

# **EXPERIENCE-BASED MODEL QUALITY ASSESSMENT METHODS AND THEIR APPLICATION TO REINFORCED CONCRETE WALLS**

A dissertation by  
**Samira Marzban**

submitted in partial fulfillment of the  
requirements for the degree of  
Dr.-Ing.

**Bauhaus-Universität Weimar**

Faculty of Civil Engineering  
Bauhaus-Universität Weimar  
Weimar, Germany  
November, 2015



## Abstract

Studies focused on models and their associated parameters are of crucial importance to engineers since models are the essential tools for structural analysis and design. Particularly, diversity of the available models has introduced difficulties on the choice of a unique model to define a desired phenomenon. Consequently, model selection techniques have been developed to address the issue. Though, they mainly rely on a benchmark model as the reference to check the other models. The benchmark is usually chosen to be the experimental measurement or the most complex model where no experimental data is accessible. In the present thesis, I propose a model selection technique which evaluates models quantitatively based on a systematic comparison considering their uncertainty and sensitivity properties. The core assumption is that any model in a group of models to be assessed has the potential to be the best abstraction of the studied phenomenon regardless of its nature (experimental or numerical) or complexity status. The proposed methodology was applied to a series of mathematical and engineering problems including the data collected in the so-called experience-based database on reinforced concrete walls. The straightforward mathematical problems were used as benchmarks whereas the engineering problems were supposed to challenge the capacity of the method in practical situations. In all the studied cases, the assessment results agreed well with the qualitative evaluation of the models.

The proposed model selection technique was founded on the ground of a conceptual implementation of the variance-based sensitivity analysis. Therefore, the conceptual implementation was exclusively investigated to shed some light on the fundamentals of the proposed method.

**Keywords:** *Sensitivity Analysis, Model Evaluation, Uncertainty Assessment, Validation, Experimental Data, Reinforced Concrete Walls, Yield Displacement*



## **Acknowledgments**

First and foremost, I wish to express my sincere gratitude towards my doctoral fathers Dr. Jochen Schwarz and Prof. Carsten Könke who supported me through out this research to experience, learn and grow in professional and personal aspects. Their different practical and theoretical attitudes led me to reach for a balanced view of the engineering problems at hand. My special thanks go to Prof. Tom Lahmer, Dr. Lars Abrahamczyk and Dipl.-Ing. Mathias Leipold for the remarkably fruitful discussions during my study and the helpful comments on the early versions of the thesis. Additionally, I would like to thank my colleagues and professors in GRK1462 for the multi-cultural, multi-discipline and friendly scientific environment in which I had the opportunity to work. GRK1462 is a research training group funded by the German Research Foundation (DFG). Their financial support for my research project is much appreciated.

Last but certainly not least, I am so grateful to my family's endless heartwarming love which is invaluable to me. They have always been my greatest support, although geographically thousands of kilometers away.

Samira Marzban  
October, 2015



*to my Mom*  
*the woman behind my big dreams*





# Contents

1. Introduction	1
1.1. State of the Art of the Assessment Techniques	2
1.1.1. Sensitivity Analysis	2
1.1.2. Model Selection	4
1.2. Problem Definition	5
1.3. Contribution of the Thesis	6
1.4. Structure of the Thesis	7
2. Reinforced Concrete Structural Walls	9
2.1. Characteristics	10
2.2. Relevant Studies	14
2.2.1. Numerical Investigations	14
2.2.2. Experimental Investigations	16
2.3. Response Parameter of Interest	19
3. Experience-Based Database	23
3.1. Experimental Tests	23
3.1.1. Typical Test Setup	24
3.1.2. Typical Wall Specimen	26
3.1.3. Recorded Input Parameters	27
3.1.4. Recorded Output Parameters	28
3.2. Numerical Simulations	29
3.2.1. Multiple Vertical Line Element Model	32
3.2.2. Flexure-Shear Interaction Displacement-Based Beam-Column	39
4. Variance-Based Sensitivity Analysis	43
4.1. First Order Effects	43
4.1.1. Implementation by SALTELLI ET AL. (2008)	44
4.1.2. Conceptual Implementation	46
4.1.3. Extended Fourier Amplitude Sensitivity Test (EFAST)	47
4.2. Analytical Benchmark Problems	48
4.2.1. General Conditions	49

4.2.2.	Sobol's g-Function . . . . .	50
4.2.3.	Polynomial Function . . . . .	54
4.2.4.	Ishigami Function . . . . .	57
4.2.5.	Parameter Study on the Number of Subdivisions . . . . .	59
4.2.6.	Parameter Study on the $N_R$ in EFAST . . . . .	62
4.3.	Engineering Problems . . . . .	63
4.3.1.	General Conditions . . . . .	64
4.3.2.	Numerical Simulations . . . . .	66
4.3.3.	Experimental Tests . . . . .	68
4.4.	Discussion of the Results . . . . .	71
5.	Model Selection . . . . .	73
5.1.	Assessment Methodology . . . . .	75
5.2.	Benchmark Problem . . . . .	79
5.2.1.	General Conditions . . . . .	79
5.2.2.	Parametric Study . . . . .	81
5.3.	Engineering Problems . . . . .	84
5.3.1.	Studied Yield Displacement Estimation Methods . . . . .	84
5.3.2.	Database: Numerical Part . . . . .	86
5.3.3.	Database: Experimental and Numerical Parts . . . . .	91
5.4.	Discussion of the Results . . . . .	96
6.	Conclusions . . . . .	99
A.	Database: Experimental Part . . . . .	103
A.1.	Squat Walls . . . . .	109
A.2.	Transition Walls . . . . .	120

# List of Figures

1.1. Uncertainty vs complexity (GABER ET AL. (2009)). . . . .	6
2.1. Structural response of RC walls in interaction with other substructures. . .	10
2.2. Typical wall forms. . . . .	11
2.3. Typical wall sections: a) rectangular, b) barbell, c) flanged, d) L-shaped and e) C-shaped. . . . .	11
2.4. Deformation components of the RC wall response. . . . .	12
2.5. Different types of the hysteretic behavior. . . . .	12
2.6. Isolation of the wall element from the real structure. . . . .	17
3.1. Distribution of the database properties. . . . .	24
3.2. Examples of typical test setup. . . . .	25
3.3. Displacement-controlled loading history and the resulting hysteretic be- havior. . . . .	26
3.4. Sample instrumentation pattern of a wall specimen. . . . .	26
3.5. Typical cross sections of the collected specimens. . . . .	27
3.6. Geometrical properties of the wall section. . . . .	29
3.7. Histogram of the parameters recorded in the database. . . . .	30
3.8. Distribution of the parameter values for the studied specimens. . . . .	31
3.9. Schematic deformation decoupling of a RC wall element in MVLEM . .	32
3.10. Center of rotation in MVLEM . . . . .	33
3.11. Concrete's stress-strain relationship . . . . .	34
3.12. Steel's stress-strain relationship . . . . .	36
3.13. Hysteretic model for force-deformation relationship in shear. . . . .	37
3.14. MVLEM as built in OpenSees. . . . .	39
3.15. Biaxial response for fibers in FSIDB. . . . .	40
3.16. Stress-strain relationship for <i>concrete06</i> . . . . .	41
3.17. Schematic of the wall models created with FSIDB as compared to the MVLEM. . . . .	41
4.1. Flowchart for the calculation of the $S_k$ based on SALTELLI ET AL. (2008). . .	45
4.2. Flowchart for the calculation of the $S_k$ based on the proposed implemen- tation. . . . .	46

4.3.	Influence of the constant parameter $a_k$ on $g_k(X_k)$ . . . . .	51
4.4.	Scatter of the output $Y$ with respect to the parameters for the Sobol problem with a) $K = 3$ and b) $K = 6$ . . . . .	52
4.5.	Scatter of the output $Y$ with respect to the parameters for the Sobol problem with $K = 12$ . . . . .	53
4.6.	Mean absolute error ( $MAE$ ) in predicting the first order effects for the three cases of the Sobol's $g$ -function. . . . .	54
4.7.	Scatter of the output $Y$ with respect to the parameters for the polynomial problems with a) $K = 3$ and b) $K = 6$ . . . . .	55
4.8.	Scatter of the output $Y$ with respect to the parameters for the polynomial problem with $K = 12$ . . . . .	56
4.9.	Mean absolute error ( $MAE$ ) in predicting the first order effects for the three cases of the polynomial function. . . . .	57
4.10.	Scatter of the output $Y$ with respect to the parameters for the Ishigami problems. . . . .	58
4.11.	Mean absolute error ( $MAE$ ) in predicting the first order effects for the three cases of the Ishigami function. . . . .	60
4.12.	The best choice of $S$ for problems with different number of parameters. . .	61
4.13.	The best choice of $S \times K$ for problems with different number of parameters. .	62
4.14.	Parametric study on $N_R$ for the three cases of the Sobol's $g$ -function. . . .	63
4.15.	Parametric study on $N_R$ for the three cases of the polynomial function. . .	64
4.16.	Parametric study on $N_R$ for the three cases of the Ishigami function. . . .	65
4.17.	Schematic of the studied numerical model from (AUSTRELL ET AL. (2004)). . .	66
4.18.	Scatter of the output $Y$ with respect to the considered parameters for the CALFEM problem. . . . .	67
4.19.	Average sensitivity index estimated for each parameter in the CALFEM problem. . . . .	68
4.20.	Sum of the average first order effects for the CALFEM problem in terms of the number of function calls. . . . .	69
4.21.	Observed yield drift for the specimens in the experimental part of the database. . . . .	70
4.22.	Scatter of the output $Y$ with respect to the parameters for the experimental problem on transition walls. . . . .	71
4.23.	Average sensitivity index estimated for each parameter in the experimental problem on transition walls. . . . .	72
5.1.	Hypothetical set of plausible models in the design space. . . . .	74
5.2.	Example parameter space for four hypothetical models. . . . .	77

5.3. Selected benchmark functions: a) scatter plot b) probabilities of failure in prediction. . . . .	80
5.4. Influence of the error parameters $\alpha$ and $\beta$ on $y^*$ when $y = x$ . . . . .	81
5.5. Recreation of the models presented in Figure 5.1: a) scatter plot b) probabilities of failure in prediction. . . . .	82
5.6. Probability distribution of the grades scored by the highest-ranked (lowest graded) models categorized according to the $\alpha$ and $\beta$ combinations. . . . .	83
5.7. Studied bilinearization methods for yield displacement estimation. . . . .	85
5.8. Mean and standard deviation of the normalized constant parameters in the experimental part of the database. . . . .	87
5.9. Estimated yield drifts for the MVLEM-generated specimens in the numerical part of the database. . . . .	88
5.10. Scatter plots of the estimated yield drifts for the MVLEM-generated specimens in the numerical part of the database. . . . .	89
5.11. First order effects of the input parameters on the estimated yield drifts for the MVLEM-generated specimens in the numerical part of the database. . . . .	90
5.12. Estimated probabilities of failure in prediction for the studied methods based on the data from the MVLEM-generated specimens in the numerical part of the database. . . . .	90
5.13. Estimated yield drifts for the squat specimens in the experimental part of the database. . . . .	92
5.14. Estimated yield drifts for the transition specimens in the experimental part of the database. . . . .	93
5.15. Estimated vs observed yield drifts for the transition specimens in the experimental part of the database. . . . .	94
5.16. Estimated probabilities of failure in prediction for $m_1, \dots, m_5$ . . . . .	95
5.17. Estimated probabilities of failure in prediction for $\mathcal{M}_1, \dots, \mathcal{M}_3$ . . . . .	96
A.1. Database force-deformation plots and the estimated yield drifts for the squat walls. . . . .	113
A.2. Database force-deformation plots and the estimated yield drifts for the transition walls. . . . .	124



# List of Tables

2.1.	Common failure mechanisms of RC walls according to EAG (2013).	13
2.2.	Features of a selected number of RC wall models in comparison.	14
3.1.	Parameter definitions for the database records.	28
3.2.	Parameter ranges in the experimental part of the database.	28
4.1.	Description of the terms in Equation 4.1.	44
4.2.	Selected $\mathbf{a}$ vectors for the Sobol's g-function.	51
4.3.	Parameter ranges for the CALFEM numerical simulations.	66
5.1.	Error parameters used for the recreation of Figure 5.1.	81
5.2.	Status of the parameters $\alpha$ and $\beta$ for the highest and lowest-ranked models.	83
5.3.	Constant parameters for the numerical simulations.	87
5.4.	Normalized final grades for the studied methods based on the data from the MVLEM-generated specimens in the numerical part of the database.	90
5.5.	Normalized final grades for $m_1, \dots, m_5$ given the data from $\mathcal{M}_1, \dots, \mathcal{M}_3$ .	94
5.6.	Normalized final grades for $\mathcal{M}_1, \dots, \mathcal{M}_3$ given the data from $m_1, \dots, m_5$ .	96
A.1.	Database sources and specimens.	103
A.2.	Database parameters for squat walls: geometry and material.	109
A.3.	Database parameters for squat walls: reinforcement and loading.	111
A.4.	Database parameters for transition walls: geometry and material.	120
A.5.	Database parameters for transition walls: reinforcement and loading.	122





# 1. Introduction

As civil engineers, we owe to design and build reliable structures which operate in the bounds of safety margins away from non-desired performances. In order to accomplish this task, we create abstractions of the *real* structures under *real* imposed loads, i.e. models, to be able to study the consequent effects. Such abstractions are developed in the form of mathematical (e.g. numerical) or physical (e.g. experimental) models. Obviously, the reliability of the resulting design depends strongly on the reliability of these models. Although, as BOX AND DRAPER (1987) put it:

*“Essentially, all models are wrong, but some are useful.”*

In structural engineering, the reality to be modeled includes, for instance, the structural materials, elements, connections, interactions and loading types and scenarios. It is readily clear that numerous unknowns shade our knowledge of the reality. Material properties, geometry of the elements, rigidity of the connections, interaction mechanisms and finally the upcoming natural/unnatural loads are all subject to uncertainties due to incomprehensibility or inherent randomness of the phenomena. Probabilistic approaches allow us to take uncertainties of these kinds into account. Nevertheless, and in spite of the significant efforts, there is still limited understanding of the real structural behavior from material level through section and element levels to the global level.

In an attempt to overcome the lack of knowledge, researchers have performed numerous experiments and proposed a diversity of models. Furthermore, the development of the technology has led to the evolution of extremely elaborate experimental models along with highly sophisticated numerical ones. On one hand, a hierarchy of numerical models from elementary to extremely complicated have been introduced. On the other hand, controlled laboratory tests have been performed for a wide range of problems from the material level all the way to the structural level. Clearly, the wide variety of the models at hand has confused the users. The choice of the appropriate model and its corresponding key parameters for a given problem has become a challenge. Probabilistic techniques, though, have been proposed to tackle the challenge. The major achievements in this regard are presented in the following section.

## 1.1. State of the Art of the Assessment Techniques

Quality evaluation of models requires careful interpretation of uncertainties as inherent properties of models and their corresponding parameters. Two crucial tools to deal with parameter and model uncertainties are sensitivity analysis and model selection techniques. A selected number of relevant studies in the literature from these two fields are reviewed and discussed here. In this context, the need for the present study and its contribution to the state-of-the-art knowledge can be easily justified.

### 1.1.1. Sensitivity Analysis

Sensitivity analysis is a powerful tool to serve model parameter studies by revealing the importance of input parameters and how they influence the uncertainty in the output of a model. Various methods of performing sensitivity analysis are available which generally fall into three categories, namely, 1) graphical, 2) mathematical and 3) statistical (CHRISTOPHER FREY AND PATIL (2002)).

Graphical methods tend to show the sensitivity visually for example in scatter plots. These methods are not able to assess the sensitivity in a quantitative manner. Mathematical methods, though, aim to measure the reactivity of the model output to the changes in the input. The proposed definition readily suggests the application of the derivatives of the output with respect to the input. The corresponding basic technique is called the brute force method. Accordingly, the input parameter is changed by small amount, the output is recalculated and the sensitivity is estimated by means of the observed difference (CHINNECK (2006)). Although, straightforward, derivative-based techniques are strongly dependent on the point at which they are applied and therefore provide only local information about the sensitivity of the output. They are relatively slow and considerably vulnerable to inaccuracies (CHINNECK (2006)).

Statistical methods determine the variance of the output with regard to the variance of the input. They offer quantitative solutions to global sensitivity analysis and therefore have gained significant attention. The developed techniques in the statistical category range from simple correlation to complicated variance decomposition analysis. The correlation coefficient by PEARSON (1901), on one hand, merely measures the linear input-output correlation. The variance-based methods, on the other hand, take advantage of the analysis of variance (ANOVA) in order to compute the sensitivity measures. In what follows, some major variance-based techniques are presented and discussed.

Fourier Amplitude Sensitivity Test (FAST) (CUKIER ET AL. (1973)), takes advantage of the multiple Fourier series expansion of the output function to calculate the conditional variances. The computation of the first order sensitivity indices relies on the choice of the

set of the frequencies to perform the transformation. FAST provides information regarding the contribution of the parameter uncertainties to the output uncertainty. Parameters which are then recognized as slightly important could be set equal to their nominal values (SALTELLI AND BOLADO (1998)). The method is, however, rather difficult to perform and unable to address higher order sensitivity indices. Though, attempts have been made to improve the method. SALTELLI ET AL. (1999), for example, extended the FAST by adding the capability to compute the total effects of the input parameters on the output. Recently, XU AND GERTNER (2008A) managed to overcome the limitation of parameter independence as well. Combination of the FAST with the random balance design from SATTERTHWAITTE (1959) has been proposed by TARANTOLA ET AL. (2006) to increase the efficiency and the range of application of the original FAST.

Uncertainty importance factor was introduced by HORA AND IMAN (1986) and further developed by IMAN AND HORA (1990) based on the logarithm of the output. Although, derivation of the results for the output itself was somewhat cumbersome (SALTELLI ET AL. (2008)).

SOBOL (1993) exploited the concept of the FAST and extended it in order to calculate the sensitivity indices via factor-based decomposition of the output variance (MOKHTARI AND CHRISTOPHER FREY (2005)). Sobol's method demands high computational effort for the calculation of the sensitivity indices because of the number of model runs it requires. For rather complex engineering models, this prohibits applicability. Some researchers have addressed this issue by implementing more efficient computation strategies (e.g. SALTELLI (2002)). In addition, it is unable to capture the sensitivity properties of model outputs which are calculated based on correlated model inputs. KEITEL AND DIMMIG-OSBURG (2010), for instance, expressed this incapability and replaced the method by a method appropriate for correlated parameters (XU AND GERTNER (2008B)). The deficiency is, apparently, a result of exchanging the columns of the sampling matrices during which the correlations between the parameters is lost (MOST (2012)). The method is checked against other existing methods in SALTELLI ET AL. (2010).

Methods based on meta-modeling have evolved to benefit from the considerably lower computational costs and simplicity of treatment of meta-models (also known as response surfaces or surrogate models). Response surfaces tend to approximate the unknown input-output relationship with relatively simple mathematical functions. Several studies have been dedicated to the development of procedures for sensitivity analysis based on simplified response surfaces (e.g. RATTO ET AL. (2007), REICH ET AL. (2009), STORLIE ET AL. (2009), RATTO AND PAGANO (2010), STORLIE ET AL. (2011) & VU-BAC ET AL. (2014) among others). Although, through the simplification process of creating the response surfaces additional uncertainties might be introduced to the problem which are certainly not desired.

### 1.1.2. Model Selection

Model selection/averaging techniques aim at finding the *best* definition of a desired phenomenon. On one hand, model selection methods tend to identify the *best* model among a set of plausible models. On the other hand, model averaging methods try to create a *best* model through a synergetic combination of the existing plausible models. In what follows, several techniques from both categories are reviewed and discussed.

The major achievements in the field of model selection are mainly based on the principle of parsimony as BURNHAM AND ANDERSON (2002) expressed. According to this theory, among all the plausible models defining a desired phenomenon, the one established on the ground of the fewest assumptions should be selected. The *best* model is, therefore, assumed to offer a balanced combination of simplicity and accuracy. Nevertheless, the search for the *best* model relying only on the capability to fit the known data (to fulfill the accuracy criterion) and the comparison of the parameter spaces (to meet the simplicity limit) does not guarantee that a good model will be chosen (BROWNE (2000)).

According to SEWELL (2008), the model selection techniques can be divided into two major categories of empirical (e.g. Adjusted  $R^2$ : WHERRY (1931), Cross-validation: STONE (1974) and GEISSER (1975) & Shibata's model selector: SHIBATA (1981) among others) and theoretical (e.g. AIC: AKAIKE (1973), Mallows's  $C_p$ : MALLOW'S (1973), FIC: WEI (1992), KIC: CAVANAUGH (1999) & Schwarz criterion: SCHWARZ (1978) among others). Majority of the techniques address specifically regression problems. The adjusted  $R^2$  (WHERRY (1931)), for instance, is the modified version of the simple coefficient of determination ( $R^2$ ) to penalize larger models ( $R^2$  increases with the model size). MALLOW'S (1973) also evaluates the fit of a regression model by means of the  $C_p$  as the criterion.  $C_p$  depends on the number of the parameters and samples, the residual sum of squares and the variance. The method worked quite well though it could not address a wide range of problems (DELEEUW (1992)).

In the very same year, AKAIKE (1973) introduced the Akaike information criterion (AIC) which could be presented in the frame of Bayesian statistics. The criterion is relative to the likelihood which made the method desirable to statisticians and easily applicable to the results of existing statistical programs (DELEEUW (1992)). As Mallows's  $C_p$  the criterion penalizes the large models by considering the number of parameters. However, in contrast to Mallows' criterion, AIC is not limited to the curve-fitting problems (KIESEPPA (1997)). AIC attempts to find the model with better prediction capabilities but it cannot avoid the pitfall of overfitting (DZIAK ET AL. (2012)). Modifications have been made to the penalty term in order to improve the performance of the AIC.

In the same category of penalized-likelihood criteria, SCHWARZ (1978) proposed the Bayesian information criterion (BIC). BIC searches for the parsimonious model although it might

result in an under-fitted model. In contrast to the AIC which assumes an unknown *best* model, BIC assumes that one of the models in the considered set of models is the *best* model. Therefore, BIC appears more consistent than AIC because there are chances that AIC selects an unnecessarily large model (DZIAK ET AL. (2012)).

As discussed above the model selection techniques seem to be considering the existence of a *true* set of data (mostly experimental), the underlying model of which is sought. However, usually the available experimental data is subject to lack of precision and incompleteness. Not to forget that it might be influenced by measurement and human errors as well.

In contrast to the model selection, model averaging attempts to avoid over-confidence due to the risky selection of a single model as the *best* model. In order to address the uncertainty affiliated to the *best* model selection, statisticians suggested a combination of plausible models could offer the *best* model with better predictive ability. Model averaging mainly involves regression problems where choices of the functions and the parameter combinations lead to a variety of models. Bayesian approach to the uncertainty evaluation, for instance, has led to the Bayesian Model averaging where models are weighted depending on how much they are supported by the data (DRAPER (1995), RAFTERY ET AL. (1997), HOETING ET AL. (1999) & RAFTERY AND ZHENG (2003)). In this case, model averaging and model selection will result in the same *best* model if a single model has a dominant posterior probability (CHIB ET AL. (2003)). Frequentistic approaches have also been used to compute the weights corresponding to each model. BUCKLAND ET AL. (1997) and BURNHAM AND ANDERSON (2002) proposed exponential AIC weights. Also, HJORT AND CLAESKENS (2003) discussed model average estimators for likelihood-based models. Likewise, JUDGE AND MITTELHAMMER (2007) used an empirical likelihood method to find the *best* combination of the competing models.

## 1.2. Problem Definition

In fact, the availability of several mathematical and physical models has puzzled the definition of the structural phenomena. It is not clear which model is the appropriate choice for a given problem. We have to select a model among a list of plausible models based on the efficiency and the reliability as the main properties of a sensible model. The challenge, here, is to evaluate the reliability as the probability that the model does not fail in realizing the corresponding phenomenon, i.e. the reality is the benchmark. Due to epistemic and aleatoric uncertainties, however, the reality has remained obscure. Notwithstanding, it is common practice to favor the most complex mathematical models along with the physical models as the best representatives. Model selection techniques have been proposed based

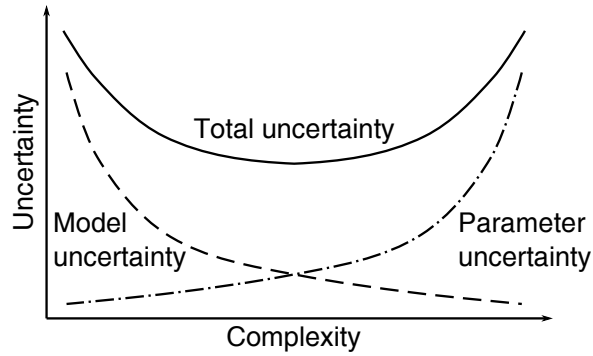


Figure 1.1. Uncertainty vs complexity (GABER ET AL. (2009)).

on the assumption that such models are the references for the quality evaluation of other models. Contradictorily, it is well understood that complex models with numerous input parameters usually suffer from parameter uncertainties (as shown in Figure 1.1), limited range of application and high computational expenses. In addition, experimental data is usually subject to lack of precision and incompleteness and can be influenced by measurement and human errors. Sometimes, as in the cases of design of experiments, there is even no access to the experimental data during the modeling phase.

As a result, model selection techniques which count solely on biased references like complex numerical models or experimental data have limited application scope and might lead to erroneous quality assessments if the references are chosen improperly.

### 1.3. Contribution of the Thesis

In this study, I propose a model selection technique which ranks the models in the studied group of models based on a systematic comparison considering their uncertainty and sensitivity properties. The method does not rely on predetermined benchmark models since it basically assumes equal probabilities for each model in a set of plausible models to be the *best* model. In other words, the models are not prejudged according to their experimental or numerical nature or their complexity status. A particular result of this assumption is that the experimental data can be regarded as a physical model along with the numerical ones. Another consequence is that a number of scenarios can be considered in each of which one model is assumed to be the *best* model. Obviously, the number of such scenarios equals the number of models in the design space. In each scenario, the performance of every studied model in predicting the temporarily selected *best* model is measured in terms of the probability of failure in prediction. The final ranking is done through the quantitative assessment of the ability of the models in representing the group of models.

The model which is best in predicting and being predicted by all the models in the design space is assumed to be the *best representative* model among them.

As mentioned above, the proposed method is independent from any specific benchmark model which implies that it is applicable to the cases where no experimental data or unknown/improper numerical reference models are available. In cases where the experimental data is included in the systematic comparison, the model selection results include the validation against the experimental data as well. In the current thesis, the proposed method was mainly targeted at the assessment of the experimental and numerical data collected in the experience-based database on reinforced concrete walls.

It should be noted that the proposed model selection technique operates on the uncertainty and sensitivity properties of the models to be assessed. It was, in fact, founded on the basis of the variance-based sensitivity analysis concept by SOBOL (1993). Since the conceptual implementation formed the foundation for the proposed model selection technique, it was exclusively investigated using different analytical and numerical benchmark problems.

## 1.4. Structure of the Thesis

The thesis is divided into six chapters including the introduction and the conclusions and one appendix. Chapter 1 starts with a broad view on the subject of model assessment. The topic is then narrowed down to the sensitivity analysis and model selection as the main focuses of the present study. With a review on the state of the art of the aforementioned fields, the reader is guided to the research gaps where the target problems are defined. A brief review of the key features of the proposed methodology to tackle the problem and the application cases followed by the justification of the study's significance finalize Chapter 1.

Chapter 2 aims at providing the reader with information regarding reinforced concrete structural walls as the engineering application case for the proposed methodology. The need for extensive probabilistic studies on reinforced concrete walls is made clear through a literature survey on numerical and experimental references. At the end of the chapter, a specific response parameter is selected for further studies. Chapter 3 introduces the created experience-based database during the course of the study. The first part of the chapter refers to the experimental part of the database whereas the second part concentrates on the numerical one. In the experimental section, general properties of the collected specimens are provided. In addition, information recorded from the specimens and the primary statistical analysis on the resulting data are presented. In the numerical section, the fundamentals of the used numerical models are discussed and the detailed modeling procedures are explained.

Chapter 4 and Chapter 5 tackle the defined problem in Chapter 1. Chapter 4 targets the sensitivity analysis. It begins with the definition of three studied implementations including the proposed conceptual implementation. The efficiency and accuracy of the conceptual implementation is then checked against the competing implementations in several analytical and numerical benchmark problems. Chapter 5 introduces the proposed model selection technique through a comprehensive description of the methodology. The technique is applied to mathematical benchmark problems in order to investigate its performance. After the methodology is justified through the benchmarks it is employed to analyze the data coming from the database as the final engineering application.

The thesis is finalized with conclusions in Chapter 6. Detailed information regarding the database are provided additionally in Appendix A.



## 2. Reinforced Concrete Structural Walls

Reinforced concrete (RC) structural walls have gained considerable attention since 1920's in construction and rehabilitation of new and existing buildings in regions with medium to high seismic hazard. They provide structures with lateral stiffness, strength and ductility if properly designed. Moreover, they have shown reasonable performance during the past earthquakes. WOOD ET AL. (1987), for instance, reported that the structural walls performed excellently during the 1985 Chile earthquake. WYLLIE (1989) mentioned that the buildings with structural walls performed much better than other structural systems in the 1988 Armenia earthquake. In addition, no building with RC walls as the lateral resisting system collapsed during the 1994 Northridge, 1995 Kobe and 1999 Kocaeli earthquakes. BIRELY (2012) provides a valuable review over the performance of RC walls in some major earthquakes since 1957.

RC walls are used in a wide range of structures from simple residential to sophisticated infrastructures (e.g. GALLITRE ET AL. (2007), GULEC ET AL. (2009)). In the most common building configuration, they are combined with gravity resisting system (usually RC moment frame) to form an integrated lateral/vertical load-carrying system. In such frame-wall structures the most lateral resistance is supplied by the walls. Their modeling and design, therefore, becomes a critical issue, since the structural performance under seismic actions relies mainly on their performance. Thus, it is logical to focus studies on the lateral response of RC walls. Although, as learned from the past earthquakes, the wall performance can be significantly affected by the interactions with other substructures (e.g. MARZBAN (2010), BAO AND KUNNATH (2010), BARBOSA (2011) and TANG AND ZHANG (2011)). Figure 2.1, for instance, schematically depicts the interaction of RC walls with the moment frame as well as the soil-foundation. In this study, since the wall is investigated as a standalone element, all interactions with other structural elements are not considered.

In the following section, general features of the RC walls and their lateral response are described. Next, a brief review on the relevant studies on RC walls is provided. The chapter ends with a discussion on the selected response parameter for further studies.

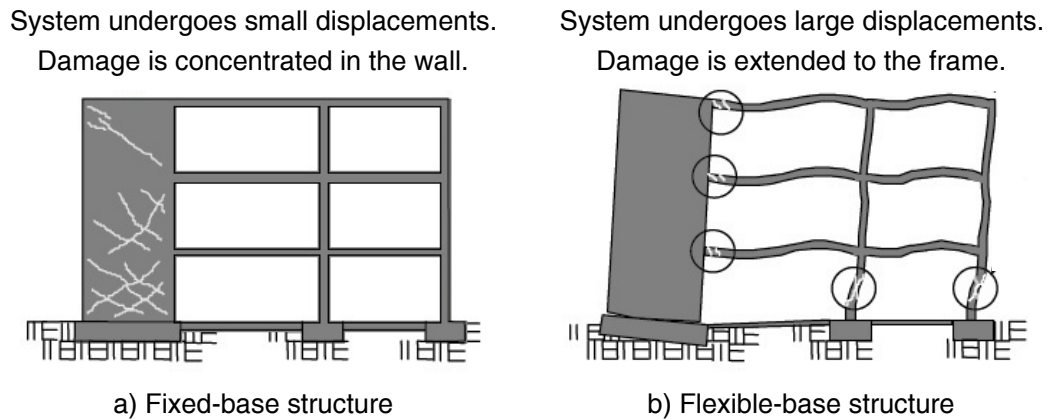


Figure 2.1. Structural response of RC walls in interaction with other substructures (modified from ATC40 (1996)).

### 2.1. Characteristics

The general form of the RC walls is dictated by the structural configuration along with the architectural plans. They are usually either single, coupled or perforated by openings (see Figure 2.2). RC walls have basically rectangular cross sections which are oriented so that the major bending occurs about the strong axis of the section. In cases where the walls interconnect with adjacent columns or perpendicular walls barbell, flanged, L-shaped and C-shaped sections are introduced (see Figure 2.3). Boundary elements add to the stiffness and strength of the wall if properly reinforced and particularly confined.

The response of RC walls to lateral loads can be described as a combination of shear and flexural deformations as seen in Figure 2.4. The contribution of each deformation type to the total response of the wall depends strongly on the geometrical, material, reinforcement layout and loading properties. In the technical literature, these properties are usually described in terms of the aspect ratio, boundary element contribution, vertical and horizontal reinforcement ratios, concrete's and steel's strength and the loading conditions. In particular, the aspect ratio defined commonly as the wall height divided by its length has a major effect on the wall behavior. This parameter determines whether the wall responds in shear, flexure or a combination of both. According to FEMA356 (2000), walls with aspect ratios less than 1.5 and greater than 3.0 are considered as squat and slender walls respectively. Walls with aspect ratios between 1.5 and 3 are defined as transition walls where both shear and flexural deformations contribute to the total response. Other categorizations may differ slightly in the definition of the ranges. GULEC AND WHITTAKER (2009), for instance, set the limit for squat walls at the aspect ratio of 2.0. In this study, the recommended criteria from FEMA356 were used to classify the walls.

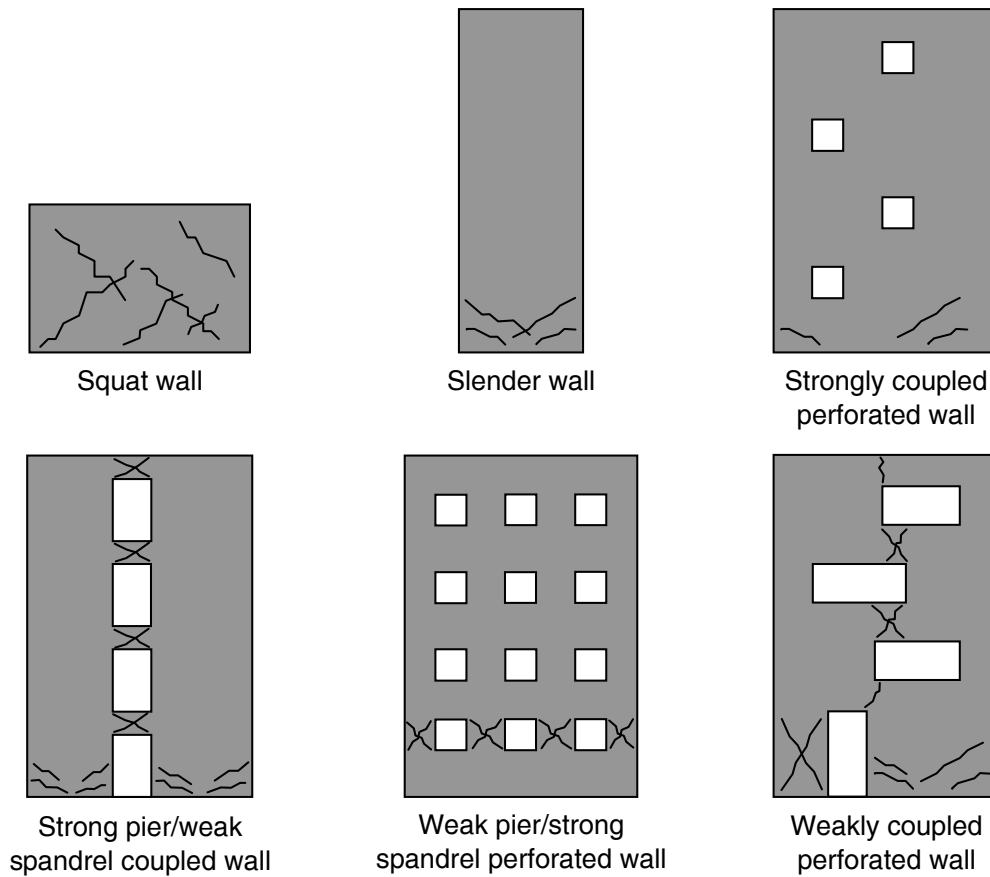


Figure 2.2. Typical wall forms (EAG (2013)).

As seen in Figure 2.5 and depending on the dominant deformation mechanism in the wall, the hysteretic behavior can change dramatically from perfectly ductile with quite wide loops to brittle with pinched loops (examples can be found, for instance, in KOLOZVARI ET AL. (2015)). The former behavior depicts the flexural response of walls with proper confinement whereas the latter is a well-known response in shear. Obviously and as for other structural members, flexural behavior is desired for RC walls due to its ductile nature.

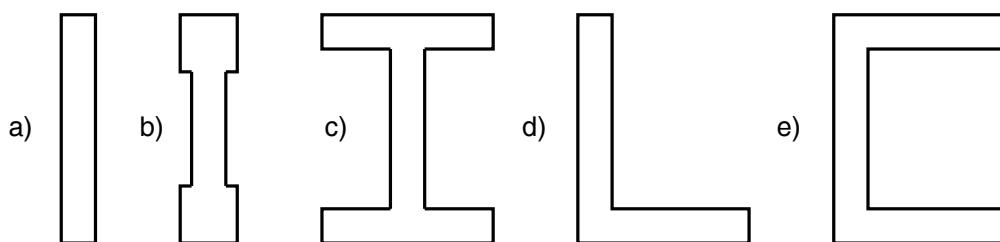


Figure 2.3. Typical wall sections: a) rectangular, b) barbell, c) flanged, d) L-shaped and e) C-shaped.

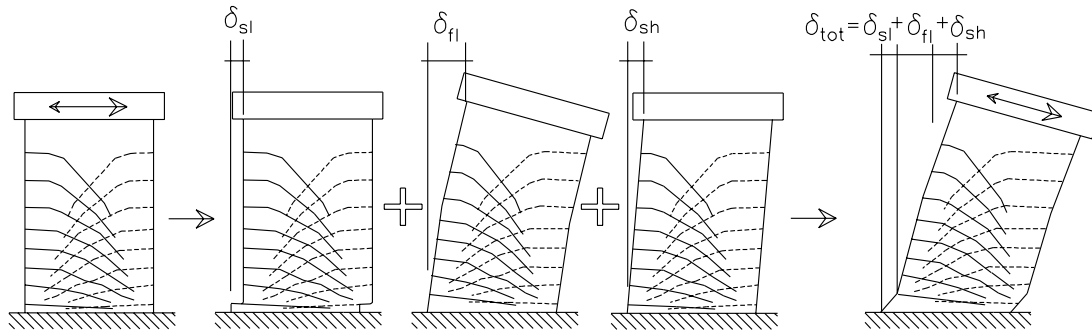


Figure 2.4. Deformation components of the RC wall response (SALONIKIOS (2004)).

The wall response could be additionally affected through its interaction with the soil-foundation substructure. The phenomenon is known as rocking and results in a favorable amount of energy dissipation without imposing severe damage to the wall. In fact, it is thought that rocking might have been the reason for some remarkable performances of poorly designed/built walls in the past earthquakes (EAG (2013)). The rocking mechanism is more likely to happen where quite stiff (e.g. squat) wall is supported by shallow or flexible foundation. Other aspects of the wall behavior include but are not limited to: neutral axis migration, concrete tension stiffening, progressive crack closure and nonlinear shear behavior (ORAKCAL ET AL. (2006)).

Severe earthquakes subject RC walls to local and global damages of various types (see, for instance, the crack patterns in Figure 2.2). The damages, normally, involve cracks in concrete, concrete crushing and spalling along with yielding and buckling of reinforcement. The main cause for such damages is usually inappropriate and/or inadequate reinforcement content. The damages are mainly concentrated at the wall base, the intersections with other structural elements and particularly where the splices occur and/or the seismic demand is high. The type of the damage that a RC wall undergoes can be roughly

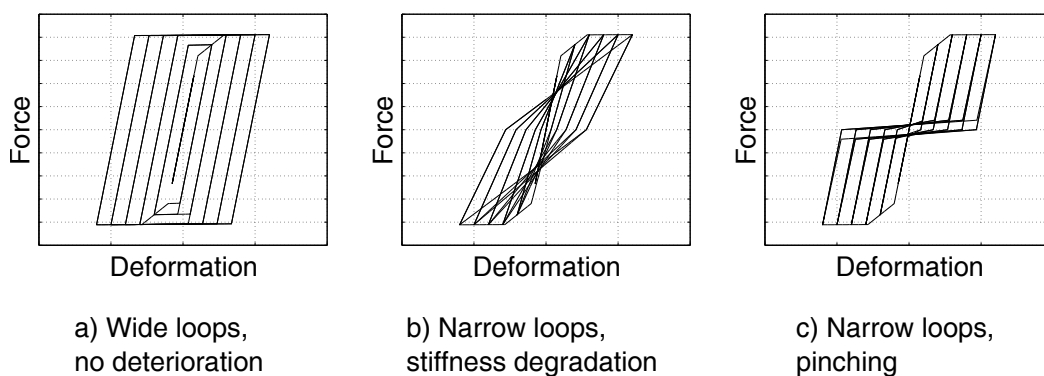
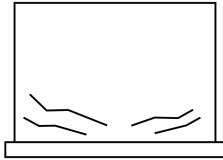
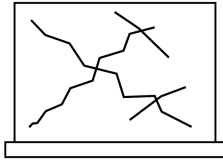
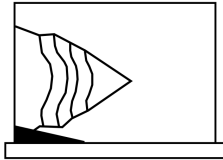
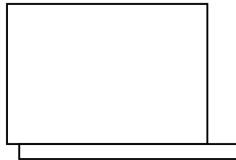
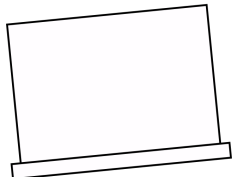


Figure 2.5. Different types of the hysteretic behavior.

determined according to its dominant behavior (namely, shear, flexural or both) and its interaction with the adjacent fundamental elements such as foundations and diaphragms. Additionally and depending on the reinforcement content and the material properties of the wall, the damages can be limited to negligible cracks or extended to overall collapse. The failure mechanism is, in fact, a function of the wall's dominant behavior mode as well (see Table 2.1). Flexural failure usually involves bar fracture/buckling and concrete spalling/crushing. This failure type is quite desirable in design due to its ductile nature through which the wall undergoes large deformations before collapse. Shear failure, however, commonly comes with damages in the diagonal directions where virtual struts develop in tension and compression. Other failures might initiate due to discontinuities in the form of damages at the construction joints and the splices (BIRELY (2012)).

Table 2.1. Common failure mechanisms of RC walls according to EAG (2013).

	Failure Mode	Favorability	Description
	Flexure	✓✓	Flexure is the ideal wall behavior. Issues to be considered are whether the remaining reinforcement capacity is sufficient and what repair may be required.
	Shear	×	Shear is generally not the desired mechanism, as vertical load-bearing capacity may be lost at relatively low strains. This is generally considered a non-ductile mechanism.
	Crushing	××	Crushing may occur where there is an inadequate confinement of the compression zone or an axial load in excess of the calculated demand. Excess axial load may result from flexural actions.
	Sliding	✓	Sliding is not generally a design failure mode but appears to have happened widely, particularly at poorly formed and compacted construction joints. However, it is not inherently an unsafe mechanism.
	Rocking	✓✓	Rocking has probably saved many walls that would have otherwise failed if they had rigid foundations. Although, inherently a simple mechanism, rocking is dynamically complex.

## 2.2. Relevant Studies

Reliable design of RC walls is achieved via the new performance-based design procedures in which the desired performance under specific seismic hazard is sought. This requires hazard, structural, damage and loss analysis which obviously should be based on comprehensive studies of RC wall behavior. A large number of studies, therefore, have been devoted to the understanding of RC wall behavior under lateral forces. Many researchers have delved into the problem from the experimental and numerical aspects.

### 2.2.1. Numerical Investigations

A transparent result of the plethora of numerical studies focused on the lateral response of RC walls, is the emerge of diverse modeling techniques to simulate the walls. Table 2.2 includes a few of the most common models. A review on a number of these models can be found in GALAL AND EL-SOKKARY (2008). The models can be roughly fit into two categories of macro- and micro-models with the macro-models being very popular due to their simplicity and computational efficiency. Consequently, they have been exposed to significant enhancements and developments. One of the early macro-models consisted of three vertical line elements connected rigidly at certain elevations to represent the web and the boundary elements. KABEYASAWA AND MILEV (1997) replaced the middle springs of the three-vertical-line-element model with a panel to enhance the shear behavior consideration. GHOBARAH AND YOUSSEF (1999) modeled the wall with springs concentrated at the base followed by linear elastic truss elements. Their model was presumed to be capable of capturing the shear deformations and was validated against experimental data.

HIDALGO ET AL. (2002) developed models for shear and flexural behaviors with validations against wall and beam experiments, respectively. The models were also used in the numerical modeling of a real building in order to evaluate their ability to predict the observed crack distribution. LEE AND MOSALAM (2003) and later LEE AND MOSALAM

Table 2.2. Features of a selected number of RC wall models in comparison.

Model	Features					
	Damage		Response		Interaction	
	Local	Global	Flexure	Shear	Flexure-Axial	Flexure-Shear
Finite element	✓	✓	✓	✓	✓	✓
Fiber section	✓	✓	✓	×	✓	×
Beam-Column	×	✓	✓	×	×	×
MVLEM	✓	✓	✓	✓	✓	×
FSIDB	×	✓	✓	✓	✓	✓

(2005) utilized the deterministic sensitivity approach to find out the relative significance of a group of selected parameters with respect to the engineering demand parameters as the outputs. On one hand, the input parameters were set to be the mass, viscous damping, structural strength and stiffness and ground motion properties. On the other hand, the roof absolute acceleration and displacement, maximum interstory drift and peak curvature at critical sections were chosen as the output parameters. The model was made of beam elements connected to the side columns through rigid beams. The first-order-second-moment (FOSM by BAKER AND CORNELL (2003)) method was used to estimate the stochastic properties of the output parameters given the uncertainty features of the input variables. According to them, the dominant parameters were the ground motion specifications and the viscous damping. MASSONE ET AL. (2004) evaluated the interaction of the flexural and shear behaviors in transition and slender walls. Accordingly, they modified the Multiple Vertical Line Element Model (MVLEM) to allow for the simulation of the observed interaction. A biaxial constitutive relationship was used for concrete. The results agreed well with the experimental results. However, the models seemed to perform better in the case of flexure-dominant walls rather than the shear-dominant ones. ERVENKA ET AL. (2005) modeled RC walls in an attempt to find a set of material properties leading to the best agreement between the simulated and the experimental responses. MO ET AL. (2008) implemented material and membrane element models in OpenSees. The smeared crack model captured the deterioration process through the constitutive relationship by DE BORST ET AL. (2004) which was checked against the experimental data. THOMSON ET AL. (2009) proposed a simple lumped plasticity model with limited application to shear-dominant walls. Stiffness reduction due to cracking was considered. They validated the results against test data. AALETI (2009) modeled walls by means of the beam-column elements with fiber section in the OpenSees. The model by MANDER ET AL. (1988) was used to define the properties of the confined concrete. They took advantage of the experimental data on shear distortion to calibrate the hysteretic material for shear.

MATSUURA ET AL. (2012) used the comparison with the experimental data to prove the accuracy of their proposed model. It consisted of two trusses as the boundary elements as well as a combination of the rotational, axial and shear springs for the mid-panel. The model which overall had three segments produced results in good agreement with the experiments. YEOW ET AL. (2012) performed damage loss estimation on walls modeled as lumped plasticity beams with hysteretic behavior and constant axial load. They compared the results with those coming from the analysis on a frame structure to observe the difference in the performance in terms of the damage loss. DARANI AND MOGHADAM (2012) conducted a study on the influence of the boundary elements on the performance of RC walls. According to their numerical analysis, in the presence of the boundary elements the strength capacity increases whereas the accompanying displacement decreases compared to the case of no boundary elements.

MAGNA AND KUNNATH (2012) compared the response of three different models, namely, the equivalent beam-column model, the multiple-vertical-line-element-model (MVLEM) (ORAKCAL ET AL. (2004)) and the flexure-shear interaction displacement-based beam-column model (ORAKCAL ET AL. (2006)). The models were built in OpenSees with experimental tests on squat, transition and slender walls as benchmark to check the results. They concluded that given a proper definition of the shear spring, the MVLEM was an appropriate choice for modeling RC walls. DASHTI ET AL. (2012) utilized MVLEM to model experimentally tested walls. They controlled both the local and the global response with respect to the experiment. The investigated local responses included: the migration of the neutral axis and the behavior of the vertical and the horizontal springs. FISCHINGER ET AL. (2012) proposed an extended version of the MVLEM. The idea was to use distributed shear springs on the vertical elements. They modeled the shear springs as a combination of three horizontal springs representing: the dowel effect of the vertical reinforcement, the axial resistance of the shear reinforcement and the interlock of the aggregate particles in the crack. The properties of the springs depended on the state of the cracks. KOLOZVARI ET AL. (2012) and KOLOZVARI ET AL. (2015) also extended the MVLEM by replacing each uniaxial fiber with a panel element subjected to membrane actions which was able to capture the interaction between shear and flexural behaviors. They compared the results to experimental data leading to the observation that the shear-flexure interaction might appear even in fairly slender walls. Although, their model failed at predicting shear deformations due to the simple elastic model chosen to relate the sliding shear strain to the shear stress along the crack surface.

### 2.2.2. Experimental Investigations

Among all the studies on RC walls, experimental tests have been very popular. They provide valuable information regarding the wall behavior and can be used to validate/calibrate numerical models and/or develop empirical equations. In experimental studies, it is far more common to study RC walls as standalone elements. Usually, it is assumed that the wall is isolated from the structural system that it belongs to (see Figure 2.6). In this case, not only setting up and performing the experiment but also comprehending the results is more feasible.

The most extensive experimental program on RC walls was conducted by the Portland Cement Association in three phases by OESTERLE ET AL. (1976), OESTERLE ET AL. (1979) and SHIU ET AL. (1981). Overall, sixteen isolated specimens of various cross sections, boundary confinement, reinforcement content, concrete's strength and loading conditions were tested. The aim was to formulate a design procedure based on the information gathered from the experimental and the analytical investigations regarding the strength



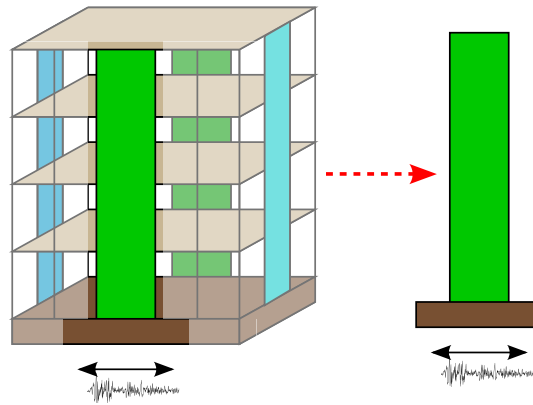


Figure 2.6. Isolation of the wall element from the real structure (modified from DAZIO ET AL. (1999)).

and deformation capacities of RC walls. In particular, the ductility, energy dissipation and strength capacities were studied. They found the shear stress level played an important role on the behavior of the walls.

BOUCHON ET AL. (2004) performed experiments on low-rise walls as one of the main structural systems in nuclear facilities in order to define the crack geometry. SU AND WONG (2007) tested three specimens of high aspect ratio ( $H/L = 4$ ) with different axial loads and transverse reinforcement. The specimens were loaded by axial and bending forces which means no direct shear force was applied. The aim was to study the behavior of the RC walls in common existing high-rise buildings in Hong Kong. PANAGIOTOU (2008) validated a proposed displacement-based seismic design approach against his experimental data from a full-scale 7-story building. The experimental results were additionally used as benchmark to check a developed strut and tie model. AALETI (2009) performed two experiments to acquire the necessary data for the validation of a model implemented in OpenSees. The sections were not symmetrical in terms of the boundary elements. DAZIO ET AL. (2009) tested six wall specimens with rectangular sections and different reinforcement content, under static cyclic loading. The results were used to develop empirical equations for the determination of the plastic hinge length and strain limit states. PENG AND WONG (2011) tested three walls under lateral load in combination with torsion. They observed that torsion led to the occurrence of the plastic hinge at higher elevations along the wall height. KONO ET AL. (2012) designed two  $\frac{4}{10}$  scale specimens with different transverse reinforcement for experimental examination. They made comparisons to numerical as well as a full-scale 4-story building shaking table test. MATSUURA ET AL. (2012) carried out two series of cyclic tests on u-shaped walls as the representatives of the three lower stories of a prototype building. The first series consisted of three  $\frac{1}{10}$  scale specimens with either constant or variable axial load in addition to different lateral load directions. The responses were compared to the corresponding results from the fiber section and three-

column models. The second series included twelve specimens with various cross section areas, load patterns and reinforcement configurations. The main purpose for the second series of the tests was to investigate the unconfined compressional characteristics of concrete. HANNEWALD AND BEYER (2012) tested seven pier specimens under quasi-static cyclic loading with the intention to study the plastic hinge properties of not-seismically-designed existing piers. BIRELY (2012) tested four large-scale walls to produce fragility curves from the resulting data. Additionally, she took advantage of the information regarding the damages to walls during the 2010 Chile earthquake as well as the photos from the damages due to the past earthquakes. TALEB ET AL. (2012) examined the lower three stories of a typical 6-story building at the  $\frac{4}{10}$  scale. The walls were designed to fail in shear. In addition to the axial load, bending moments were applied to keep the shear span ratio constant and equal to one. The experimental results were used to study the shear strength of walls with different opening layouts. NAGAE ET AL. (2012) Performed shaking table tests on two full-scale 4-story buildings with RC walls in one direction. The intensity of the input ground motion was gradually increased in order to capture the damage development. They reproduced the system with a single-degree-of-freedom to calculate the global response which led to the conclusion that a properly characterized model could respond reasonably well. TRAN AND WALLACE (2012B) validated their numerical model against 5 large-scale transition walls with significant contribution of the shear deformations to the lateral response. The cyclic loading scheme comprised of a force-controlled loading followed by a displacement-controlled one. Using the experimental data, the influence of the aspect ratio, average shear stress and the axial stress on the wall deformation and axial load-bearing capacities were investigated.

The review of the experimental studies can go further on due to its broad nature. In fact, the diversity of the available data has complicated the research on RC walls. Collecting such data and organizing it in databases facilitates data management as well as probabilistic analysis on the data. In the case of RC walls, for instance, many researchers created databases of wall experiments in order to study different aspects of the wall behavior. GULEC AND WHITTAKER (2009), for instance, assembled a database including 434 squat walls with three different cross sections based on loading type, aspect ratio, shear span ratio, axial load ratio, material properties and type of failure. The goal was to find out which factors affect the performance of the wall and to introduce new models capable of simulating the wall behavior. BEYER ET AL. (2011) listed the results of 34 tests on RC walls. According to them, the shear-to-flexural deformation ratio is constant and reveals the significance of the shear deformations in the total response. The ratio increases as the wall behavior enters the nonlinear range with less shear resistance along the open cracks. They used the data to propose an empirical equation for the calculation of the shear-to-flexural deformation ratio. TUNA (2012) developed a database of 124 walls with the purpose of studying the effects of a set of selected parameters on shear and deformation capacity of

RC walls. The data, taken from 19 different sources, included information about loading and section type, geometry, shear span ratio, axial load ratio and reinforcement properties. BIRELY (2012) collected the data from 66 slender wall specimens. The data was organized according to geometry and reinforcement properties, loading type and shear strength. The database was built to create fragility functions for slender walls with the shear span ratio of greater than or equal to 2.0.

Although, databases do not necessarily limit to the laboratory experiments, cases proving otherwise can rarely be found. JÜNEMANN ET AL. (2012) and (2015), for example, created a database of wall buildings damaged during the 2010 Chile earthquake. They collected information regarding 34 out of 47 moderately to severely damaged wall buildings. The focus was the common fishbone Chilean buildings with more than 9 stories. In this type of construction the walls carry the gravity loads as well. They concluded that despite the standard wall to floor area ratio for the new buildings, they accounted for the majority of the damaged buildings.

As it was mentioned in Chapter 1, what might be disregarded in experimental studies is that experiments can be as fragile as the numerical simulations. In fact, uncertainties can affect the experimental data as well. Therefore, a proper model quality evaluation through validation against experimental data should take the mentioned uncertainties into account. This issue will be addressed in Chapter 5.

## 2.3. Response Parameter of Interest

In order to study the wall performance, it should be quantified in terms of the wall response. Strength and deformation components, for instance, are well known as convenient response parameters to be used in performance-based design. One of the characteristic points in the strength-deformation relationship is where the global yield happens, i.e. where a major loss in the stiffness occurs. Since the yield point plays an important role during the design process based on the performance-based codes, it was chosen as the focus of the present study. Particularly, the probabilistic aspects in the estimation of the yield displacement for RC walls were addressed.

The yield point has become a crucial part of many simplified seismic design procedures. This specifically includes methods involving the simplification of multi-degree of freedom systems to the equivalent single-degree of freedom systems. The simplification process normally takes advantage of some linearization method (ATC40 (1996) for instance) which indeed requires a simplified definition of the yield point. Since this point characterizes the idealized force-deformation relationship (or the capacity curve), careful attention should be paid to its definition.

Many researchers have focused on yield displacement calculations. PARK (1988), for instance, considered the four following definitions for the yield point. According to him, the yield point corresponds to the displacement: 1) where the first yield occurs (based on material nonlinearity), 2) of the equivalent elasto-plastic system with the same elastic stiffness and ultimate load as the real system, 3) of the equivalent elasto-plastic system with the same energy absorption as the real system and 4) of the equivalent elasto-plastic system with reduced stiffness found as the secant stiffness at 75% of the ultimate lateral load of the real system. Such definitions later set the ground for the approaches recommended by some design codes (e.g. ATC40 (1996)).

PAULAY AND PRIESTLEY (1992), estimated the yield curvature based on Equation (2.1). Here,  $\epsilon_y$  is the yield strain of the steel at the extreme fiber and  $\epsilon_{ce}$  is the corresponding concrete's elastic compression strain on the opposite edge of the wall. Obviously, this estimation is based on the local response of the concrete and the steel which might not always be accessible (as for some experimental data for example).

$$\phi_y = \frac{\epsilon_y + \epsilon_{ce}}{L_w} \xrightarrow[\epsilon_{ce} \approx 0.0005]{\epsilon_y \approx 0.002} \phi_y \approx \frac{0.0033}{L_w} \quad (2.1)$$

In the same category, lies the formulation from PRIESTLEY AND KOWALSKY (1998). They proposed the dimensionless Equation (2.2). The idea is to calculate the yield displacement ( $\Delta_y$ ) in terms of the yield strain of the longitudinal reinforcement ( $\epsilon_y$ ), the wall length ( $L_w$ ) and the effective wall height ( $h_e$ ).  $K_1$  is the coefficient found based on the level of axial load and the reinforcement distribution.

$$\Delta_y = \left( \frac{K_1 \epsilon_y}{l_w} \right) \frac{h_e^2}{3} \quad (2.2)$$

A large number of methods have been introduced to estimate the yield displacement based on the global response. Majority of such methods, specifically those addressed in design codes, rely on bilinearization techniques. ATC40 (1996) recommends bilinearizing the force-deformation relationship by an elastic branch followed by an inclined post-yield branch. The post-yield stiffness is found through minimizing the difference between the area under the main curve and its idealization. This is to satisfy the equal energy concept which requires that the idealized model absorbs the same amount of energy as the main model. The intersection of the two branches is then known to be the global yield point. In contrast to ATC40, FEMA273 (1997) suggests a secant stiffness through 60% of the yield strength for the first branch. The rest of the procedure, though, is the same as that of the ATC40. An application and a comparison of some of the code-recommended methods

can be found in IBRAHIM (2000). Though, the purpose was to evaluate Ibrahim's method to calculate the effective flexural stiffness of RC walls. He estimated the effective flexural stiffness by means of a piece-wise flexural model. Later, TJHIN ET AL. (2004) proposed Equation (2.3) for the calculation of the yield displacement. In this equation,  $\kappa_{\Delta}$  denotes the yield displacement coefficient with  $\phi_y$  being the effective yield curvature at the bottom of the wall.  $h_w$  is the height of the wall.

$$\Delta_y = \kappa_{\Delta} \phi_y h_w^2 \quad (2.3)$$

SULLIVAN ET AL. (2004) related the yield displacement of RC wall to the corresponding yield curvature considering the curvature distribution. Another comparative study has been done by KADAŞ (2006). He studied the influence of different idealization techniques on the seismic response of moment frames. The methods were taken from PAULAY AND PRIESTLEY (1992), FEMA273 (1997) and ATC40 (1996). He concluded that all the methods resulted in more or less the same amount of error and uncertainty in the seismic response. The idealization technique, therefore, is of less importance compared to the hysteretic behavior (loading-unloading model), ground motion characteristics and frame properties. PRIESTLEY ET AL. (2007) defined the yield displacement in a very similar way to PRIESTLEY AND KOWALSKY (1998). Using the 3/4-rule from PRIESTLEY AND PARK (1987), DAZIO ET AL. (2009) calculated the yield displacement for a series of wall specimens. The method needs a prior knowledge of the yield force.

FAZILEH (2011) idealized pushover curves of RC frame-wall systems to apply displacement-based design approach. The bilinearization was done by drawing a horizontal line at 95% of the maximum strength and then trying to find the elastic branch stiffness by minimizing the difference between the area under the main and the idealized curves. The resulting yield displacement at the intersection was checked with empirical relations as well. As an application of the relation proposed in PRIESTLEY ET AL. (2007), KAZAZ ET AL. (2012) calculated the yield displacement for several RC walls in a parametric study. The studied parameters included: shear-span-to-wall-length ratio, wall length, axial load ratio, normalized shear stress, horizontal web reinforcement and longitudinal reinforcement at the confined boundary of the wall. As a result, they derived empirical formulations for the calculation of the yield deformation components in terms of the influential parameters.

HAGEN (2012) bilinearized the moment-curvature curves of RC walls for performance-based analysis purposes. The idealization was done through considering a secant stiffness to the point where either the reinforcement yields or the concrete cracks (in case of no yield, where the strength is maximum). The second branch was then found using the concept of equal energy absorption by the main and the idealized curves.

Having reviewed all the above sources, it is clear that a lot of work has been devoted to the calculation of the yield displacement for RC walls. However, probabilistic assessment of the available methods still requires further studies. In order to take a step forward in the evaluation process, five of the above-mentioned methods were selected as discussed in Chapter 5.

## 3. Experience-Based Database

As mentioned earlier in Chapter 1, the proposed model selection technique was aimed at the assessment of the numerical and experimental data collected in an *experience-based database*. The idea was to take advantage of the knowledge coming from a variety of numerical and experimental sources to ensure an inclusive assessment of the models at hand. This was a few steps forward from the conventional model validation since the validation was done against a wider range of both numerical and experimental models. Additionally, the uncertainties in experimental data were properly addressed. Further details on the proposed model selection methodology are presented in Chapter 5. Here, the two main components forming the experience-based database, namely, the experimental tests and the numerical simulations, are introduced.

### 3.1. Experimental Tests

The experimental part of the database was created from a total of 48 sources and nearly 300 specimens. There was an attempt to include sources from various authors, years and types (i.e. papers, thesis and reports). Some of the already available databases and statistical studies were searched for references to potential sources (GULEC AND WHITTAKER (2009), TUNA (2012) and BIRELY (2012) among others). Each source was assigned a grade based on its quality in presenting the essential material regarding the experimental study (see Table A.1). The key parameters in the qualification were: the quality of the graphs and the charts and the adequacy of the information about the material properties, the reinforcement layout and the ultimate force and displacement. From the 300 collected specimens, 162 walls were selected for further checks based on the availability of their force-deformation relationships and the possibility to digitize them. The list of the chosen specimens is presented in Appendix A.

The type of walls was determined based on FEMA356 as mentioned previously in Chapter 2. Accordingly, walls with aspect ratios less than 1.5 and greater than 3.0 were defined as squat and slender, respectively. Out of 162 walls, 94 were squat whereas only 2 were slender. A total of 66 fell in the transition category in between the squat and slender walls. Obviously, the final study was limited to squat and transition walls due to lack

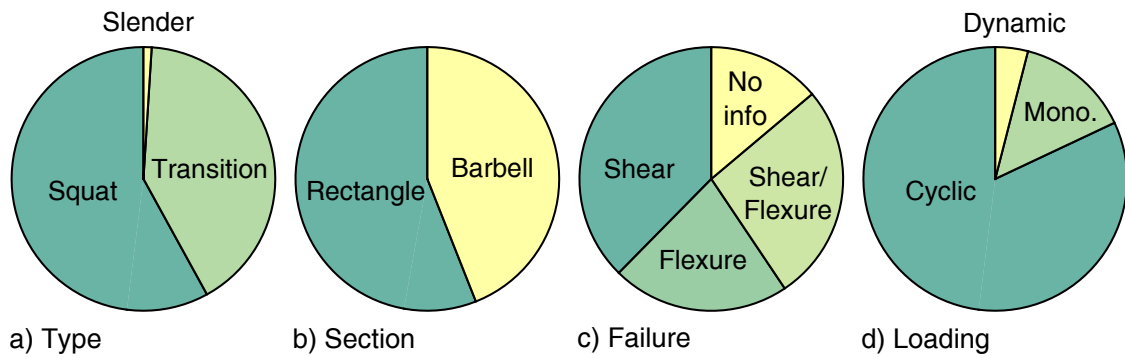


Figure 3.1. Distribution of the database properties.

of statistical data for slender walls. Additional filtration of the data was performed according to the numerical analysis results in the simulation part of the database. 60 wall specimens were stricken out due to problematic numerical analysis which means the experimental database ended up with 51 squat (see Tables A.2 and A.3) and 55 transition (see Tables A.4 and A.5) walls. Some principal properties of the database are shown schematically in Figure 3.1. Detailed information regarding the database can be found in Appendix A.

### 3.1.1. Typical Test Setup

It is common practice to test RC walls as standalone elements (see Figure 3.2 for some examples). As Figure 3.2 shows and although different tests have different characteristics, majority of them seem to follow a generic setup convention. A typical test setup for RC walls attempts to have the wall fixed at one end and loaded axially/laterally at the other end as a simple cantilever.

In the collected experimental data, the end support mostly consisted of a large concrete block which was properly fixed to the underlying ground and, therefore, was supposed to be rigid. The wall connected to the rigid foundation by means of overlapping reinforcement from both the wall and the foundation. The intention was to avoid rocking and sliding modes of failure as they are usually not desired in RC wall testing. In addition, the out of plane behavior was blocked through appropriate side supports. Steel and concrete frames enclosing the wall were very common in this regard.

Most of the walls were loaded in the axial and/or lateral directions only. In the technical literature, quite a few tests have moments applied at the top in order to simulate the pure bending state (e.g. HART ET AL. (2008)). The loads were applied by means of loading cells/jacks at the top of the walls. In most cases (contributing to 82% of the total number of the recorded specimens), the walls were loaded cyclically to capture the potential stiffness



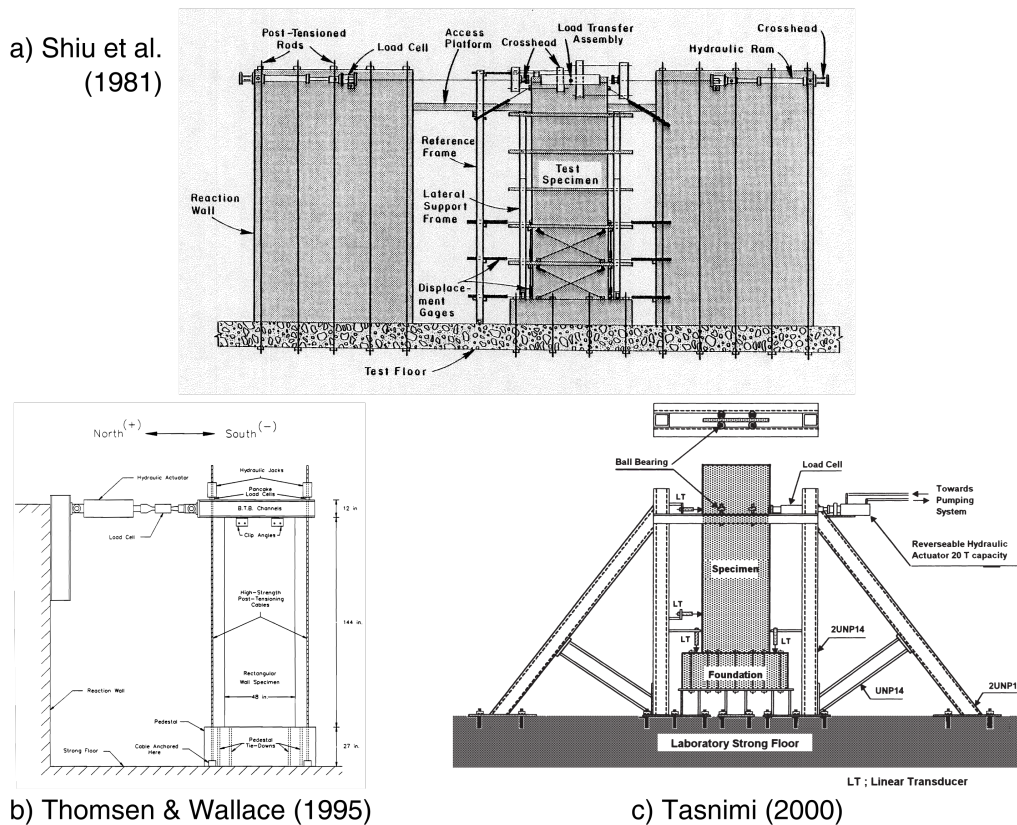


Figure 3.2. Examples of typical test setup.

and strength degradation. Some walls, accounting for 14% and 4% of the total number of the walls, were tested under monotonic and dynamic loads, respectively.

The loads were applied in a displacement-controlled scheme which was normally dependent on the characteristic properties of the walls such as their yield displacement (e.g. DAZIO ET AL. (2009)). Although, this implies different walls would produce non-comparable cyclic responses, the resulting envelope curves remain less affected and, therefore, comparable. Figure 3.3 shows an example of displacement loading history along with the resulting hysteretic force-deformation and the corresponding envelope.

One of the main outputs of the tests was the lateral forces applied at the top (or the corresponding shear at the base) and the corresponding lateral displacement at the top. Other than the global response, sensors were arranged over the wall specimens in order to record the local responses. The typical sensor arrangement follows the pattern shown in Figure 3.4. LVDTs (linear variable differential transformers) and strain gauges were the most commonly utilized sensors. They were primarily intended to provide information regarding the flexure- and shear-induced deformations as well as the internal local stresses and strains in concrete and steel.

### 3. Experience-Based Database

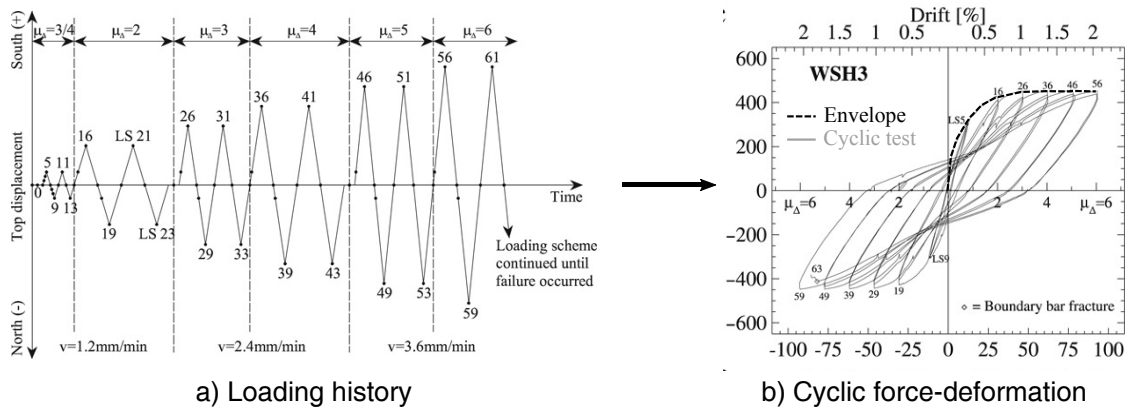


Figure 3.3. Displacement-controlled loading history and the resulting hysteretic behavior (DAZIO ET AL. (2009)).

#### 3.1.2. Typical Wall Specimen

As seen in Figure 3.1b, rectangular and barbell sections had a quite close contribution to the database, i.e. 56% and 44%, respectively. Although, the cross sectional shape only mattered when the boundary elements were properly confined. Generally, three main boundary element configurations of non-confined, weakly-confined and confined could be observed in terms of the reinforcement and regardless of the shape of the wall section. In cases where the confining reinforcement was not particularly supplied at the ends of the sections, no boundary elements were considered. Sections with no boundary elements were mostly rectangular. Figure 3.5 shows the typical cross sections, among the collected specimens, with and without the boundary elements. The confining effect of the transverse reinforcement was as well considered in the numerical part of the database (see for example Equation 3.3) and was similarly limited to the boundary elements.

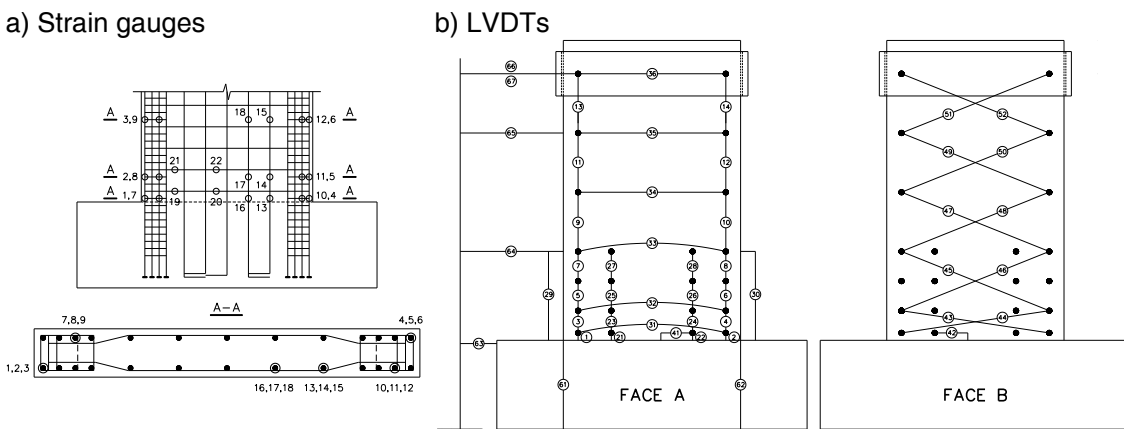


Figure 3.4. Sample instrumentation pattern of a specimen (TRAN AND WALLACE (2012A)).

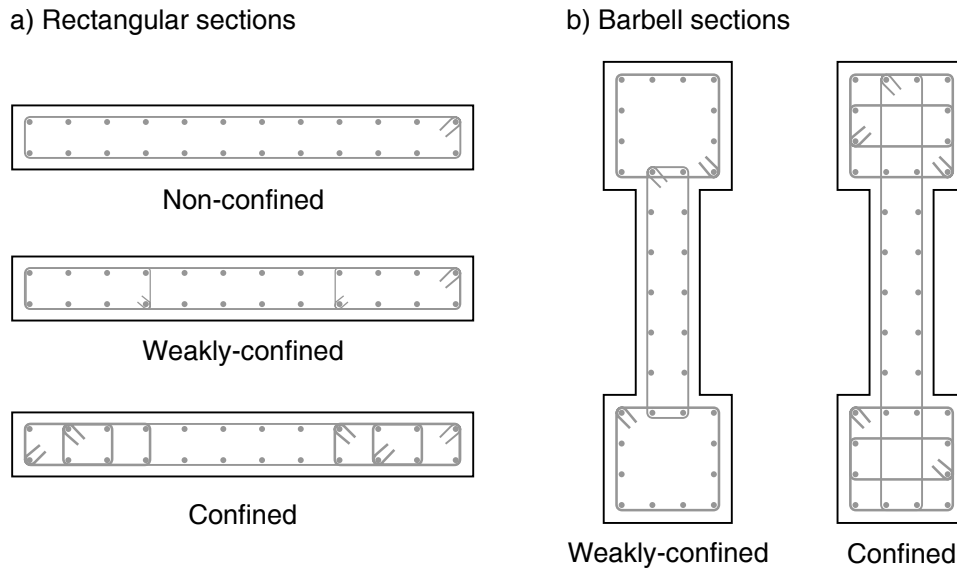


Figure 3.5. Typical cross sections of the collected specimens.

### 3.1.3. Recorded Input Parameters

A very important step in the database development was to determine the parameters to be collected. This should be done considering the purpose of creating the database. There was a need to be able to perform uncertainty analysis on the experimental data along with the numerical simulations in a comparable way. Thus, the variable parameters in the database and the numerical simulation had to be the same. In the ideal situation, the minimum number of parameters providing the most information regarding the walls would be selected. The required information included geometry, material, reinforcement layout and loading properties of the walls. Consequently, ten parameters were selected in which three were used to define the geometry of the wall, two included information regarding the material properties and four specified the reinforcement layout. The last parameter was used to record the axial loading. All the recorded parameters are presented in Table 3.1. The geometrical variables required for the definition of these parameters are shown in Figure 3.6. It should be noted that for most of the parameters a normalized value was preferred in order to make comparisons easier. As seen in Table 3.1, except for concrete compressive strength and steel yield strength, all parameters were normalized based on engineering judgment. Table 3.2 includes the parameter ranges for the final group of the studied wall specimens. The same parameter ranges were used when necessary to generate samples for numerical simulations in the simulation part of the database.

Figure 3.7 depicts the histogram of the studied parameters for the squat and transition walls separately. The values for each parameter were normalized to fit in the  $[0, 1]$  interval for the sake of convenience. As expected, random selection of the wall specimens has

Table 3.1. Parameter definitions for the database records.

Parameter	Definition
$H/L$	Wall aspect ratio
$A_b/A$	Boundary area ratio
$L_b/L$	Boundary length ratio
$\rho_{vw} = A_{svw}/A_w$	Web vertical reinforcement ratio
$\rho_{hw} = A_{shw}/(s_w t_w)$	Web horizontal reinforcement ratio
$\rho_{vb} = A_{svb}/A_b$	Boundary vertical reinforcement ratio
$\rho_{hb} = A_{shb}/(s_b t_b)$	Boundary horizontal reinforcement ratio
$f'_c$	Concrete compressive strength
$f_y$	Reinforcement yield strength
$P/(f'_c A)$	Axial load ratio

$A_b$  Boundary element area and  $A$  total area.

$A_{svw}$  and  $A_{svb}$  Vertical reinforcement area at the web and the boundary, respectively.

$A_{shw}$  and  $A_{shb}$  Horizontal reinforcement area at the web and the boundary, respectively.

$s_w$  and  $s_b$  Horizontal reinforcement spacing at the web and the boundary, respectively.

resulted in complicated distributions of the parameter values along their corresponding ranges. This might be reasonably explained based on Figure 3.8. The figure shows the rough value of each parameter for each specimen. It shows that for the most part of the specimens, the majority of the parameters were kept to the minimum values (blue tones) while a few were raised to the average (green tones) or higher (red tones) values probably with the intention to be studied.

### 3.1.4. Recorded Output Parameters

In addition to the input parameters, several output parameters were chosen to be recorded in the database. The outputs would later be used in the uncertainty analysis of the ex-

Table 3.2. Parameter ranges in the experimental part of the database.

Parameter	Squat	Transition
Wall aspect ratio	[0.5 – 1.5]	[1.8 – 3.0]
Boundary area ratio	[0.15 – 0.55]	[0.11 – 0.59]
Boundary length ratio	[0.09 – 0.40]	[0.15 – 0.43]
Web vertical reinforcement ratio	[0.0024 – 0.0156]	[0.0021 – 0.0150]
Web horizontal reinforcement ratio	[0.0023 – 0.0109]	[0.0025 – 0.0162]
Boundary vertical reinforcement ratio	[0.0085 – 0.0820]	[0.0100 – 0.0925]
Boundary horizontal reinforcement ratio	[0.0031 – 0.0170]	[0.0028 – 0.0382]
Concrete compressive strength, [MPa]	[20.3 – 47.8]	[22.0 – 64.0]
Reinforcement yield strength, [MPa]	[366.9 – 610.0]	[216.0 – 753.0]
Axial load ratio	[0.00 – 0.31]	[0.00 – 0.24]

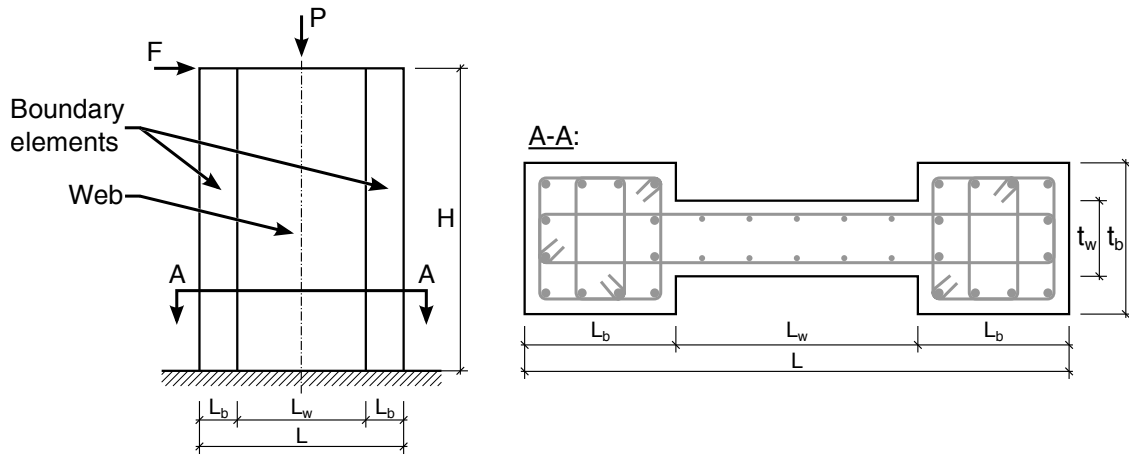


Figure 3.6. Geometrical properties of the wall section.

perimental data and assessment of the desired numerical model. For this purpose, the force-deformation relationships of the specimens were collected in the form of force and deformation vectors. Commonly, the aforementioned relationship was presented as plots in the original sources. The desired information was, therefore, attained by digitizing the plots. Figures A.1 and A.2 depict the recorded force-deformation curves for all the squat and transition wall specimens, respectively. The maximum shear and the corresponding displacement recorded for each specimen were also added to the database.

## 3.2. Numerical Simulations

The simulation part of the database was created using two well-known macro-models designed particularly for RC wall modeling, namely, the *multiple-vertical-line-element-model* (MVLEM) and the *Flexure-shear interaction displacement-based beam-column element* (FSIDB). Selection of only two models was a difficult task since numerous micro and macro models for structural walls have been developed (see Section 2.2.1). The choice was made based on the efficiency of the models in terms of the computational costs as well as the adaptability for extensive parametric simulations. Micro-models, therefore, were excluded in the first step due to their time-consuming nature. Not to mention that the detailed information coming from the micro-models on the local response could barely be useful since the comparable data in the experimental counterpart was very scarce.

The fiber section model could be potentially used. It is able to predict both the local and the global damages with reasonable computational effort. The essential feature of the fiber section model, though, is the ability to capture the interaction between the flexural and axial behaviors. The main drawback, however, is that the fibers merely undergo axial deformations which implies the model fails to go through shear deformations. This

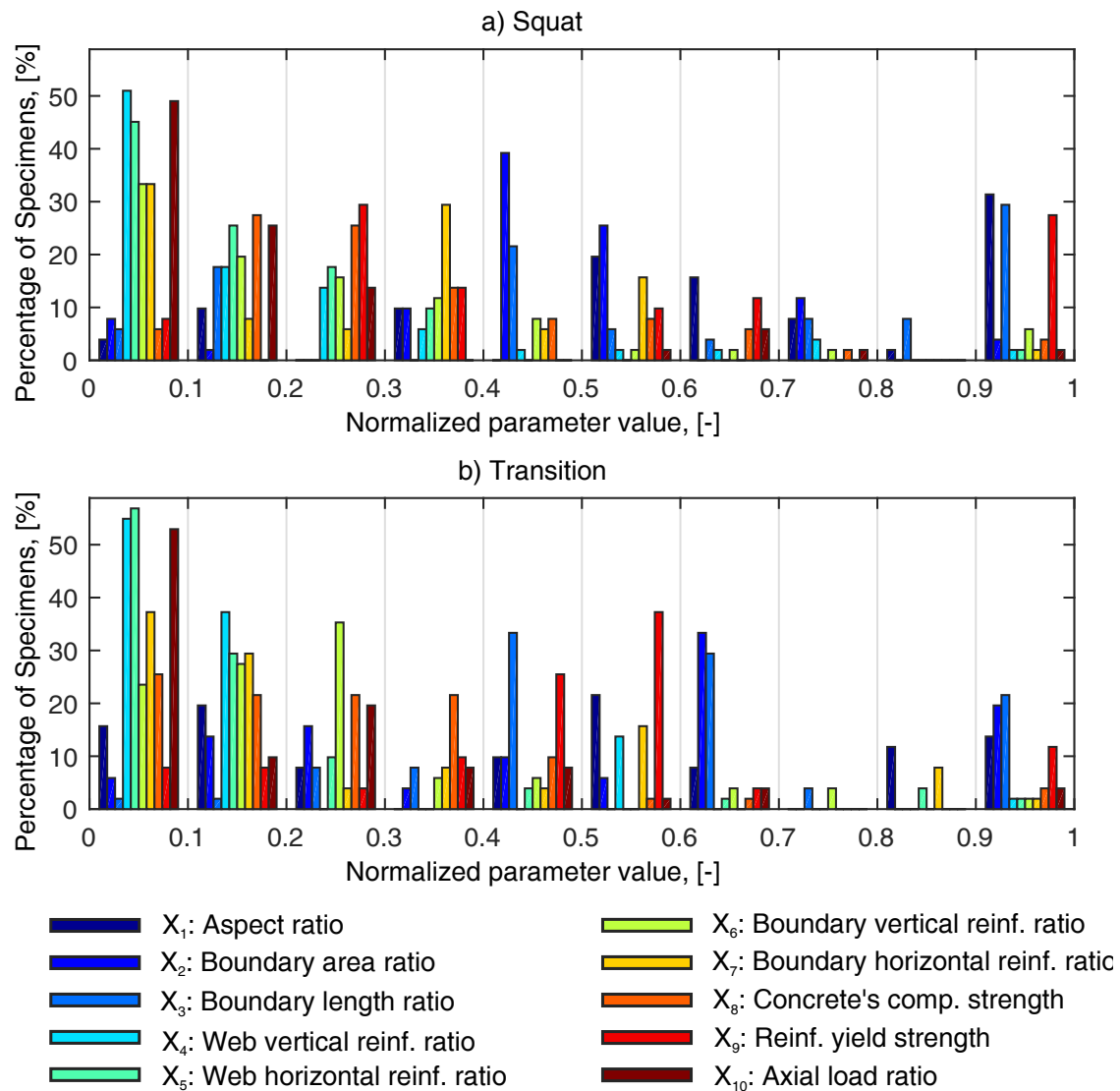
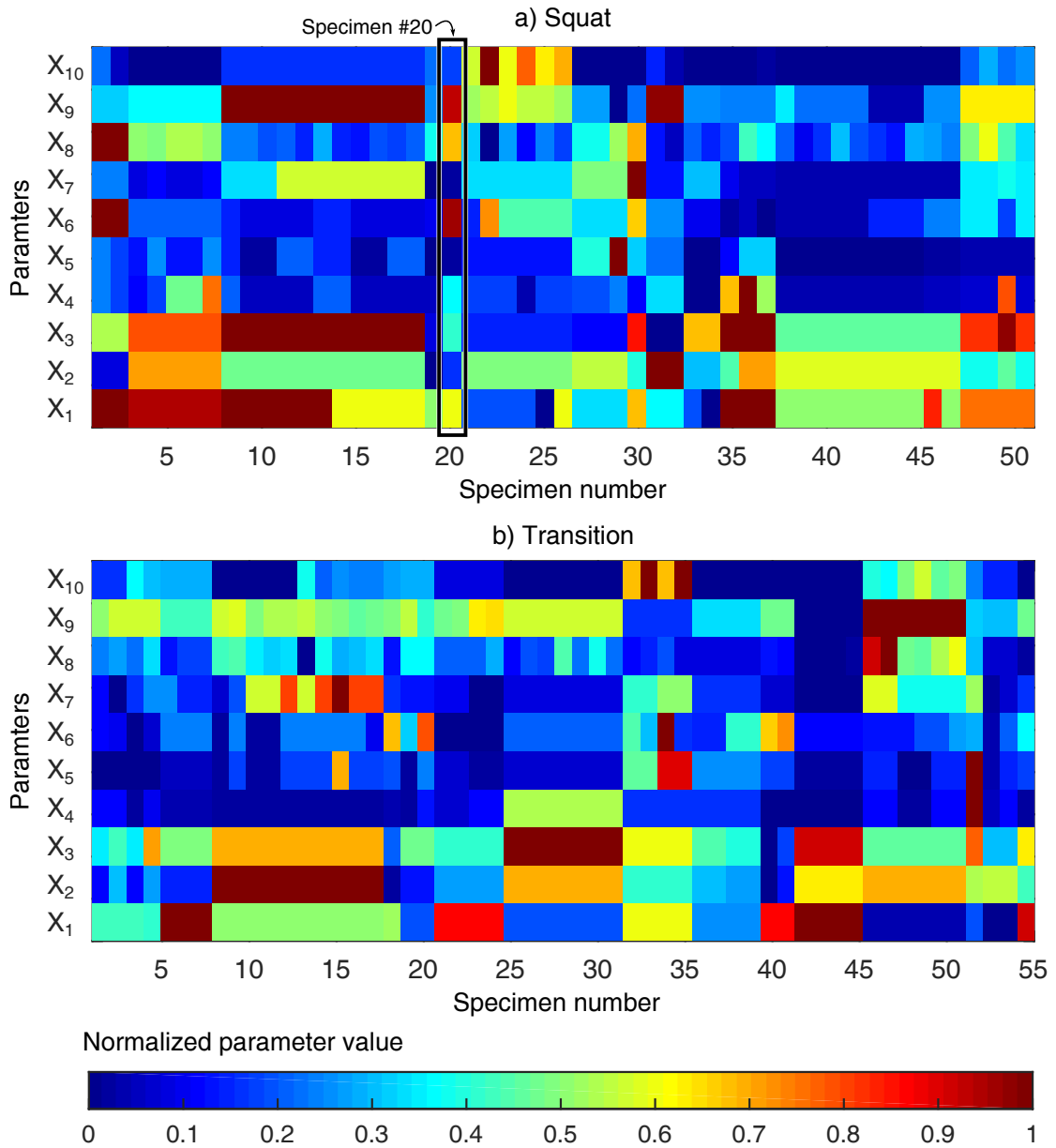


Figure 3.7. Histogram of the parameters recorded in the database.

results in unrealistic predictions of the wall response, specifically, in the case of squat and transition walls. Moreover, some observed phenomena such as neutral axis shift cannot be represented by the fiber section model. In order to overcome the aforementioned shortcomings yet exploiting the fiber section model, several macro-models were proposed based on the fiber section concept. As seen in Table 2.2, MVLEM and FSIDB provide comparable features to the micro-models like finite element models (FEM). In addition they are easy to implement for parametric studies. In this study, therefore, MVLEM and FSIDB were selected to perform the simulations in the numerical part of the database. In the following sections these models are described in detail.

It should be noted that the simulation part of the database included the analysis results not only from the numerical recreations of the specimens in the experimental part but also



Guide to read the plot:

1. Pick a column, e.g. squat wall, specimen #20



Note: Each small block in this column stands for the parameter corresponding to its row

2. Interpret the colors using the colorbar

3. The normalized values of the 10 parameters for the selected specimen are:

$X=[0.60, 0.17, 0.41, 0.37, 0.02, 0.96, 0.02, 0.67, 0.93, 0.18]$

Figure 3.8. Distribution of the parameter values for the studied specimens.

from a group of randomly generated sample walls. In both cases, the modeling parameters were chosen to be the same as those of the experiments (see Table 3.1) varying within the corresponding ranges (see Table 3.2). The results, therefore, could be compared between the two parts of the database. A set of six constant parameters were additionally required to create the models but not necessary to vary separately. The wall length, the web thick-

ness and the vertical and horizontal reinforcement sizes in the web and the boundary belonged to the latter group of the constant parameters. When modeling the experimental specimens, these parameter values were set to be the same as those specifically describing the specimen. Figures A.1 and A.2 show, in the same order, the force-deformation curves of the squat and transition wall specimens recreated using the MVLEM and the FSIDB. In the case of the generated wall samples, the constant parameters were set to the average values of the experimental counterpart parameter ranges. More details on the parameter settings are provided in Chapter 5.

### 3.2.1. Multiple Vertical Line Element Model (MVLEM)

The MVLEM is one of the most notable macro-models developed for RC walls. Its idea practically originates from the fiber section concept. The wall section is divided into a number of fibers which are then modeled as *vertical line* truss elements. They are connected at the top and the bottom by means of rigid beams to ensure the integrity of the system. The global behavior of the wall under axial and bending forces generates from the local axial behavior of the mentioned truss elements. The model, as described so far is unable to simulate the behavior of the wall under shear actions. A shear spring is, therefore, added to the central vertical element to allow for the shear deformations. Obviously, in this way, no interaction between the flexural and shear behaviors is considered (see Figure 3.9 for the decoupling mechanism). The latter seems to be inconsistent with experimental observations according to ORAKCAL ET AL. (2006). Nevertheless, the model has proven to be an efficient tool for the modeling of RC wall elements demanding reasonable computational time and effort while providing promising results (ORAKCAL ET AL. (2004) and JALALI AND DASHTI (2010)).

A characteristic point in the MVLEM is the center of rotation where not only the shear spring is placed but also the relative rotation of the top of the wall with respect to its

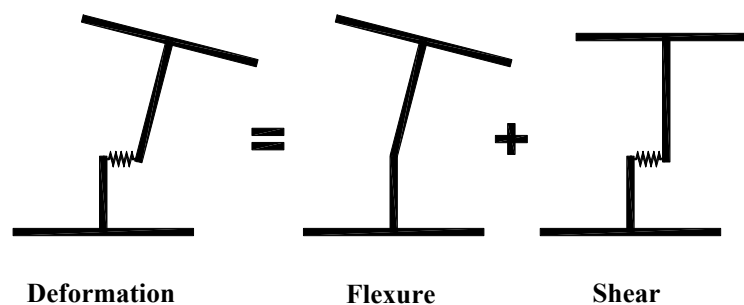


Figure 3.9. Schematic deformation decoupling of a RC wall element in MVLEM (ORAKCAL ET AL. (2006))



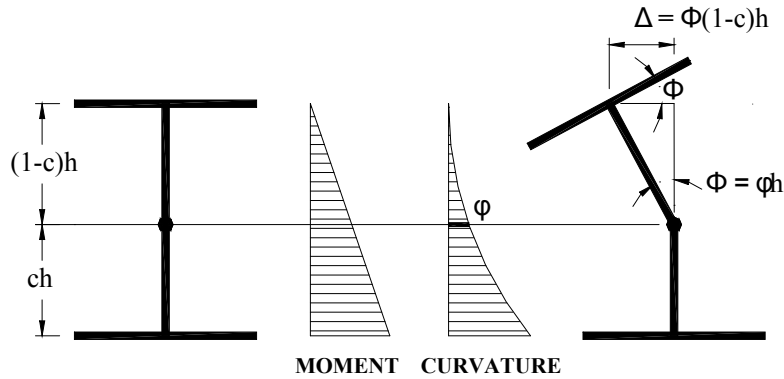


Figure 3.10. Center of rotation in MVLEM (ORAKCAL ET AL. (2006))

base occurs (see Figure 3.10). The ability to simulate the neutral axis shift is also a result of considering the center of rotation. The point is located on the central element at the height of  $ch$  where  $h$  is the height of the segment and  $c$  is empirically found based on the nonlinear distribution of the curvature along  $h$ . Practically,  $c$  is set equal to 0.4 for common applications (VULCANO AND BERTERO (1987) and ORAKCAL ET AL. (2004)). It is recommended to stack more than one MVLEM segments on top of each other along  $H$ , particularly, where significant nonlinear behavior is expected. According to FISCHINGER ET AL. (1992), this is to avoid probable misestimating of the curvature distribution in the regions where it is highly variable. Though, the total number of the divisions along the height (or the length) does not considerably influence the global response of the wall. Notwithstanding, addition of more divisions leads to a more accurate detection of the local response (ORAKCAL ET AL. (2004) and JALALI AND DASHTI (2010)).

#### 3.2.1.1. Materials

For the MVLEM, a minimum of two material models for the concrete and the steel had to be defined. According to the variable parameters, though, there was a need to distinguish the confined concrete from the unconfined one in order to capture the effects of the transverse reinforcement. Therefore, three material models were finally used. The confinement feature was only considered in the boundary elements where large compressional forces might apply.

One of the most practical and well-known material models for concrete was developed by KENT AND PARK (1971) and extended by SCOTT ET AL. (1982) (see Figure 3.11). The modified Kent-Park model, as shown in Figure 3.11, is comprised of three portions in the compression side. The stress-strain relationship in each portion is described by Equation 3.1 for compression and Equation 3.2 for tension.

In compression:

$$\begin{aligned}
 \text{OA: } \epsilon_c \leq \epsilon_0 \quad \sigma_c &= Kf'_c \left[ 2 \left( \frac{\epsilon_c}{\epsilon_0} \right) - \left( \frac{\epsilon_c}{\epsilon_0} \right)^2 \right] \\
 \text{AB: } \epsilon_0 < \epsilon_c \leq \epsilon_{20} \quad \sigma_c &= Kf'_c [1 - Z(\epsilon_c - \epsilon_0)] \\
 \text{BC: } \epsilon_c > \epsilon_{20} \quad \sigma_c &= 0.2Kf'_c
 \end{aligned} \tag{3.1}$$

where:

$$\begin{aligned}
 \epsilon_0 &= 0.002K \\
 K &= 1 + \frac{\rho_s f_{yh}}{f'_c} \\
 Z &= \frac{0.5}{\frac{3+0.29f'_c}{145f'_c-1000} + 0.75\rho_s \sqrt{\frac{h'}{s_h}} - 0.002K}
 \end{aligned}$$

In tension:

$$\begin{aligned}
 \text{OA': } \epsilon_c \leq \epsilon_n \quad \sigma_c &= E_t \epsilon_c \\
 \text{A'B': } \epsilon_n < \epsilon_c \leq \epsilon_u \quad \sigma_c &= \sigma_n + E_t \epsilon_c \\
 \text{B'C': } \epsilon_c > \epsilon_u \quad \sigma_c &= 0
 \end{aligned}$$

where:

$$\begin{aligned}
 f'_t &= 0.6228 \sqrt{f'_c} \\
 \epsilon_n &= \frac{f'_t}{E_c} \\
 \sigma_n &= f'_t \left( 1 + \frac{E_{ts}}{E_c} \right) - E_{ts} \epsilon_n \\
 \epsilon_u &= f'_t \left( \frac{1}{E_{ts}} + \frac{1}{E_c} \right)
 \end{aligned} \tag{3.2}$$

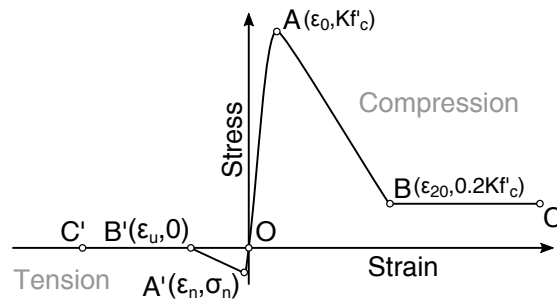


Figure 3.11. Concrete's stress-strain relationship (based on KENT AND PARK (1971))

Here,  $\epsilon_0$  and  $\epsilon_{20}$  are, in the same order, the concrete strains at the maximum and the residual stresses.  $K$  stands for the overstrength due to confinement which is calculated in terms of the  $f'_c$ , the concrete's compressive strength (in MPa),  $f_{yh}$ , horizontal reinforcement's yield strength (in MPa) and the horizontal reinforcement ratio. For the unconfined concrete,  $K$  is set equal to 1.  $Z$  is the strain softening slope with  $h'$  being the width of the concrete core and  $s_h$  designating the horizontal reinforcement spacing.

The modified Kent-Park model has been implemented in OpenSees (McKENNA ET AL. (2000)) as *concrete02* uniaxial material. In the present study, *concrete02* was used to define both the unconfined and the confined concrete behaviors. Although, the current model could capture the confinement effects, the more rigorous method from RAZVI (1995) was used to compute the properties of the confined concrete. Accordingly, the stress-strain relationship of an unconfined concrete could be modified to achieve the confined properties by considering the confinement capacity of the transverse reinforcement. It is needless to say that the boundary horizontal reinforcement ratio (as defined in Table 3.1) was the parameter to control the confinement effects. The aforementioned modification could be accordingly done through Equation 3.3.

$$f'_{cc} = f'_{c0} + k_1 f_{le}$$

where:

$$\begin{aligned} f_{le} &= \frac{f_{lex}b_{cx} + f_{ley}b_{cy}}{b_{cx} + b_{cy}} \\ k_1 &= 6.7 (f_{le})^{-0.17} \\ f_{lex(y)} &= k_{2x(y)} f_{lx(y)} \\ k_{2x(y)} &= \sqrt{\left(\frac{b_{cx(y)}}{s_{x(y)}}\right) \left(\frac{b_{cx(y)}}{s_{lx(y)}}\right) \left(\frac{1}{f_{lx(y)}}\right)} \leq 1.0 \end{aligned} \quad (3.3)$$

Here,  $f'_{c0}$  and  $f'_{cc}$  stand for the concretes strength in the unconfined and confined states, respectively. For the rectangular sections, the equivalent uniform confinement pressure,  $f_{le}$ , is calculated in terms of the equivalent uniform confinement pressures along both axis of the section, i.e.  $f_{lex}$  and  $f_{ley}$ . In the corresponding computations,  $s_{x(y)}$ ,  $s_{lx(y)}$  designate the spacing between the laterally supported longitudinal reinforcement and the lateral ties in  $x(y)$  direction, respectively. Finally,  $b_{cx(y)}$  measures the center to center of the peripheral transverse reinforcement along the  $x(y)$  direction.

For the reinforcing steel, it is very common to use the material model implemented by MENEGOTTO AND PINTO (1973) due to its efficiency and accuracy (FILIPPOU ET AL. (1983)). The model as shown in Figure 3.12, follows the stress-strain relationship defined in Equation 3.4.

$$\sigma^* = b\epsilon^* + \frac{(1-b)\epsilon^*}{(1+\epsilon^{*R})^{\frac{1}{R}}}$$

where:

$$\begin{aligned} \epsilon^* &= \frac{\epsilon - \epsilon_r}{\epsilon_0 - \epsilon_r} \\ \sigma^* &= \frac{\sigma - \sigma_r}{\sigma_0 - \sigma_r} \end{aligned} \tag{3.4}$$

$(\epsilon_0, \sigma_0)$  and  $(\epsilon_r, \sigma_r)$  are, in the same order, the strain and stress coordinates of the points A and B in Figure 3.12.  $b$  is the strain-hardening ratio defined as  $E_1/E_0$  which was set to the practical value of 0.02.  $R$  controls the curvature of the transition area and physically represents the Bauschinger effect. In the case of monotonic loading  $R$  equals to an initial value  $R_0$  which was chosen to be 18.5 according to the literature (MENEGOTTO AND PINTO (1973)).

Last but not least, there was a need to determine the sectional force-deformation relationship under shear actions to be assigned to the shear springs. A handful of choices are available for RC walls (e.g. KABEYASAWA ET AL. (1983), FISCHINGER ET AL. (1990), ORAKCAL ET AL. (2006), XIAOLEI ET AL. (2008) and JALALI AND DASHTI (2010)). Here, the major concern was to represent the low capability of hysteretic energy absorption in shear. This is, mostly, done by means of origin-oriented or pinching hysteretic materials. In this study, the *Hysteretic* material model with trilinear backbone curve as seen in Figure 3.13 was used.

The characteristic points A, B and C on the hysteretic force-deformation curve in Figure 3.13 stand, in the same order, for the cracking, yield and ultimate states of the wall behavior in shear. The coordinates of the points and their negative counterparts were calculated according to KABEYASAWA ET AL. (1983) and PARK AND HOFMAYER (1994). The corresponding formula are presented in Equation 3.5 (Note: the units are in *kgf* and *cm* for the force and length, respectively).

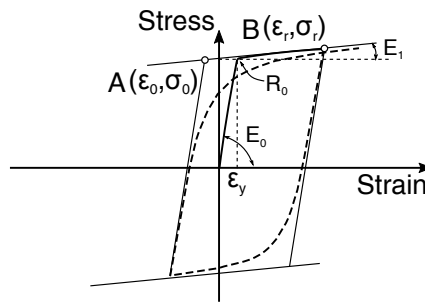


Figure 3.12. Steel's stress-strain relationship (based on MENEGOTTO AND PINTO (1973))

Elastic stiffness:

$$K_0 = \frac{GA}{\kappa h}$$

$$\kappa = \frac{3(1+u)[1-u^2(1-\nu)]}{4[1-u^3(1-\nu)]}$$

$$L_1 = L = L_3 + 2L_b$$

$$L_2 = (1+u)\frac{L_1}{2}$$

$$L_3 = uL_1$$

$$\nu = \frac{t_w}{b_e}$$

$$b_e = \frac{2t_b L_b + L_3 t_w}{L_1}$$

Cracking point (A):

$$F_{cr} = 1.4 \sqrt{f'_c} A$$

Post-cracking stiffness:

$$\beta = \frac{K_1}{K_0} = 0.14 + \frac{0.46 \rho_{hw} f_y}{f'_c}$$

Yield point (B):

$$F_y = b_e j \left[ \frac{0.0679 \rho_t^{0.23} (f'_c + 180)}{\sqrt{M/(VL)} + 0.12} + 2.7 \sqrt{f_y \rho_{hw} + 0.1 \sigma_0} \right]$$

$$j = \frac{7}{8} (L_1 - L_b/2)$$

$$\rho_t = \frac{100 A_{st}}{b_e (L_1 - L_b/2)}$$

Post-yield stiffness:

$$K_2 = 0.001 K_0$$

(3.5)

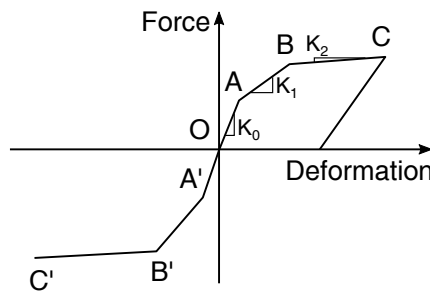


Figure 3.13. Hysteretic model for force-deformation relationship in shear.

In this equation  $G$  is the shear modulus of concrete,  $h$  is the height of the wall segment,  $F_{cr}$  and  $F_y$  are in the same order the shear forces at the cracking and the yield states,  $M/(VL)$  is the shear-span ratio with  $M$  being the moment at the top and  $V$  being the base shear,  $\sigma_0$  is the average axial stress over the wall section, and  $\rho_t$  is the effective tensile reinforcement ratio in which  $A_{st}$  designates the area of the longitudinal reinforcement in the tension side of the boundary element. All the geometrical variables were previously defined (see Figure 3.6).

It is worth to mention that an elastic compression-only material was assigned to the axial spring on the central column. The properties of the unconfined concrete were used to define the modulus of elasticity for this material.

#### 3.2.1.2. Elements

As seen in Figure 3.14, the numerical model built in OpenSees consisted of truss and beam elements together with vertical and horizontal springs. The beam elements were defined as *elasticBeamColumns* with large flexural stiffness. The trusses were modeled by means of *truss* elements to which fiber sections were assigned. The sectional dimensions of the vertical elements were determined based on the corresponding tributary area. The material properties of the concrete and steel fibers were set to be as described in the materials section. *zeroLength* elements in the vertical and the horizontal translational degrees of freedom represented the axial and shear springs on the central column. The number of segments per wall model was decided according to the aspect ratios. The squat walls were divided into a minimum of two segments. For the transition walls, this number was increased to four. The axial and shear springs were placed at 0.4 of each segment's height.

#### 3.2.1.3. Constraints and Restraints

Obviously, the walls were fixed at the base which implies the truss elements were pinned whereas the central rigid columns were constrained in all the degrees of freedom. At each segment level, all the nodes lying on the same elevation were rigidly connected through the *rigidLink*. It restrained the axial and bending degrees of freedom. In addition, the central rigid column was fixed at the joint to the beam in each segment, creating a rigid cross as the main skeleton of the wall. The crosses joined all the elements to build an integrated system. Axial and shear springs linked the vertical and horizontal translational degrees of freedom on the two disconnected parts of the central column. The rotational degree of freedom at this point was not restrained to allow for the interaction of the truss elements with the rigid beam at each section.

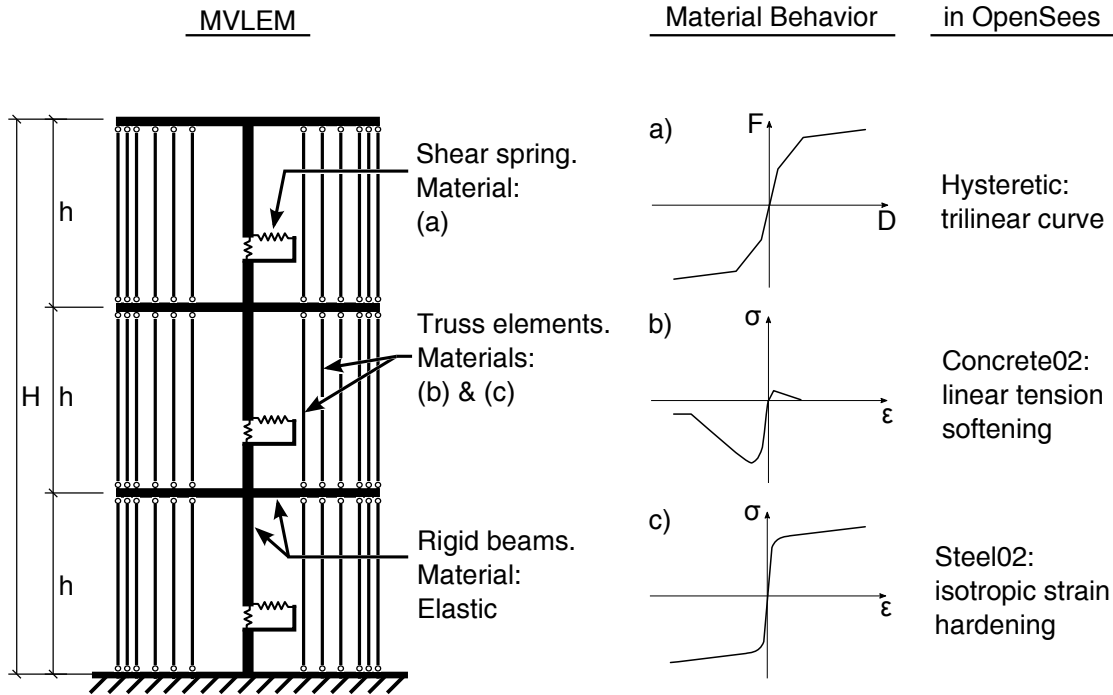


Figure 3.14. MVLEM as built in OpenSees.

#### 3.2.1.4. Analysis

The walls were, first, axially loaded according to the axial load ratio parameter. Later, concentrated lateral loads were imposed at the top of each cantilever wall. The loading was applied in a displacement-controlled manner in which the displacement of the top middle node was monitored. An adaptable analysis procedure was used to perform the analysis in order to overcome the numerical issues on convergence and instability. In case of such numerical problems, the adaptable procedure modified the loading steps and/or the solution algorithm if necessary. The walls, for which the undertaken steps could not succeed in solving the aforementioned issues, were not considered for further studies. In case of a successful, analysis, the final force-deformation relationship corresponding to the base shear versus the top displacement was recorded as the output.

### 3.2.2. Flexure-Shear Interaction Displacement-Based Beam-Column Element (FSIDB)

The FSIDB was developed on the same basis as the MVLEM (ORAKCAL ET AL. (2006)). The interaction between the flexural and shear behaviors, though, was additionally considered in FSIDB. The model was implemented in OpenSees by upgrading the original fiber element with an additional strain component to represent the behavior under shear

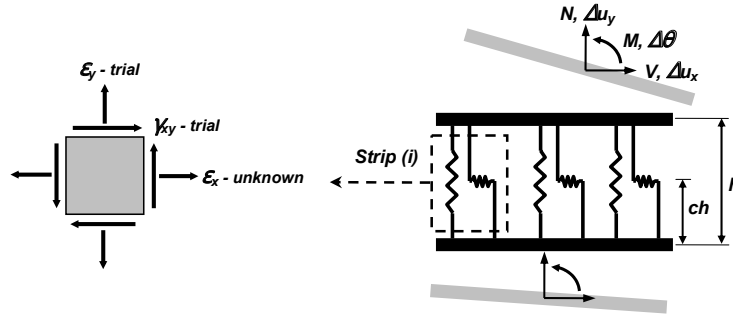


Figure 3.15. Biaxial response for fibers in FSIDB (ORAKCAL ET AL. (2006)).

actions. Therefore, a biaxial response based on the uniaxial material models for concrete and steel was provided. The concept is schematically shown in Figure 3.15. The model was formulated only in 2D and has, so far, been verified only under static monotonic loading. As in the case of MVLEM, the center of rotation is defined in order to determine the contributions of the flexural and shear components to the total displacement.

### 3.2.2.1. Materials

All the material properties were defined in the same way as for the MVLEM. Only, the concrete material for the FSIDB was modified to address the behavior in membrane elements. The *concrete06* uniaxial material in OpenSees captures the required considerations. The corresponding material model is based on Equation 3.6 from Popovics (1973) and BELARBI AND HSU (1994) (see Figure 3.16).

In compression:

$$\sigma = f'_c \frac{n \left( \frac{\epsilon}{\epsilon_0} \right)}{n - 1 + \left( \frac{\epsilon}{\epsilon_0} \right)^{nk}} \quad (3.6)$$

In tension:

$$\begin{aligned} \epsilon \leq \epsilon_{cr} & \quad \sigma = \left( \frac{f_{cr}}{\epsilon_{cr}} \right) \epsilon \\ \epsilon > \epsilon_{cr} & \quad \sigma = f_{cr} \left( \frac{\epsilon_{cr}}{\epsilon} \right)^b \end{aligned}$$

In this equation  $n$ ,  $k$  and  $b$  are the compressive shape factor, post-peak shape factor and the exponent of the tension softening curve, respectively. According to the literature the values of 2.0, 1.0 and 4.0 were in the same order selected for these parameters.  $\epsilon_0$  and  $\epsilon_{cr}$  designate the strains at the peak compressive strength and at the tensile strength ( $f_{cr}$ ), respectively (see Figure 3.16).



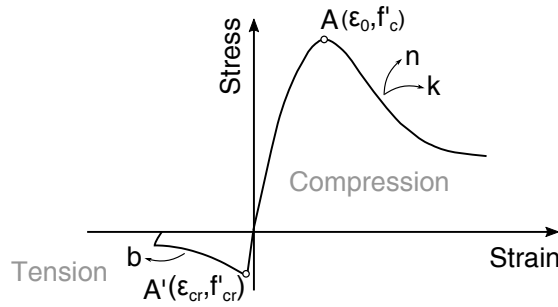


Figure 3.16. Stress-strain relationship for *concrete06* (based on MAZZONI ET AL. (2006)).

### 3.2.2.2. Elements

The FSIDB is built upon the original displacement-based beam-column element, i.e. the *dispBeamColumn* in OpenSees. The element is known as the *dispBeamColumnInt* and requires specific definitions of the cross section and geometric transformation properties. The fiber section assigned to the aforementioned element, i.e. the *FiberInt*, was constructed with strips as the unit membrane elements. Using this command the horizontal and vertical fibers could be defined separately for each sectional strip to form the panel element. The amount of the horizontal reinforcement in each strip in the boundary (or the web) was found based on the boundary (or the web) horizontal reinforcement ratio as defined in Table 3.1.

The implemented FSIDB has the possibility to model the wall section including the boundary elements. However, since the major shear resistance in the squat and transition walls is provided by the web, FSIDB was only used to represent the web as seen in Figure 3.17. The boundary elements were modeled in the same manner as the counterparts in the MVLEM (see Figure 3.17). Given that the FSIDB was developed based on the MVLEM, the same assumptions in terms of the segmentation along the height and the length were applied to the corresponding FSIDB models.

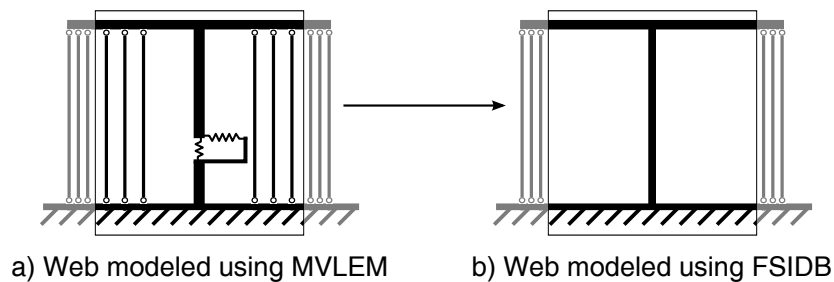


Figure 3.17. Schematic of the wall models created with FSIDB as compared to the MVLEM.

#### 3.2.2.3. Constraints

The central FSIDB was connected to the boundary elements modeled as trusses through rigid beams in order to create an integrated system. The wall base was fixed as in the case of the MVLEM. At each segment level, the nodes at equal elevations were restrained in the axial and bending degrees of freedom by means of the *rigidLink*.

#### 3.2.2.4. Analysis

The analysis procedure followed the exact same routine as that of the MVLEM in order to produce comparable results.

## 4. Variance-Based Sensitivity Analysis

Global sensitivity analysis is a versatile tool for model evaluation. It attempts to discover the relation between the uncertainty in the input and the output in a general context. The variance-based sensitivity analysis, in particular, is able to determine not only the parameters' importance, but also the significance of the interactions among them. The prominent parameters can be found by means of the first order sensitivity indices. The corresponding interactions, however, are only revealed through the computation of the total order indices. The present study is concentrated on the first order effects and thus the total order effects are not further discussed.

### 4.1. First Order Effects

The very basic idea of the variance-based sensitivity analysis is to examine how the variance of the output reacts to the variance of the input parameters. An idea is to scan the changes in the output uncertainty as a response to fixing a parameter, the importance of which is under question, to a predefined value. Since the parameter is actually made constant, a source of uncertainty is effectively removed from the parameter space. Here three possible outcomes can be expected depending on the significance of the reduction that is observed in the output uncertainty. Considerable reduction points to an influential parameter whereas negligible reduction means an unimportant parameter. A moderate change in the output uncertainty implies the parameter is not crucially important, yet, it cannot be ignored either. The above mentioned procedure should be repeated for all the possible values of the parameter under study in order to reach a final understanding of its importance with respect to the output uncertainty.

In order to mathematically execute the procedure, assume a model  $Y = f(X_1, \dots, X_K)$  which maps the input space  $\mathbf{X}$  to the output space  $\mathbf{Y}$ . The model has  $K$  parameters which directly reveal the dimensionality of the parameter space or in other words the model size.  $N$  samples are considered to study the model. To begin with, take a look at the mathematical basis for the variance-based sensitivity analysis which is the well-known variance decomposition formulation given in Equation 4.1 from SOBOL (1993).

Table 4.1. Description of the terms in Equation 4.1.

$Y X_k$	Output calculated when $X_k$ is fixed on a selected value
Variance term	
$E_{X_{-k}}(Y X_k)$	Average of the conditioned output over all parameters but $X_k$
$V_{X_k}(E_{X_{-k}}(Y X_k))$	Variance of the computed means over the $X_k$
Mean term	
$V_{X_{-k}}(Y X_k)$	Variance of the conditioned output over all parameters but $X_k$
$E_{X_k}(V_{X_{-k}}(Y X_k))$	Average of the computed variances over the $X_k$

$$V(Y) = V_{X_k}(E_{X_{-k}}(Y|X_k)) + E_{X_k}(V_{X_{-k}}(Y|X_k)) \quad \text{where: } k = 1, \dots, K \quad (4.1)$$

The corresponding terms are separately described in Table 4.1. In Equation 4.1, the term  $V_{X_k}(E_{X_{-k}}(Y|X_k))$  is known as the first order effect of  $X_k$  on  $Y$ . The significance of the  $k$ th parameter can, then, be expressed in terms of the first order sensitivity index,  $S_k$ , following Equation 4.2 (SOBOL (1993)).

$$S_k = \frac{V_{X_k}(E_{X_{-k}}(Y|X_k))}{V(Y)} \quad \text{where: } k = 1, \dots, K \quad (4.2)$$

Theoretically, for additive models, the sum of the  $S_k$  should equal to 1 which can be regarded as a quality criterion for the sensitivity analysis. Close values of the  $\sum_{k=1}^K S_k$  to 1 indicate a successful sensitivity analysis (SALTELLI ET AL. (1999)).

#### 4.1.1. Implementation by SALTELLI ET AL. (2008)

The widely used formula for the calculation of the  $S_k$  was developed by SALTELLI ET AL. (2008) in the form of Equation 4.3.

$$S_k = \frac{(1/N) \sum_{j=1}^N Y_A^j Y_{C_k}^j - f_0^2}{(1/N) \sum_{j=1}^N (Y_A^j)^2 - f_0^2} \quad \text{where: } f_0^2 = \left( (1/N) \sum_{j=1}^N Y_A^j \right)^2 \quad \text{and } k = 1, \dots, K \quad (4.3)$$

Here,  $Y_A$  and  $Y_{C_k}$  refer to the outputs computed using the sample matrices  $A$  and  $C_k$ , respectively (see Figure 4.1 for the corresponding definitions). According to Equation 4.3,

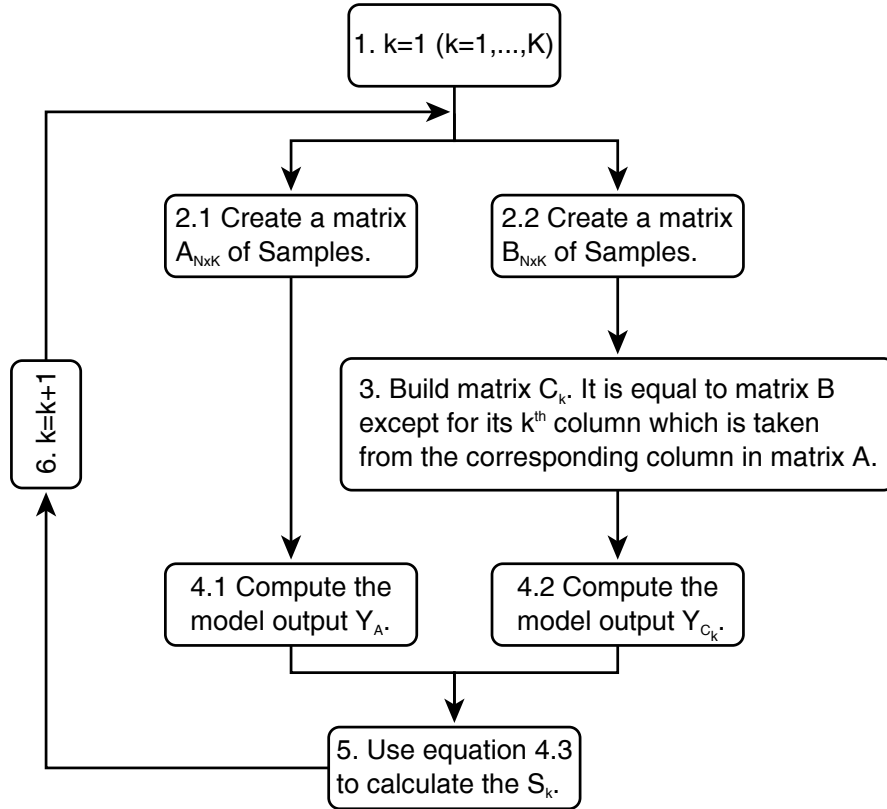
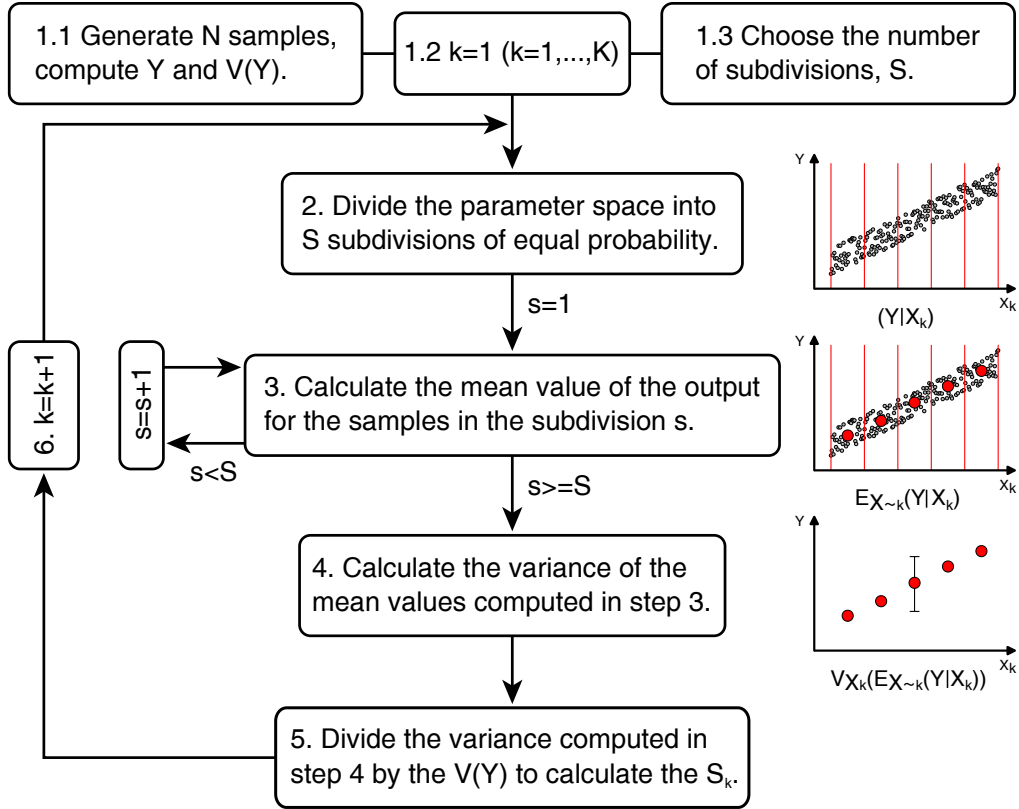


Figure 4.1. Flowchart for the calculation of the  $S_k$  based on SALTELLI ET AL. (2008).

the first order sensitivity indices can be determined through the steps shown in Figure 4.1. In the generated matrices  $A$  and  $B$ , element  $ij$  always denotes the value of parameter  $j$  from sample  $i$ . The intention in building matrix  $C_k$  from matrix  $B$  is to have two sets of samples, namely,  $A$  and  $C_k$  which differ in the values for all parameters but  $X_k$ . This resembles the parameter fixing at specific values, as discussed earlier.

Throughout the whole procedure, matrix  $A$  stays unchanged which means  $Y_A$  is calculated only once, accounting for  $N$  model runs. In addition and during each run of the flowchart, the output must be calculated for matrix  $C_k$  i.e.  $N$  extra model runs per parameter. The total model runs, then, sums up to  $N \times (K + 1)$  which can be quite large in case of huge models with numerous parameters or studies on extensive number of samples. Moreover, the technique requires model runs on predefined sample sets which limits its application to the problems with readily available objective functions. As a result, the method cannot be used on experimental data and existing sample sets (e.g. generated for reliability analysis) with no access to the objective function. Last but not least, the technique is unable to address the problems in which the parameters are correlated (KEITEL AND DIMMIG-OSBURG (2010)). This is, apparently, a result of exchanging the columns of the sampling matrices during which the correlations between the parameters are lost (MOST (2012)).


 Figure 4.2. Flowchart for the calculation of the  $S_k$  based on the proposed implementation.

#### 4.1.2. Conceptual Implementation

Deficiencies of the aforementioned implementation drew the attention to the basic concept which could be easily understood and developed. The technique conceptually originates from SOBOL (1993) and SALTELLI ET AL. (2008). The corresponding implementation uses the basic concept directly as shown in Figure 4.2 and in Equation 4.4.

$$S_k = \frac{V_s(E_{X_k}(Y|X_k^s))}{V(Y)} \quad \text{where: } k = 1, \dots, K \quad \text{and} \quad s = 1, \dots, S \quad (4.4)$$

Here,  $X_k^s$  represents part of the parameter space corresponding to  $X_k$  which we tend to call the subdivision  $s$  and has an equal probability of occurrence as all the other  $S - 1$  subdivisions of the mentioned space. The subdivisions can be interpreted as the substitute for the parameter fixing at specific values which is quite inefficient. They allow the parameter to change within a predefined range rather than to set it to a constant value. At adequately large number of subdivisions, the fixing concept can be essentially fulfilled. Although, in order to achieve a reliable estimation of the first order effects, the samples per subdivision should be sufficient to provide the statistical basis for the prediction of the mean value.

Obviously, the proposed implementation overtakes the existing one from SALTELLI ET AL. (2008) in terms of efficiency since it merely demands  $N$  model runs. In addition, the described approach, basically, reduces the remaining uncertainty of the estimated variance of the conditional means. In other words and when compared to the variance, the mean is considerably less influenced by the number of samples involved. Therefore, properly sized subdivisions are more likely to provide accurate estimates of the mean values and not necessarily the variances. Saltelli's implementation has the potential to converge slowly or even fail in case of highly scattered input parameters.

#### 4.1.3. Extended Fourier Amplitude Sensitivity Test (EFAST)

The Fourier amplitude sensitivity test was proposed by CUKIER ET AL. (1973) on the basis of the variance decomposition concept. The Fourier decomposition is done along a search curve over the parameter space in the form of Equation 4.5 where  $-\infty < t < \infty$  and  $\omega_k$ s are the frequencies corresponding to the different parameters.

$$X_k(t) = G_k(\sin(\omega_k t)) \quad (4.5)$$

$G_k$ s are the transformation functions with several suggestions from different researchers. They differ in terms of the efficiency and the coverage offered over the sample space. Here, the well-known function from SALTELLI ET AL. (1999) was used as presented in Equation 4.6.

$$X_k(t) = \frac{1}{2} + \frac{1}{\pi} \arcsin(\sin(\omega_k t + \varphi_k)) \quad (4.6)$$

Clearly, the proposed function has a phase shift of  $\varphi_k$  which is chosen randomly from a uniform distribution in the  $[0, 2\pi)$  interval. The move along the search curve occurs with the change of  $t$  upon which the  $X_k$ s vibrate with the  $w_k$  frequencies. Obviously, the mentioned vibrations result in an oscillatory output  $Y$ . The amplitude of the oscillations in  $Y$  in the frequency  $w_k$  indicates the influence of the parameter  $k$  on the output  $Y$ . Larger amplitudes imply more influential factors. The set of the frequencies must fulfill the condition as stated in Equation 4.7 to ensure a space-filling search curve.

$$\sum_{k=1}^K r_k \omega_k \neq 0 \quad -\infty < r_k < \infty \quad (4.7)$$

Given that the  $w_k$ s are positive integers, the Fourier transformation of  $Y$  can be written following Equation 4.8 according to SALTELLI ET AL. (1999).

$$Y = f(t) = \sum_{j=-\infty}^{+\infty} A_j \cos(jt) + B_j \sin(jt)$$

where:

$$A_j = \frac{1}{2\pi} \int_{-\pi}^{\pi} f(t) \cos(jt) dt$$

$$B_j = \frac{1}{2\pi} \int_{-\pi}^{\pi} f(t) \sin(jt) dt$$
(4.8)

Finally, the first order effect of the input  $X_k$  on the output  $Y$  can be computed by means of the Equation 4.9 in which  $\Lambda_j = A_j^2 + B_j^2$  and  $p\omega_k$  are the higher harmonics of  $\omega_k$ .

$$S_k = \frac{\hat{D}_k}{\hat{D}} = \frac{2 \sum_{p=1}^{+\infty} \Lambda_{p\omega_k}}{2 \sum_{j=1}^{+\infty} \Lambda_j}$$
(4.9)

The total cost of the analysis, here, equals to  $N_S \times K \times N_R$ . The number of samples per search curve is defined as  $N_S = N_R(2M\omega_{max} + 1)$  where  $N_R$  is the number of resampling,  $M$  is the interference factor (usually  $\geq 4$ ) and  $\omega_{max}$  is the largest frequency among the  $\omega_k$ s. The resampling scheme was introduced to the FAST by SALTELLI ET AL. (1999) to increase the efficiency of the procedure. They recommended a minimum value of 65 for the  $N_S$ .

In order to shed some light on the performance of the three discussed implementations, they were applied to a series of analytical and numerical benchmark problems. The intention was to investigate the capabilities of the three approaches in producing accurate results with affordable computational costs.

## 4.2. Analytical Benchmark Problems

It should be noted that several improved sophisticated methods of variance-based sensitivity analysis have already been developed. Therefore, a legitimate performance comparison of the above-mentioned implementations must include the enhanced cutting-edge techniques. Very good examples of such methods are the widely used Fourier amplitude sensitivity test (FAST) and its extension the EFAST (extended Fourier amplitude sensitivity test). They use multiple Fourier series expansion of the output to compute the conditional variances. Although, FAST and EFAST are rather complicated to implement with several parameters to be adjusted. Nevertheless, EFAST was selected to be part of the



performance comparison together with the two implementations of the Sobol's method.

Three well-known mathematical functions, namely, the g-function (SOBOL (1993)), the polynomial model (SUDRET (2008) and SOBOL (1993)) and the Ishigami function (ISHIGAMI AND HOMMA (1990)), were chosen to test the implementations. It is quite common to use the aforementioned functions as the benchmark for sensitivity analysis problems since they come with analytical solutions for the first and total order effects (see SUDRET (2008) for example). As a result, the performance of the questioned implementations can be easily judged in terms of the effort required to produce the least error with respect to the analytical solutions. SALTELLI ET AL. (2010) formulated the error as seen in Equation 4.10.

$$MAE = \frac{1}{N_r} \sum_{j=1}^{N_r} \sum_{k=1}^K |S_k^{Estimated}(j) - S_k^{Analytical}| \quad (4.10)$$

*MAE* stands for the mean absolute error which intends to calculate the error of the estimated value with respect to the analytical one in a stochastic style, i.e. in a set of  $N_r$  repetitions. The error is additionally summed up for all the  $K$  parameters. In the present study *MAE* was used to assess the precision of the implementations. It should be noted that *MAE* merely concerns the accuracy and not the efficiency. Further evaluation of the implementations in terms of the required *number of function calls* had to be done in order to comment on their efficiency. The highlighted term was named the *total cost of the analysis* by SALTELLI ET AL. (2010). Before jumping to the benchmark examples, some general conditions applied to all the cases are discussed.

#### 4.2.1. General Conditions

As mentioned above, *MAE* was used to control the ability of the considered implementations in predicting accurate first order sensitivity indices. The process was repeated  $N_r$  times to accommodate to the dependability of the calculations on the specifically generated sample sets.  $N_r$  was set to 50 as in the work by SALTELLI ET AL. (2010). In addition, the required number of function calls was changed to capture, if at all, the convergence towards the analytical results with relatively large sample sizes. Accordingly, 1000, 2500, 5000, 7500, 10000, 25000, 50000, 75000 and 100000 function calls were examined for each implementation. The corresponding numbers of samples for each implementation were chosen based on the underlying algorithms in order to achieve the mentioned numbers of function calls. In the case of the implementation by SALTELLI ET AL. (2008),  $N$  should be equal to the number of function calls divided by  $k + 1$ . For the EFAST, the number of the samples per search curve  $N_S$  was changed so that the final product of the  $N_S$ ,  $K$  and  $N_R$  resulted in the required number of function calls. The number of resam-

pling  $N_R$  was set to be 5 for all the problems. Although, a case study was done to check how the choice of  $N_R$  affected the results. The conceptual implementation does not rely on function evaluations at specific points in the parameter space rather than the existing  $N$  sample points. Obviously, therefore, the number of function calls equaled the number of samples.

Samples were always generated randomly from uniform distributions unless otherwise stated. Since the proposed implementation was founded on the ground of subdividing the input space, there was a need to select,  $S$ , the number of subdivisions which was clearly unknown. Hence, different values were assigned to  $S$  in order to study its influence on the results of the conceptual implementation. The selection of the values for  $S$  was done under the condition that the ratio  $N/S$  was kept below 40 to ensure statistically worthy calculations of the mean value. Accordingly, the results could be interpreted in two distinct ways concerning the prior knowledge of the  $S$ . On one hand where no prior knowledge was available, the mean of the *MAEs* for different values of  $S$  could shed light on how far away from the analytical solution could we get on average. On the other hand the minimum calculated *MAE* could point to the *best* choice of  $S$ . The two mentioned interpretations were selected to visualize the results. This way, the influence of the choice of the  $S$  on the results could be easily understood. An additional study on the best choice of  $S$  was performed in an attempt to introduce probable relevant instructions/recommendations. The corresponding results are presented later in Section 4.2.5.

#### 4.2.2. Sobol's g-Function

The Sobol's g-function, a very popular analytical benchmark for sensitivity analysis (see for example SALTELLI ET AL. (2010)), was introduced by SOBOL (2003) as seen in Equation 4.11.

$$g = \prod_{k=1}^K g_k(X_k) \quad \text{where:} \quad g_k(X_k) = \frac{|4X_k - 2| + a_k}{1 + a_k} \quad (4.11)$$

$g$  is a function of  $X_1, \dots, X_K$  as the uniformly distributed variables in the  $[0, 1]$  intervals and  $a_1, \dots, a_K$  as the constants. As the Equation 4.11 suggests a larger value of  $a_k$  corresponds to an ignorable parameter  $X_k$  whereas its smaller values point to an influential parameter  $X_k$ . This is schematically shown in Figure 4.3. Accordingly, the constant  $\mathbf{a}$  vectors were selected such that not only a combination of slightly versus highly influential parameters were selected but also parameter spaces of different dimensions were explored (see Table 4.2). The scatter of the output  $Y$  with respect to all the input parameters is presented in Figures 4.4 and 4.5 for the chosen  $\mathbf{a}$  vectors and an example set of 250 samples.

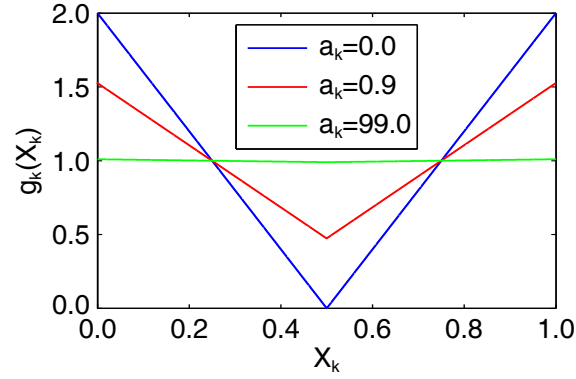


Figure 4.3. Influence of the constant parameter  $a_k$  on  $g_k(X_k)$ .

It is readily apparent that except for the 3-parameter problem, graphical interpretation of the scatter plots is out of question. In such cases, therefore, statistical techniques similar to the implementations applied here, are required in order to comment on the input-output correlation in the context of uncertainty.

According to SOBOL (2003), the analytical solution for the corresponding first order effects is as given in Equation 4.12.

$$S_k = \frac{V_k}{V} = \frac{1}{\prod_{k=1}^K (1 + V_k) - 1} \frac{3(1 + a_k)^2}{3} \quad (4.12)$$

Figure 4.6 shows the *MAEs* calculated using the studied methods. The minimum and the average errors resulted from the conceptual implementation are presented. This is done, as mentioned in Section 4.2.1, in order to clarify the influence of the choice of  $S$  on the *MAE*. In the case with three parameters, the conceptual implementation performs significantly better than Saltelli's implementation. Although, it converges much slower than the EFAST. In the latter case, the error produced from the conceptual implementation is almost four times that of the EFAST for 1000 function calls. Still, the overall performance of the proposed implementation is very promising.

Table 4.2. Selected  $\mathbf{a}$  vectors for the Sobol's g-function.

$K$	$\mathbf{a}$
3	[0.0, 0.9, 99.9]
6	[0.0, 0.001, 0.005, 0.002, 0.0015, 0.01]
12	[0.0, 0.01, 0.2, 0.3, 0.0, 0.5, 1.0, 1.5, 3.0, 4.5, 9.0, 99.0]

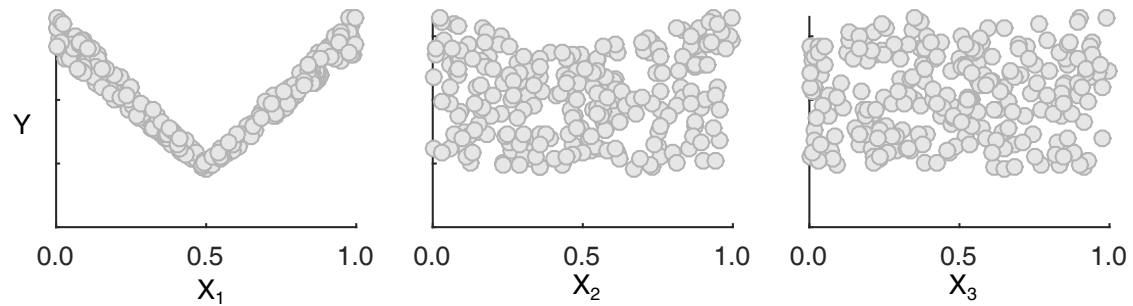
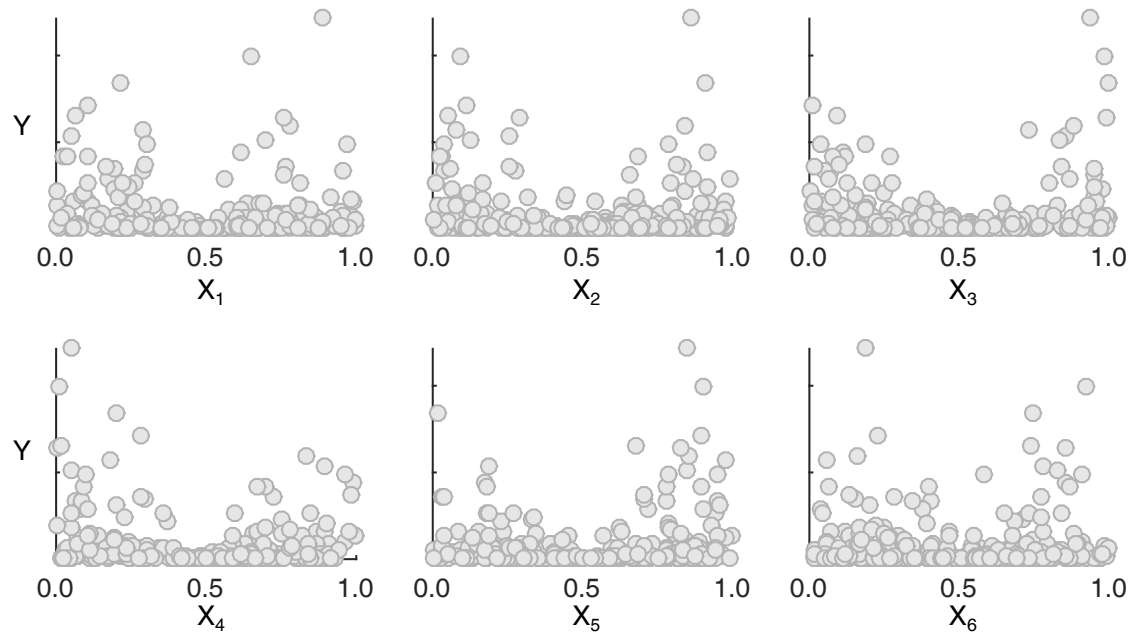
a)  $\mathbf{a}=[0.9, 9.0, 99.0]$ b)  $\mathbf{a}=[0.0, 0.001, 0.005, 0.002, 0.0015, 0.01]$ 

Figure 4.4. Scatter of the output  $Y$  with respect to the parameters for the Sobol problems with a)  $\mathbf{a} = [0.0, 0.9, 99.9]$  and b)  $\mathbf{a} = [0.0, 0.001, 0.005, 0.002, 0.0015, 0.01]$ .

The breakthrough performance of the conceptual implementation is observed when the number of parameters is doubled to six. Note that, in this particular case,  $\mathbf{a}$  was intentionally chosen to include values close to zero corresponding to parameters of roughly equal importance. As seen in Figure 4.6, Saltelli's implementation returns even larger errors and EFAST starts to converge considerably slower. For 2500 function calls, for instance, both Saltelli's implementation and EFAST predict results with errors more than 4 times larger than those of the conceptual implementation. This distance grows even larger in the case of twelve parameters, in spite of the fact that the selected  $\mathbf{a}$  directly pointed to the influential parameters. It can be clearly seen that at low computational costs Saltelli's implementation and EFAST simply fail at predicting the correct sensitivity indices for larger models. In contrast, the conceptual implementation performs rather stable regardless of the size of the model.

$\mathbf{a}=[0.0, 0.01, 0.2, 0.3, 0.0, 0.5, 1.0, 1.5, 3.0, 4.5, 9.0, 99.0]$

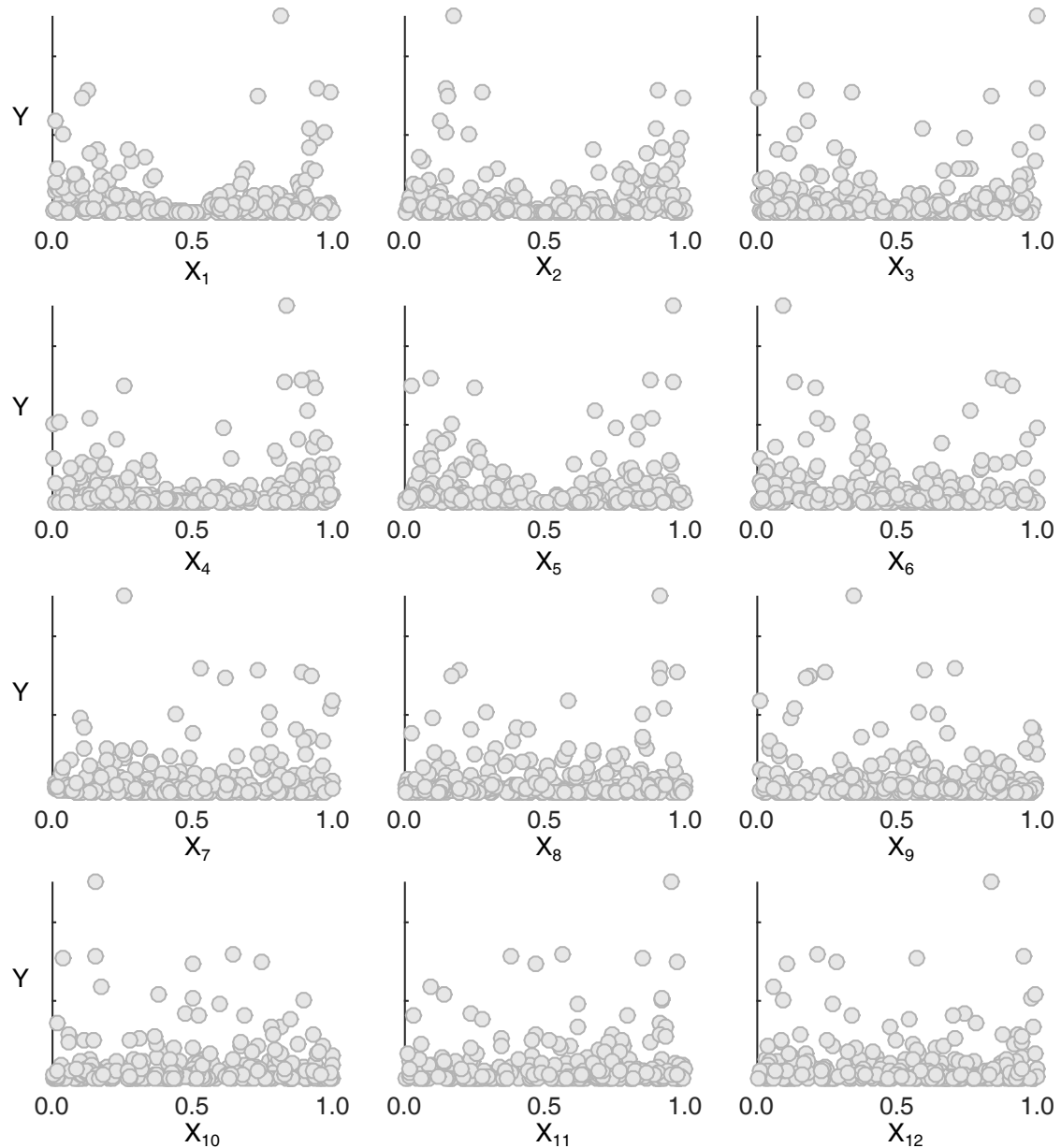


Figure 4.5. Scatter of the output  $Y$  with respect to the parameters for the Sobol problem with  $\mathbf{a} = [0.0, 0.01, 0.2, 0.3, 0.0, 0.5, 1.0, 1.5, 3.0, 4.5, 9.0, 99.0]$ .

Additionally, based on Figure 4.6, the minimum and the average errors generated by the conceptual implementation are quite close to each other which suggests that the choice of the number of subdivisions does not notably affect the results. This statement holds true as long as the subdivisions contain enough samples for statistically reliable predictions of the mean values. As expected the minimum and the average values of the  $MAEs$  from the conceptual implementation tend to depart more for larger models. The observed deviation is all outcome of the larger scatter in the results coming from larger models.

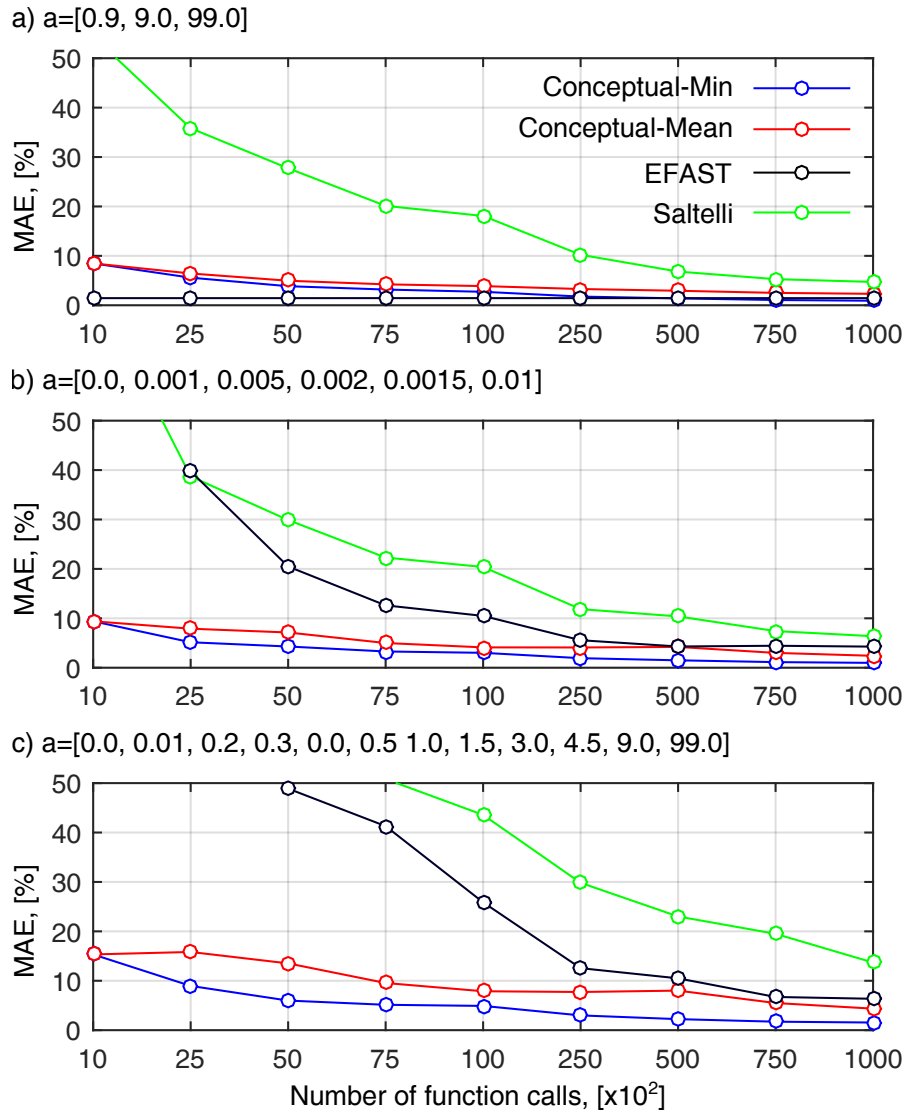


Figure 4.6. Mean absolute error (*MAE*) in predicting the first order effects for the three cases of the Sobol's *g*-function.

### 4.2.3. Polynomial Function

The polynomial function as given in Equation 4.13 has also been defined as the benchmark model for sensitivity analysis problems (see for example SUDRET (2008)).

$$Y = \frac{1}{2^K} \prod_{k=1}^K (3X_k^2 + 1) \quad (4.13)$$

It provides an analytical solution in the form of Equation 4.14 for the calculation of the first order sensitivity indices (SOBOL (1993)).

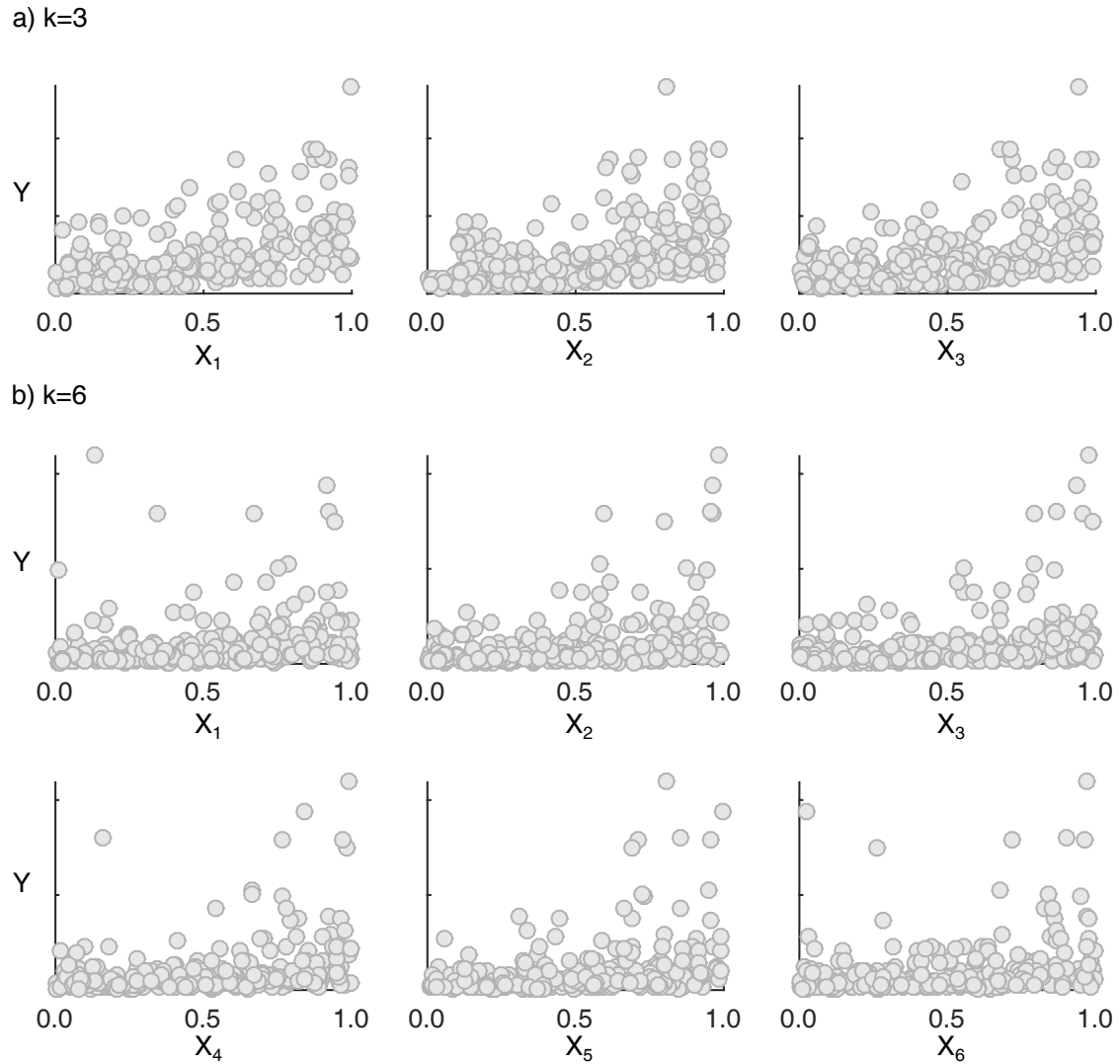


Figure 4.7. Scatter of the output  $Y$  with respect to the parameters for the polynomial problems with a)  $K = 3$  and b)  $K = 6$ .

$$S_k = \frac{5}{(6/5)^K - 1} \quad (4.14)$$

The function maps the input variables  $X_1, \dots, X_K$ , uniformly distributed over the  $[0, 1]$  interval, to the output variable  $Y$ . Similar to the previous benchmark, different sizes of the parameter space, namely  $K = 3, 6$  and  $12$  were selected to perform the tests. The polynomial function with large number of parameters could additionally confirm the efficiency of the conceptual implementation in the case of large models. The double check with the polynomial model was quite necessary, since the other considered benchmark function, i.e. the Ishigami function, had a constant number of parameters and was rather a small model which could not help in the efficiency control.

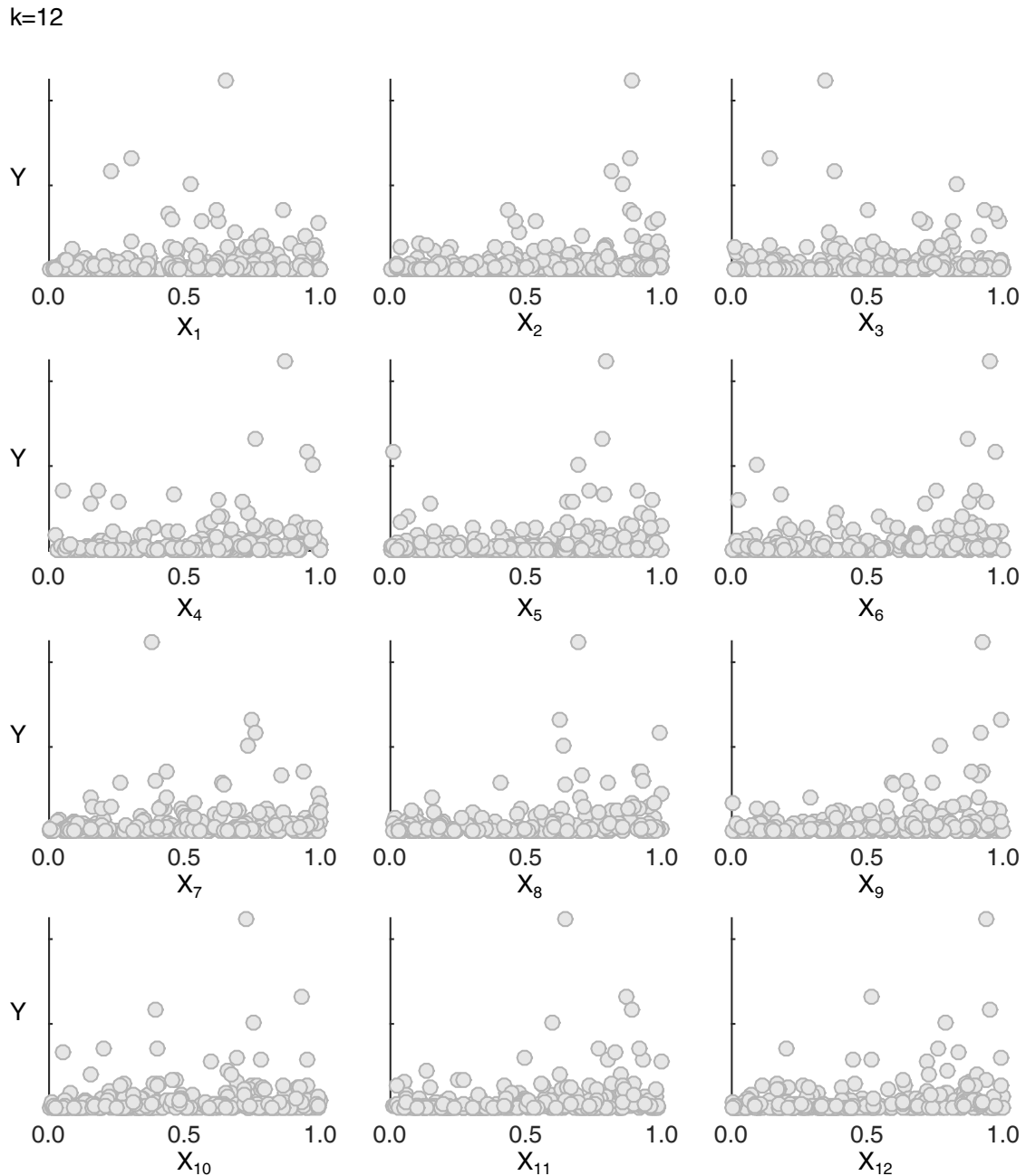


Figure 4.8. Scatter of the output  $Y$  with respect to the parameters for the polynomial problem with  $K = 12$ .

Figures 4.7 and 4.8 depict the corresponding  $X$ - $Y$  scatter plots. The parameters have clearly identical effects on the output  $Y$  as seen in the aforementioned Figures and supported by Equation 4.14. Figure 4.9 shows the computed  $MAEs$  by means of the studied techniques. Again, for the conceptual implementation the average and the minimum achieved errors are presented. The same observations as those made for the Sobol's  $g$ -function can be made here for the polynomial benchmark. The performance of the conceptual implementation is quite promising in the case of three parameters and is excellent



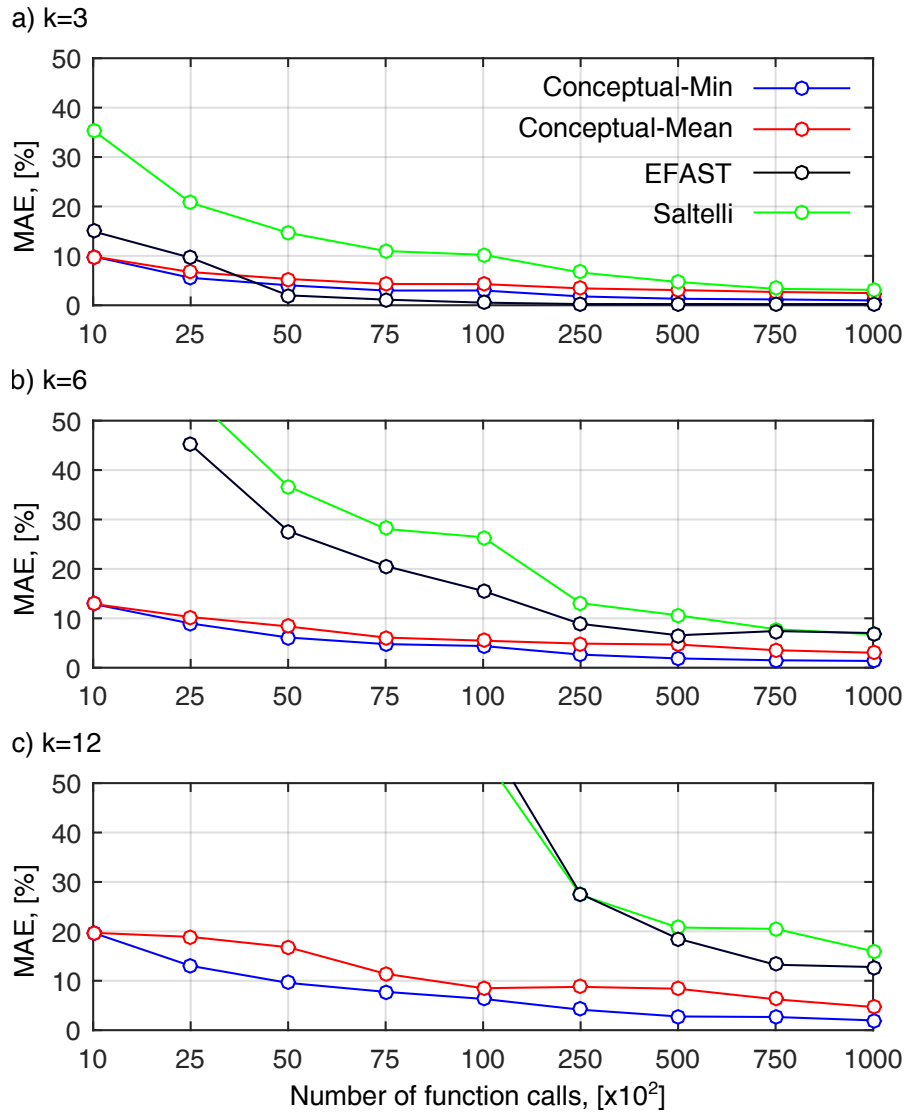


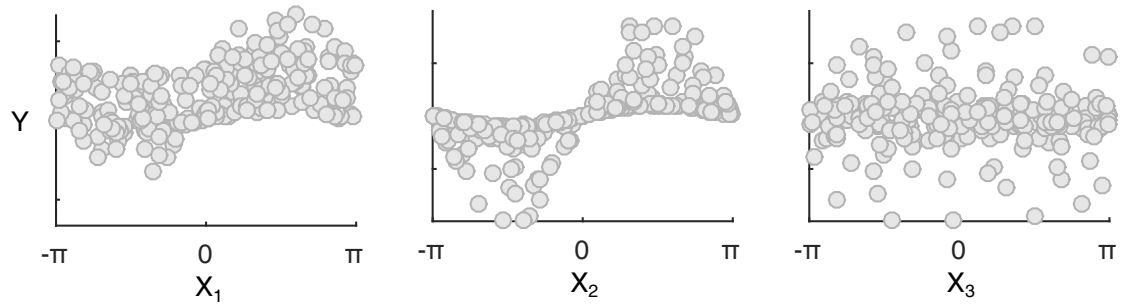
Figure 4.9. Mean absolute error (*MAE*) in predicting the first order effects for the three cases of the polynomial function.

in the case of larger models when compared to the other two implementations. The results, so far, demonstrate the efficiency and accuracy of the proposed implementation particularly when dealing with highly dimensional parameter spaces. In such cases, Saltelli's implementation and EFAST require considerable amount of function calls to come close to predicting the sensitivity indices within an acceptable range. In other words, they fail at providing accurate results with reasonable computational effort.

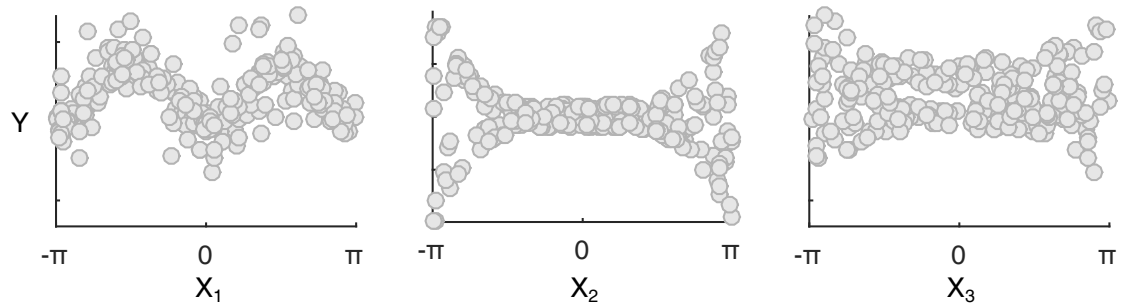
#### 4.2.4. Ishigami Function

Another well-known benchmark for sensitivity analysis tests is the Ishigami function by ISHIGAMI AND HOMMA (1990). The function is as given in Equation 4.15.

a)  $a=0.1, b=0.1$



b)  $a=7.0, b=0.1$



c)  $a=0.1, b=7.0$

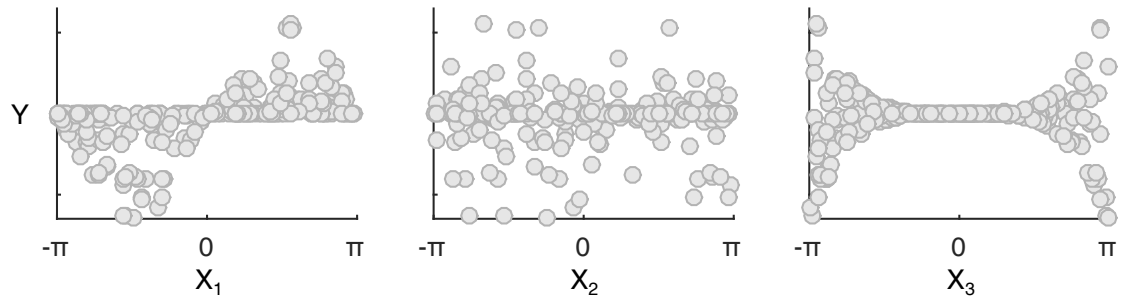


Figure 4.10. Scatter of the output  $Y$  with respect to the parameters for the Ishigami problems.

$$Y = \sin X_1 + a \sin^2 X_2 + bX_3^4 \sin X_1 \quad (4.15)$$

The function defines the output  $Y$  in terms of the input parameters  $X_1$ ,  $X_2$  and  $X_3$ . Obviously, the number of variable parameters is constant and therefore the model size cannot be changed. All the three parameters belong to the  $[-\pi, \pi]$  interval and are assumed to be uniformly distributed. The constant parameters  $a$  and  $b$  were varied to form three different cases similar to the other benchmark tests. The selected  $a$  and  $b$  pairs included:  $(0.1, 0.1)$ ,  $(7.0, 0.1)$  and  $(0.1, 7.0)$ . The resulting scatter plots are shown in Figure 4.10. In contrast to the previously studied benchmark functions, they are graphically interpretable.

The analytical solution to the sensitivity analysis could be found following Equation 4.16.

$$S_k = \frac{V_k}{V}$$

where:

$$\begin{aligned} V &= \frac{a^2}{8} + \frac{b\pi^4}{5} + \frac{b^2\pi^8}{18} + \frac{1}{2} \\ V_1 &= \frac{b\pi^4}{5} + \frac{b^2\pi^8}{50} + \frac{1}{2}, \quad V_2 = \frac{a^2}{8}, \quad V_3 = 0 \end{aligned} \quad (4.16)$$

The sensitivity indices were, accordingly, computed and the corresponding *MAEs* were calculated as shown in Figure 4.11. It should be noted that, here, the model size was the same in all the three cases. Hence, the performance of the implementations in terms of the efficiency and accuracy almost remained unchanged. Although, in some cases EFAST has apparently converged to a slightly different value than the analytical solution. As for the other two benchmarks, the conceptual implementation proves to be stable in producing minimal errors at low computational costs.

#### 4.2.5. Parameter Study on the Number of Subdivisions

To take the investigation one step further, a parameter study was performed on the unknown parameter,  $S$ , i.e. the number of subdivisions. The intention was to provide recommendations on the choice of the parameter, particularly in relation to the number of function calls. Although, the main focus should be on the lower number of function calls where limited samples are available and accordingly, every single sample is of high value in the uncertainty analysis.

For the sake of convenience, the studied parameter was chosen to be  $S^{-1}$  instead of  $S$ .  $S^{-1}$  is a normalized representative of the number of samples per subdivision, i.e.  $\frac{N/S}{N}$ . Additionally and in contrast to  $S$  itself,  $S^{-1}$  has a limited range between 0 and 100 percent. In the first step of the investigation, the number of  $S$  resulting in the lowest error (*MAE*) was found for the previously studied benchmark problems. The problems were divided into three categories with respect to the number of parameters, namely, 3, 6 and 12. The categorization allowed to capture the potential influence of the number of parameters on the choice of  $S$ . Consequently, the best choices of  $S$  are presented in Figure 4.12 in terms of the number of function calls for the selected categories.

As expected the required samples per subdivision contributes to a smaller percentage of the total samples in the case of larger number of function calls. The underlying logic could be clarified through a straightforward example. Assume a minimum of 40 samples

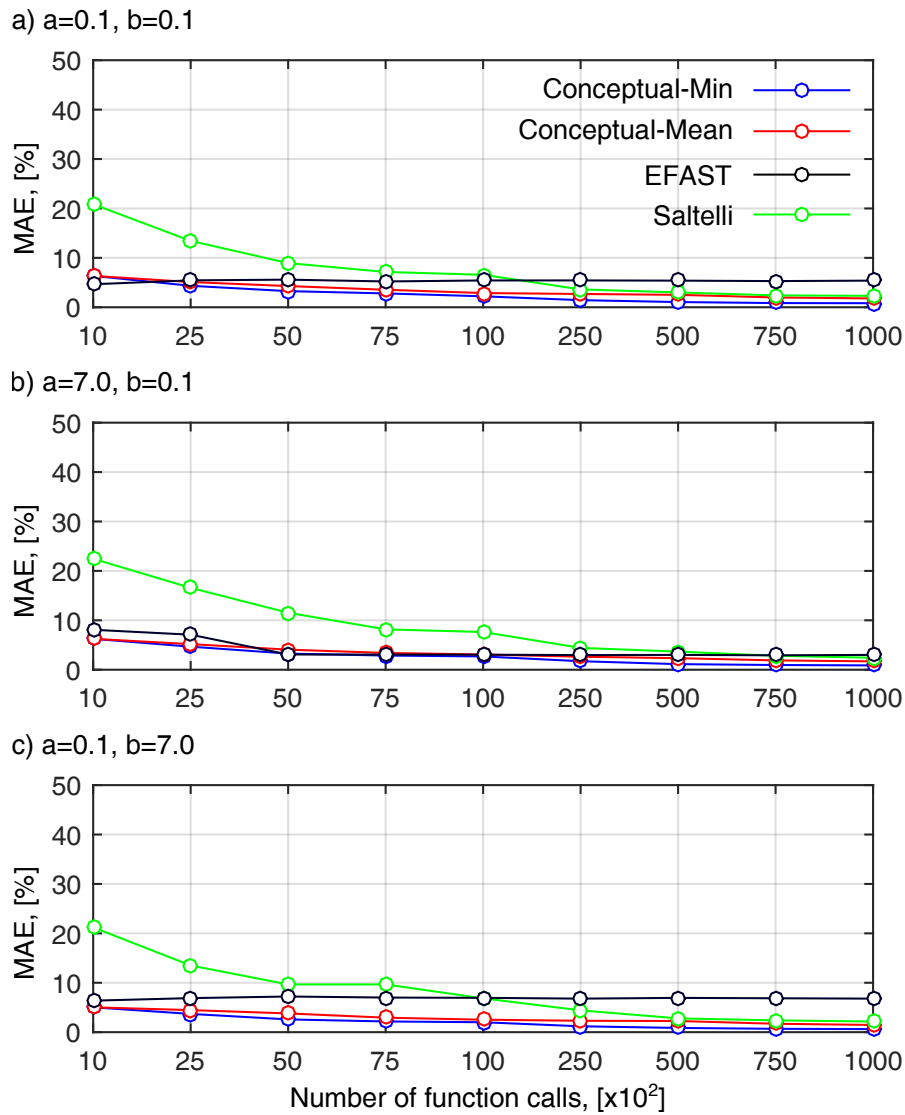


Figure 4.11. Mean absolute error (*MAE*) in predicting the first order effects for the three cases of the Ishigami function.

per subdivision is needed to predict the mean value within an acceptable range. In 1000 samples this is equal to 4% of the total number of samples whereas in 10000 samples it hardly even reaches a half percent. As previously discussed, though, the investigation should be concentrated on the lower number of function calls where the majority of the practical problems maneuver. In the following discussions, therefore, we are mainly interested in the best choice of  $S$  in this region.

A second look at Figure 4.12, reveals that the number of parameters do play a role on the choice of  $S$ . This becomes more evident when the existing tendency in each parameter category is visualized by means of fitting functions. Here, linear, quadratic and cubic polynomials have been fitted to the data from each category. The results are also shown in Figure 4.12. Clearly, larger parameter spaces demand more samples per subdivision,

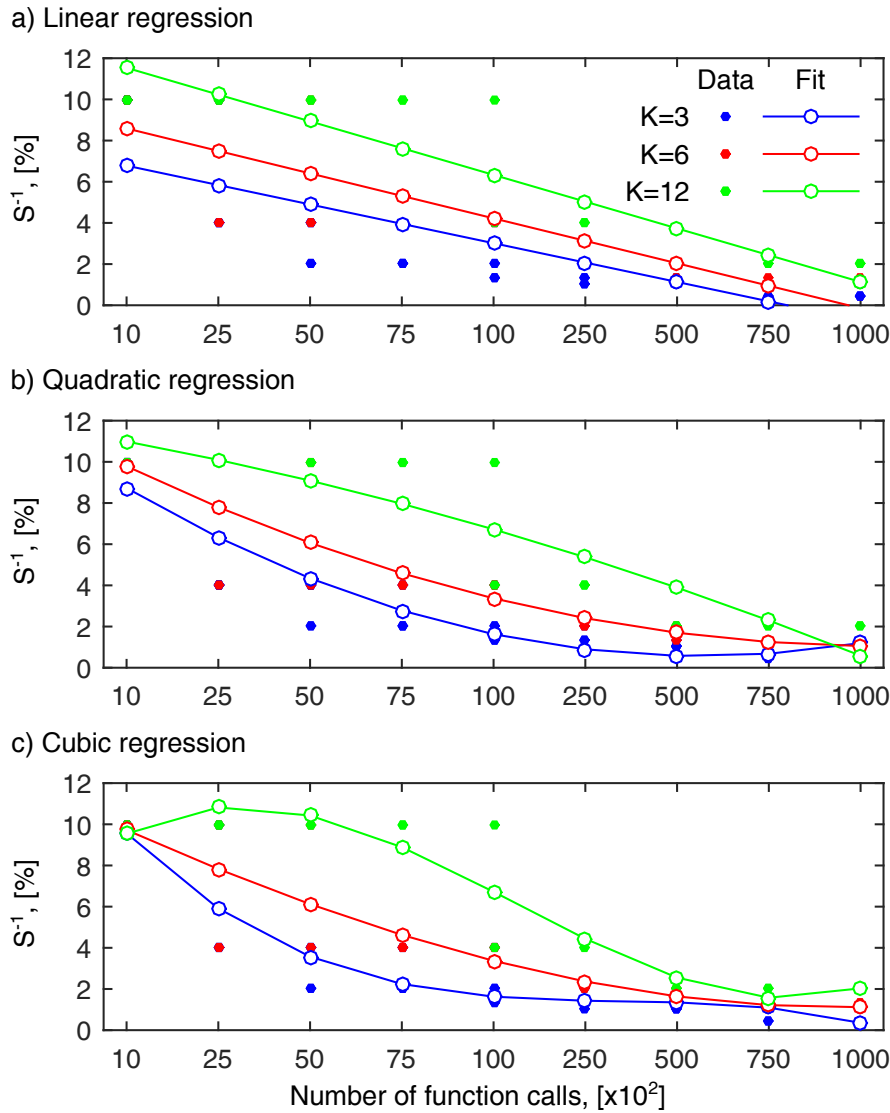


Figure 4.12. The best choice of  $S$  for problems with different number of parameters.

namely, larger  $S^{-1}$ . Among the fitted curves, the quadratic one appeared to imitate the trend in the data satisfactorily.

As the influence of the  $K$  on the choice of  $S$  was confirmed through the primary examination, the study was extended to find out any potential correlation among  $S$ ,  $K$  and the number of function calls. This time, the studied parameter was chosen to be  $(S \times K)^{-1}$  to include both parameters. It roughly represents the number of samples required per subdivision per parameter to achieve a reasonable prediction of the mean value. The results are shown in Figure 4.13. Here, the data is less scattered and appears to follow a trend along the number of function calls. Similar to the previous case, linear, quadratic and cubic functions were fitted to the data in order to capture any plausible relationship. The quadratic curve, apparently, offers a satisfactory fit to the data.

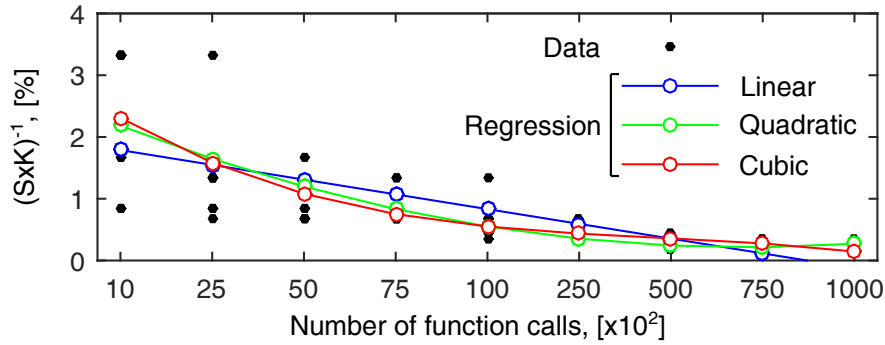


Figure 4.13. The best choice of  $S \times K$  for problems with different number of parameters.

#### 4.2.6. Parameter Study on the $N_R$ in EFAST

In Section 4.1.3 it was mentioned that EFAST relies on a number of computational parameters such as  $N_R$ , the number of resampling. Although, for the purpose of comparison,  $N_R$  was set to 5 as recommended by the literature, its direct relation to the number of function calls led to the need for an extended study on it. The preliminary perception on the parameter ended up with two quite paradoxical conclusions. On one hand, according to the definition, an increment in the  $N_R$  is followed by an increase in the number of samples per search curve. This possibly results in more accurate estimations of the sensitivity indices, though at higher computational cost. On the other hand, for a fixed number of function calls (namely, a constant  $N_S \times K \times N_R$ ) a larger  $N_R$  implies a smaller  $N_S$ . It should be noted, however, that the minimum value recommended for  $N_S$  is 65. Naturally with the latter constraint, EFAST range of application reduces to only larger number of function calls given that larger  $N_R$  is chosen. For instance, the minimum number of function calls required for a problem with 12 parameters and  $N_R = 10$  is 7800.

The influence of the choice of  $N_R$  on the performance of EFAST was further studied with two additional values of 1 and 10 for the parameter. The calculation of the  $MAE$  was repeated for the previously discussed benchmark problems. The resulting values are plotted against the number of function calls in Figures 4.14, 4.15 and 4.16 for all the studied benchmarks. According to the figures a few observations can be made. To begin with, the effect of  $N_R$  on the performance of the EFAST depends on the number of parameters involved in the problem. In the majority of the problems with  $K = 3$  the choice of  $N_R$  seems to be of negligible importance. Although, for the problems with  $K = 6$  and 12, the  $MAE$  plots corresponding to different  $N_R$  values begin to diverge, particularly in the region with lower number of function calls. In addition, EFAST plots with larger  $N_R$ s appear steeper compared to the plots corresponding to smaller  $N_R$ s which means they converge with more noticeable improvements in steps taken along the horizontal axis. As expected, however, increasing  $N_R$  to 10 has not resulted in better estimations of the

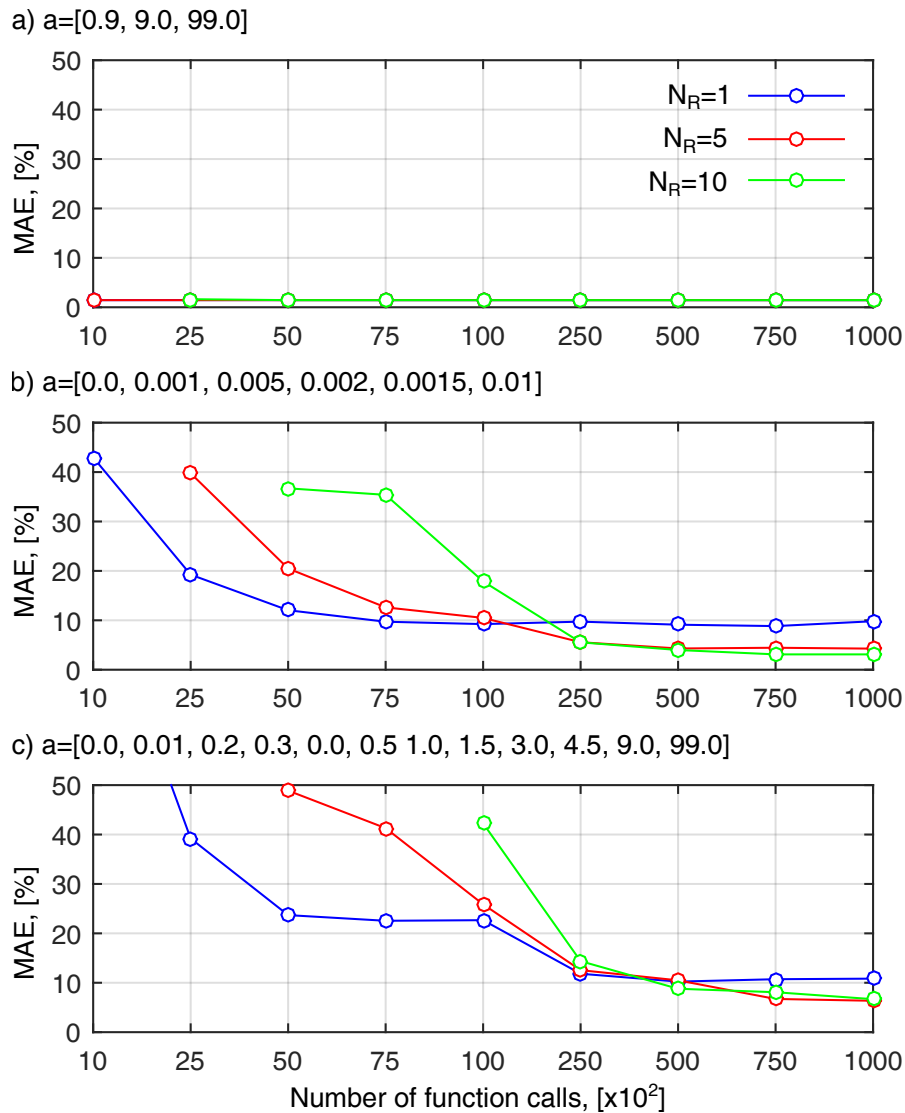


Figure 4.14. Parametric study on  $N_R$  for the three cases of the Sobol's g-function.

sensitivity indices for fixed number of function calls. It has, even, led to larger errors in the region with lower number of function calls. The above discussion confirms that the choice of 5 as the value for  $N_R$  was a reasonable decision.

### 4.3. Engineering Problems

As it was clarified in Section 1.3, the conceptual implementation formed the ground for the proposed model selection technique which is discussed later in Chapter 5. The main challenge for the proposed method was the assessment of the experimental and numerical models collected in the database described in Chapter 3. As a result, application of the conceptual implementation of the sensitivity analysis to the aforementioned models

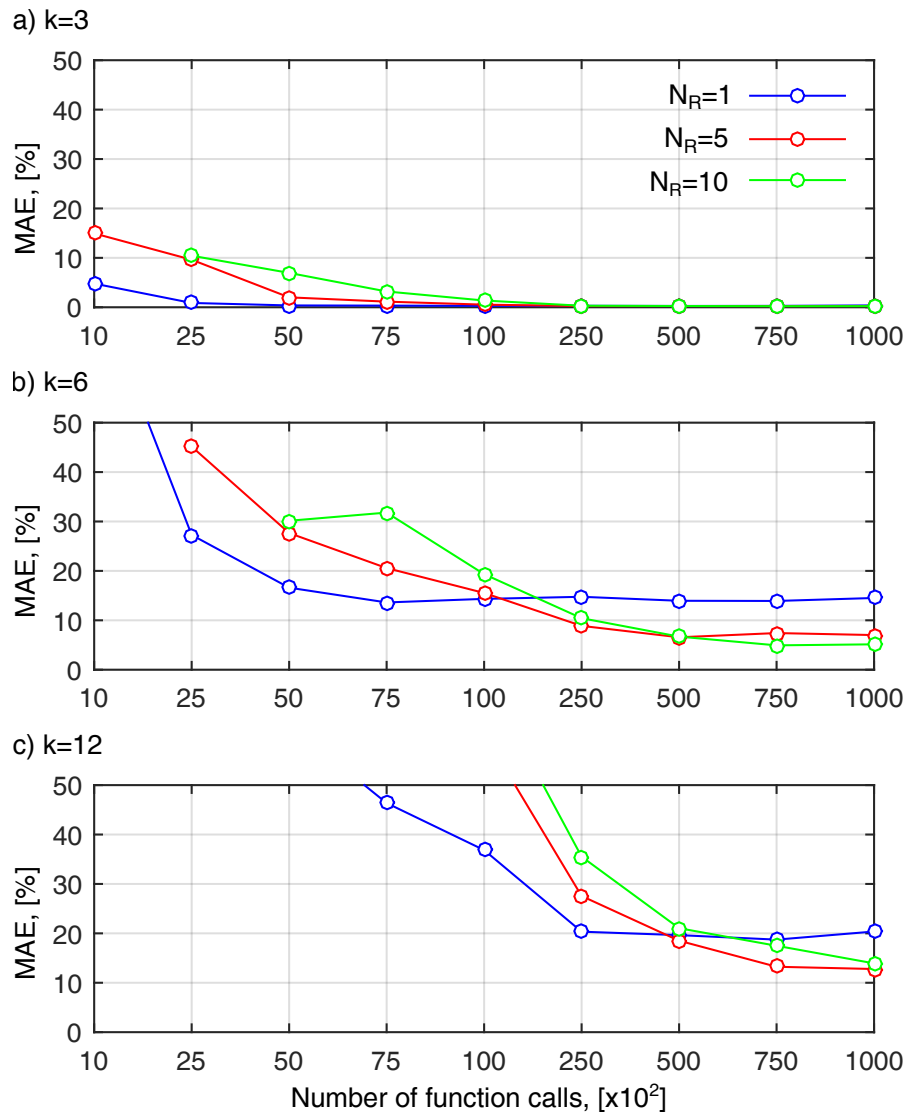


Figure 4.15. Parametric study on  $N_R$  for the three cases of the polynomial function.

was inevitable. It was, therefore, necessary to have an understanding of the performance of the proposed implementation in real engineering problems rather than simple analytical benchmarks. For this purpose, the studied sensitivity analysis implementations were further applied to two engineering problems, one numerical and the other experimental. The intention was to figure out their strengths and weaknesses in dealing with practical problems.

#### 4.3.1. General Conditions

The majority of the setup required for the performance test on the above mentioned engineering problems was assumed to be the same as that of the analytical benchmarks. For instance, the exact same series of values as those used in the analytical benchmarks were



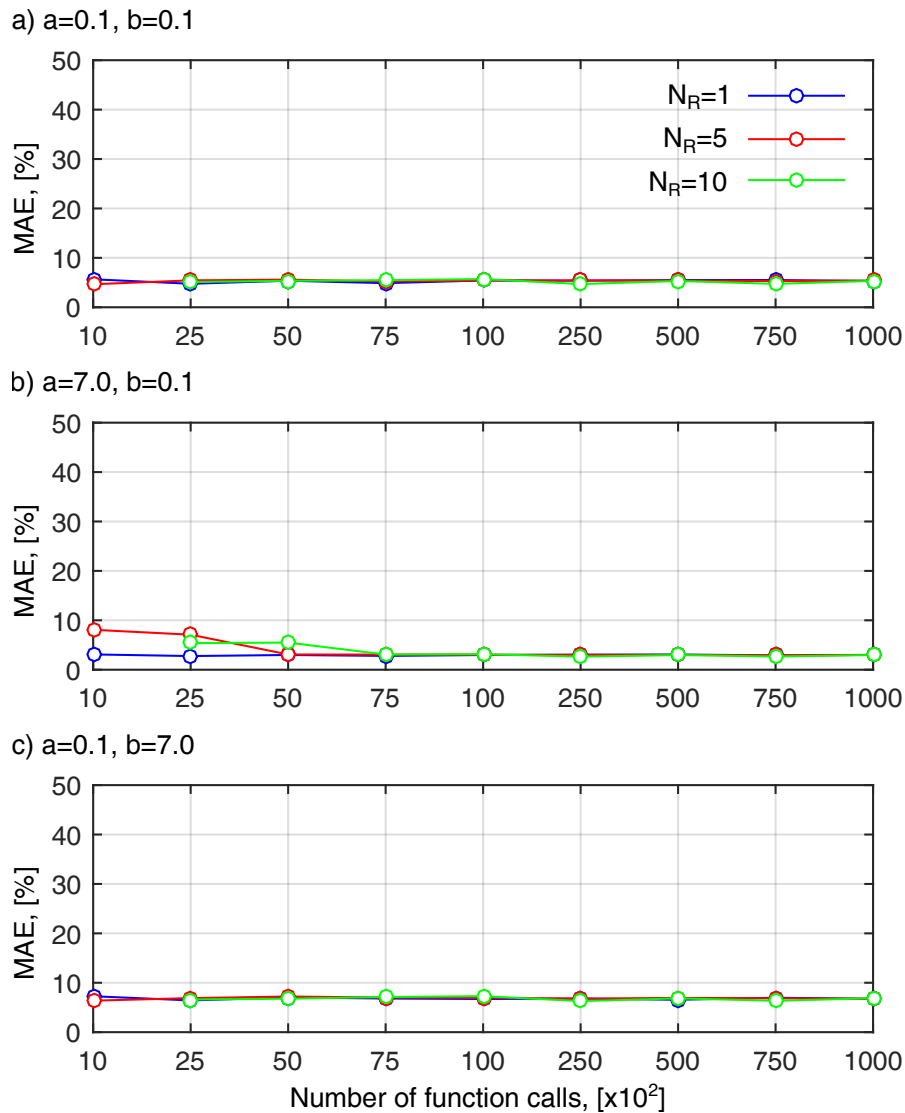


Figure 4.16. Parametric study on  $N_R$  for the three cases of the Ishigami function.

used for the number of function calls and the number of subdivisions. Similarly, the tests were run with  $N_r = 50$  repetitions. The first order effects were calculated using the three studied implementations. In the case of the EFAST,  $N_R$  was set to 5 as it appeared to produce the most reliable results in the previously performed parameter study.

It is needless to say that no analytical solution to the first order sensitivity analysis of the selected problems was available. In other words, no  $MAE$  could be computed for the engineering problems. For the purpose of visualization, therefore, the average value of the first order effect over the  $N_r$  repetitions was employed. In the case of the conceptual implementation, this implied that only the mean value of the estimated first order effects over different numbers of subdivisions could be computed. An extra averaging was later performed over the  $N_r$  for the sake of comparison with the results from the other two implementations.

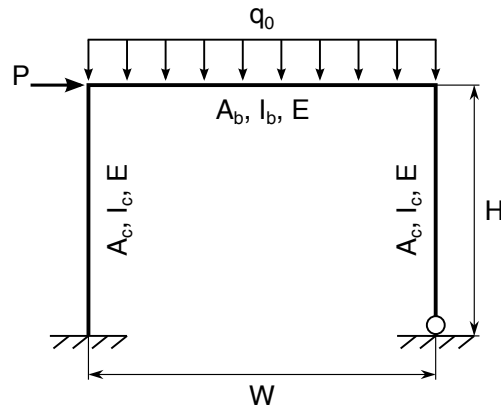


Figure 4.17. Schematic of the studied numerical model from (AUSTRELL ET AL. (2004)).

#### 4.3.2. Numerical Simulations

Performing sensitivity analysis on numerical simulations is a very common engineering problem. In order to see how the studied sensitivity analysis implementations competed in this field, they were applied to the straightforward 2nd-order analysis of a 2-dimensional frame from AUSTRELL ET AL. (2004). The single-story single-span frame was assumed to be under concentrated lateral and uniformly distributed gravity loads as seen in Figure 4.17. The study was focused on the lateral performance of the frame under influence of the given scheme. The input parameters were chosen such that the geometrical, material, sectional and loading properties of the frame were covered. Accordingly,  $H$  and  $W$  the frame height and width, respectively,  $E$  the modulus of elasticity of the frame's material,  $A_c$  and  $I_c$  ( $A_b$  and  $I_b$ ) the area and the moment of inertia of the columns (beam) cross section, respectively,  $P$  the concentrated lateral load and finally  $q_0$  the uniformly distributed load were set to be the variable parameters. The average value of each parameter was selected based on the engineering judgment. The coefficient of variation was then set equal to 0.25 which implies each parameter was allowed to vary in the range of  $\pm 25\%$  of its mean. The resulting intervals are presented in Table 4.3.

The analysis was performed using the well-known CALFEM toolbox by AUSTRELL ET AL. (2004). The code takes the input parameters, constructs a numerical model of the corresponding frame, performs 1st and 2nd-order analysis and finally returns the lateral top

Table 4.3. Parameter ranges for the CALFEM numerical simulations.

	Parameters								
	$H$	$W$	$E$	$A_c$	$I_c$	$A_b$	$I_b$	$P$	$q_0$
	[m]	[m]	[N/m <sup>2</sup> ]	[m <sup>2</sup> ]	[m <sup>4</sup> ]	[m <sup>2</sup> ]	[m <sup>4</sup> ]	[N]	[N/m]
Minimum	2.55	3.0	150e9	1.5e-3	1.2e-5	4.5e-3	4.05e-5	7.5e3	37.5e3
Maximum	4.25	5.0	250e9	2.5e-3	2.0e-5	7.5e-3	6.75e-5	12.5e3	62.5e3

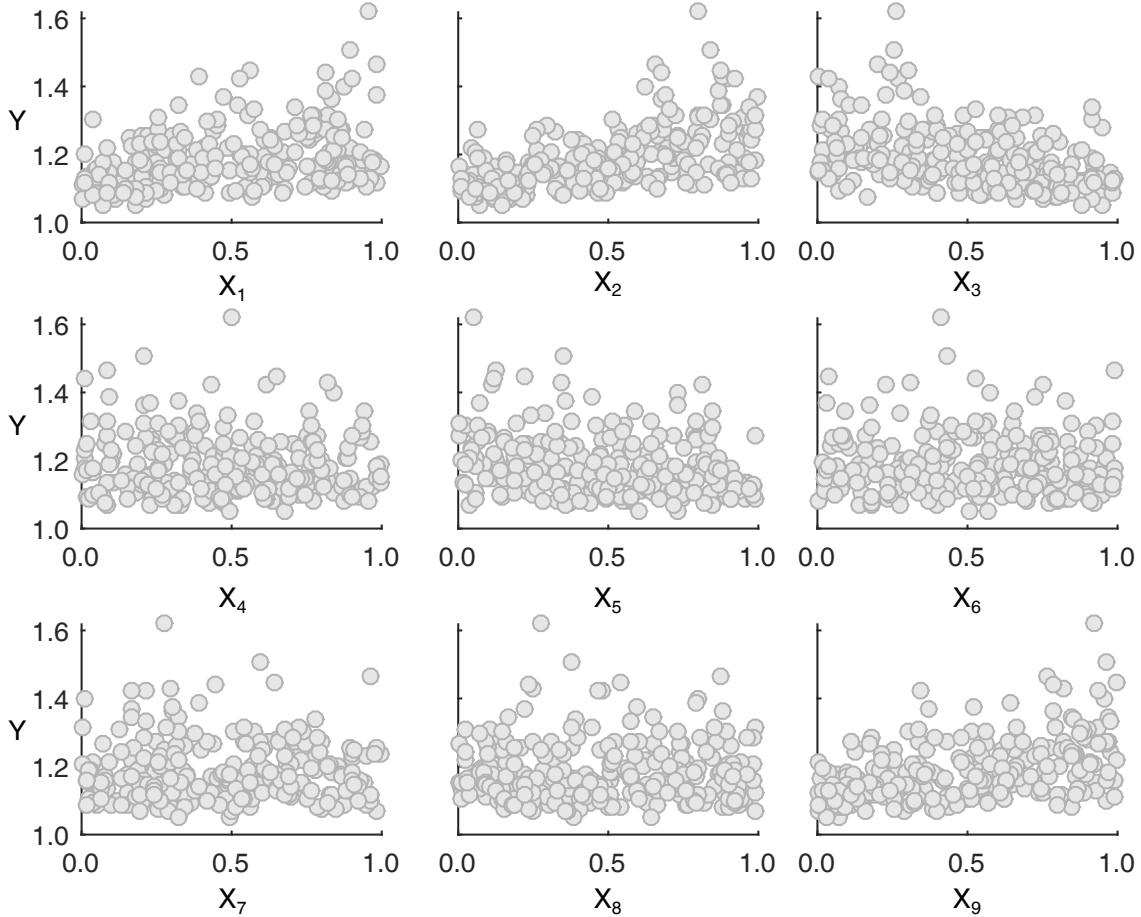


Figure 4.18. Scatter of the output  $Y$  with respect to the considered parameters for the CALFEM problem.

displacements from each analysis. Significant difference between the top displacements from the 1st and 2nd-order analysis points directly at the importance of performing the 2nd-order analysis. Therefore, the unitless parameter defined as the ratio of the 2nd-order to the 1st-order top displacements was selected as the only output parameter to be studied. To begin with the sensitivity analysis, samples were generated randomly according to uniform distribution assumption for all the parameters. The resulting scatter plots are shown in Figure 4.18 for 250 illustrative samples.

The first order sensitivity indices were then computed using the three studied implementations. The average estimated values were used to compare the results as depicted in Figure 4.19. The figure shows the performance of the implementations at the smallest and largest considered number of function calls. It should be noted that  $N_R = 5$  and  $K = 9$  dictated a minimum of 2925 function calls for the EFAST to operate. Therefore, the performance comparison was additionally done at 5000 function calls where EFAST first enters the match. Figure 4.19 once more confirms the efficiency and reliability of the conceptual implementation even for the numerical simulations. The reliability can be

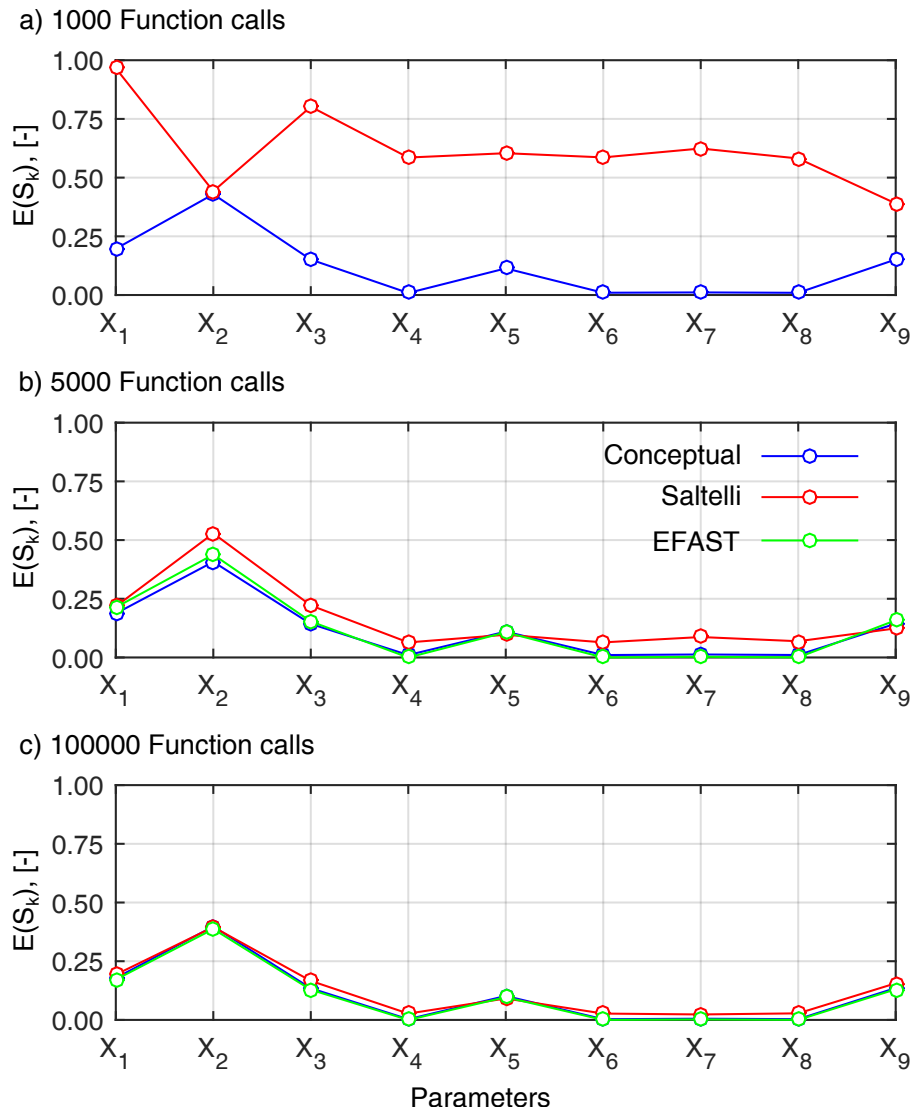


Figure 4.19. Average sensitivity index estimated for each parameter in the CALFEM problem for a)  $1 \times 10^3$  b)  $5 \times 10^3$  and c)  $100 \times 10^3$  function calls.

further proved based on Figure 4.20 in which the sum of the estimated first order effects is presented. It was already mentioned that the unit sum could act a criteria for the qualification of the sensitivity analysis. The conceptual implementation successfully passes this quality control as the sums of its results are in close proximity of one even in the case of smaller sample spaces. In contrast, though, we have the poor performance of Saltelli's implementation probably due to the large coefficient of variation of the studied data.

### 4.3.3. Experimental Tests

The final examination on the performance of the studied implementations was on the experimental part of the database, since it was an essential step toward the quality assess-

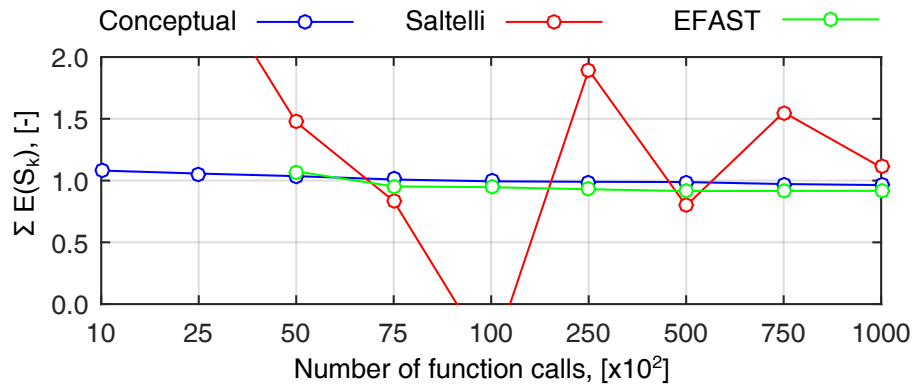


Figure 4.20. Sum of the average first order effects for the CALFEM problem in terms of the number of function calls.

ment. As mentioned in Section 2.3, the parameter of interest was the yield displacement which was also chosen as the output for the performance check. For the purpose of the investigation, the yield displacement was not computed individually for the specimens but rather fished out of the literature sources which recorded it during the corresponding experiments. In other words, the reported yield displacement was used as the output. Obviously, the set of specimens to be studied was limited to the ones that provided the observed yield point. As seen in Figure 4.21, not many specimens featured the required information, particularly, in the case of squat walls. Therefore, only a group of 33 transition walls with the available observed yield point were selected for further investigations. The sample set, hence, consisted of a  $33 \times 10$  matrix in which each column represented one of the ten parameters defined for the database in Table 3.1. The corresponding scatter plots are shown in Figure 4.22. As expected the data is very sparse following inconsistent distributions along the parameter range with the exception of a few parameters. Being well aware that the sparseness would certainly affect the final results, the data was considered for the performance check. The current conditions of the problem at hand could perfectly resemble the majority of the real engineering problems in which the available data is very limited.

The use of the experimental data implies that no random generation of samples was performed. It is needless to say that Saltelli's implementation and EFAST were stricken out of the performance check on the very same ground. Both of the aforementioned implementations require on-demand estimations of the output through the objective function. For experimental data, the objective function is not available or known. The only way to fulfill the need for it is to hypothesize the underlying physics and try to replace it with known functions. The technique which is established as the response surface method introduces its own uncertainties to the problem which was out of the scope of the current study. Therefore, Saltelli's implementation and EFAST were left out of the performance

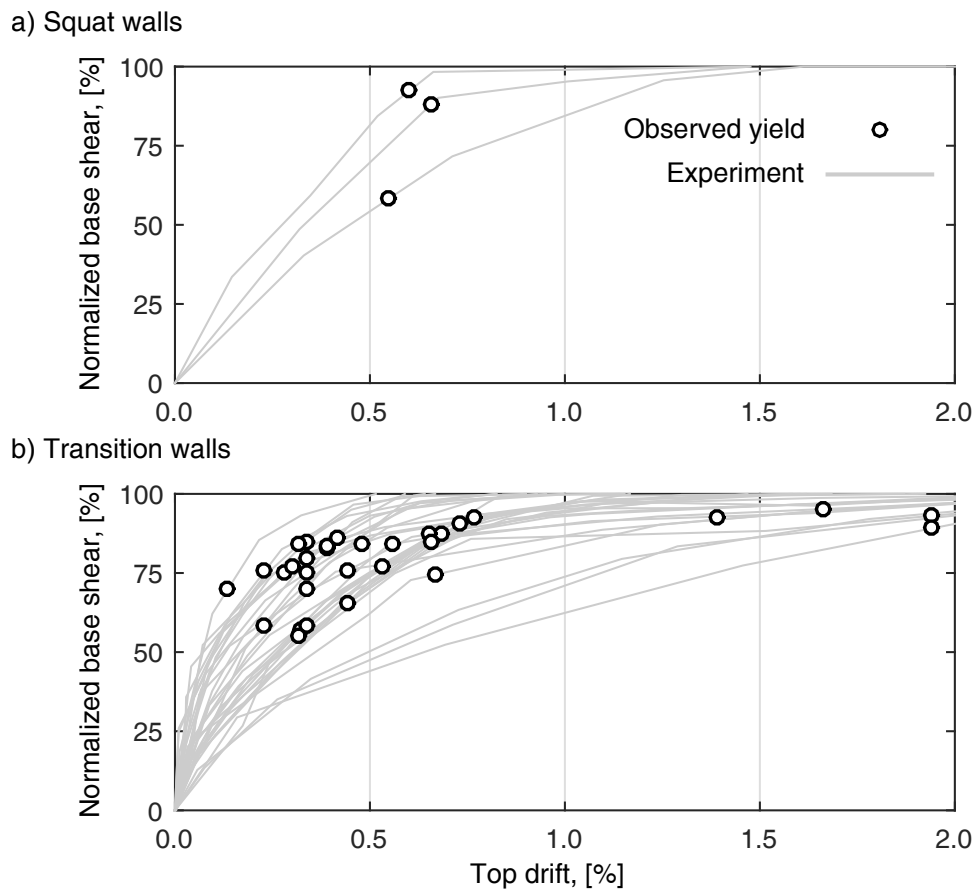


Figure 4.21. Observed yield drift for the specimens in the experimental part of the database (base shear is normalized to its maximum value for each wall).

check. The inability of the two above-mentioned implementations in treating the experimental data was already a plus for the conceptual implementation.

The first order sensitivity indices were computed using the proposed implementation with 3, 4 and 5 as the number of subdivisions. A few points regarding the results could be observed. Generally, none of the choices of  $S$  produced a set of  $S_k$ s with  $\sum S_k$  equal to one. In all the cases,  $\sum S_k$  was notably larger than one. Nevertheless, the individual  $S_k$ s were normalized to achieve a unit sum. Consequently, the resulting  $S_k$ s estimated using different numbers of subdivisions turned out to be quite similar with the exception of a few parameters. The average predicted  $S_k$  and its standard deviation are shown in Figure 4.23 for all the parameters. It is clear that  $X_1$ ,  $X_4$ ,  $X_8$  and particularly  $X_{10}$  are more influenced by the uncertainty in the estimation of the  $S_k$ , i.e. the choice of  $S$  made a quite significant difference in their results. This could be expected on the account of using the sparse data. The conceptual implementation, anyhow, provided a rough, though not exact, estimation of the first order effects on the basis of the limited available data. The results, basically, prepare the ground for further detailed studies on such data.

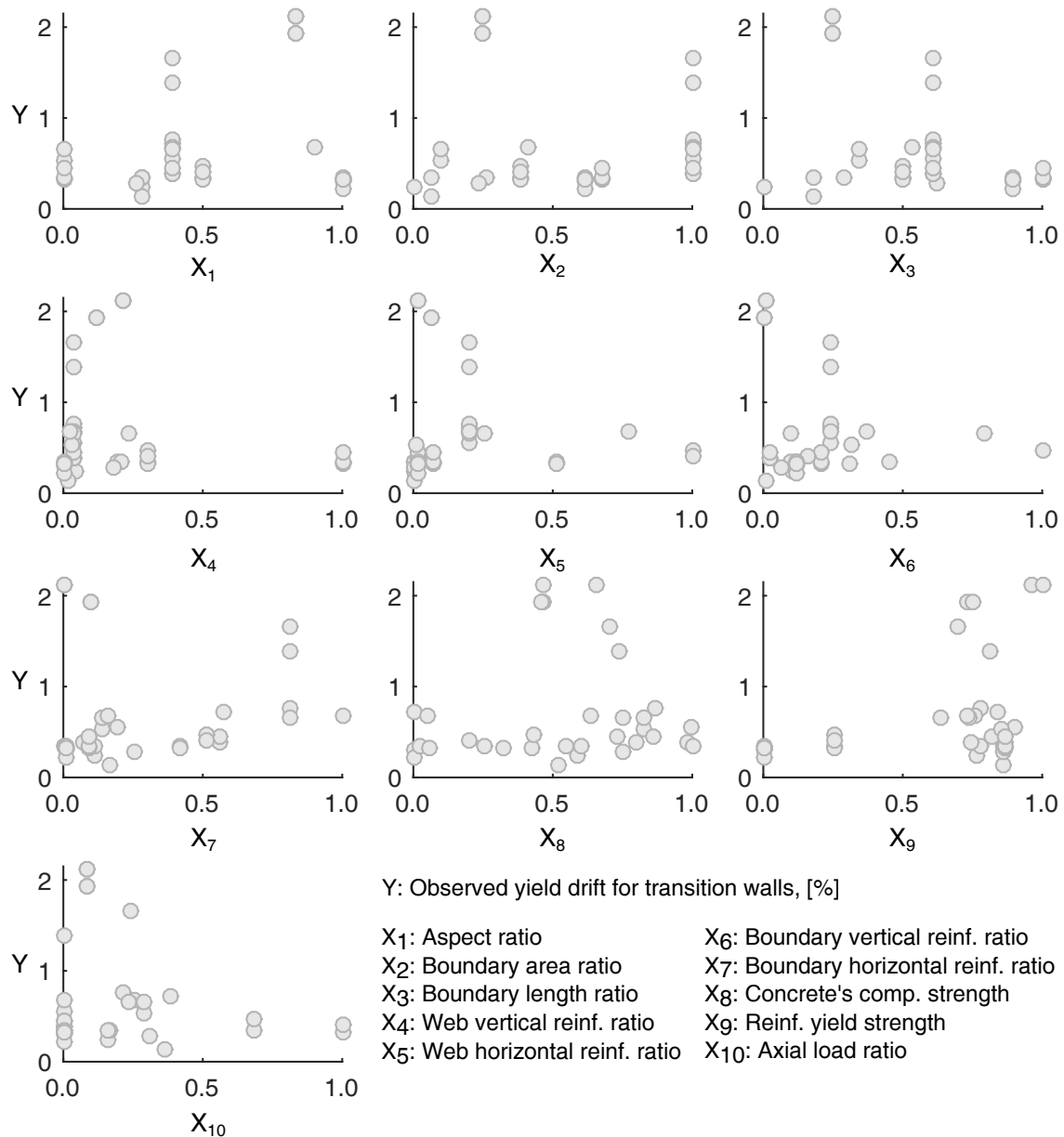


Figure 4.22. Scatter of the output  $Y$  with respect to the parameters for the experimental problem on transition walls.

## 4.4. Discussion of the Results

In the previous sections, several applications of the variance-based sensitivity analysis were used as the ground to evaluate the efficiency and accuracy of the proposed conceptual implementation. Its competency was checked against Saltelli's implementation and EFAST which, along with the conceptual implementation, were applied to the selected benchmark problems. The investigation featured problems of different sizes and of analytical, numerical and experimental backgrounds. The conceptual implementation firmly succeeded in treating all the problems at hand. Particularly, it led to very promising results

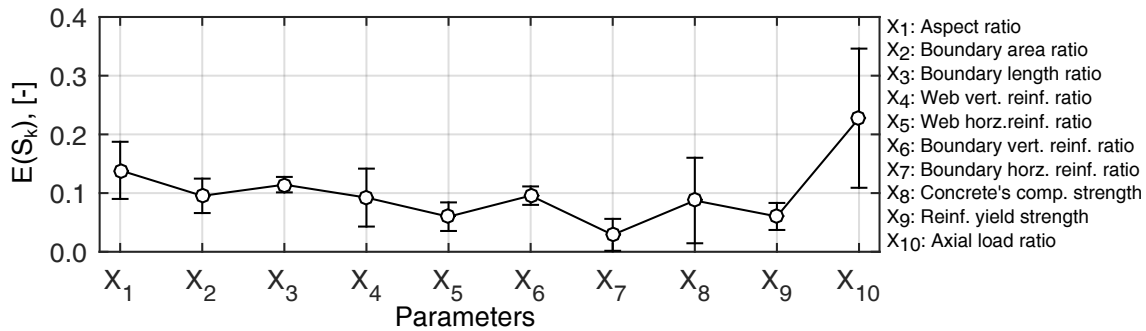


Figure 4.23. Average sensitivity index estimated for each parameter in the experimental problem on transition walls.

in the cases with large parameter spaces and limited samples. It, additionally, proved to be a competent approach as Saltelli's implementation and EFAST both performed poorly in the practical regions of engineering problems, namely, small sample spaces with large number of parameters.

The excellent performance of the conceptual implementation mainly relies on its effective use of the available data. For a problem with  $K$  parameters, for instance, all the samples are used in the calculation of every single  $S_k$ . In contrast, Saltelli's implementation and EFAST generate samples for each  $S_k$  estimation separately. This procedure is not efficient since it employs merely parts of the data in each computation. Furthermore, as suggested by the results of the conceptual implementation, the average value of the data in each subdivision is a reliable representative in terms of the statistics. In fact the number of samples needed to make a sound prediction of the mean value is considerably less than that required to estimate the reflective variance. This could be the reason for the superior and stable performance of the conceptual implementation even with relatively few function calls. Here, it is noteworthy to mention the unsatisfactory performance of Saltelli's implementation and EFAST for highly dimensional parameter spaces. With a look back at the number of function calls necessary for the two implementations to operate, the direct relation between the number of parameters and the number of function calls becomes clear. Though, this is not the case for the conceptual implementation as the number of samples required is independent of the number of parameters and equals to the number of function calls. Finally and as discussed in Section 4.2.5, a rough measure of the optimal number of subdivisions could be derived which tends to improve the efficiency of the proposed implementation.

Last but not least, the successful application of the conceptual implementation on the mathematical and engineering problems served as a confirmation of its capacity to form the foundation of the proposed model selection technique.



## 5. Model Selection

For a quick restatement of the problem justified in Chapter 1, assume a group of models describing the output  $Y$  in terms of the input  $X$  are available. For some reason, mostly being the future predictions we need a reliable model out of this group. Computational and time limitations usually force us to pick only one model which supposedly offers the highest accuracy and efficiency. The search for this *best* model has resulted in the evolution of the model assessment strategies which are inherently in need of benchmarks to come up with quantitative measures of how models perform in predicting a desired phenomenon. A benchmark model could be defined as the closest possible abstraction of the mentioned phenomenon to be used as its representative in validation and assessment problems. Experimental data, for instance, is widely employed as benchmark for model validation and further for model selection. Though, it is, commonly, mistaken as the exact counterpart of the real phenomenon to be studied. Practically, if a model fails at resembling the experiment, it will be readily rejected. However, as discussed before, experimental data is no exception to being susceptible to imprecision, incompleteness and human-made/systematic error. The same characteristics apply to the numerical solutions even in their highest levels of complexity. In fact, complicated models are rather more uncertain than simpler models since they are grounded on the basis of more assumptions and subsequently are more limited in the range of application. Yet, in the absence of any experimental data, the most complex models are taken as the benchmarks for the validation of a group of less known models. The point to be made here is that neither experimental background nor more complexity necessarily suggest a model is a suitable choice for benchmark in assessment problems.

In order to clarify the point, consider the models shown in Figure 5.1 which are supposed to define the response  $y$  on the account of having parameter  $x$ . Note that, here,  $x$  and  $y$  represent a two-dimensional problem (Multidimensional problems are designated by  $X$  and  $Y$ ). We could immediately recognize model (d) as an outlier and pick, most probably, model (a) or (c) as the best model due to their least uncertainty. Before commenting on this judgment, let us define the probable output space as the range in which the output  $y$  could land in according to our current knowledge. We shall call this the design space because it forms the foundation for the engineering design. Needless to say, how an underestimation of the design space would lead to a nonconservative design. Also, note

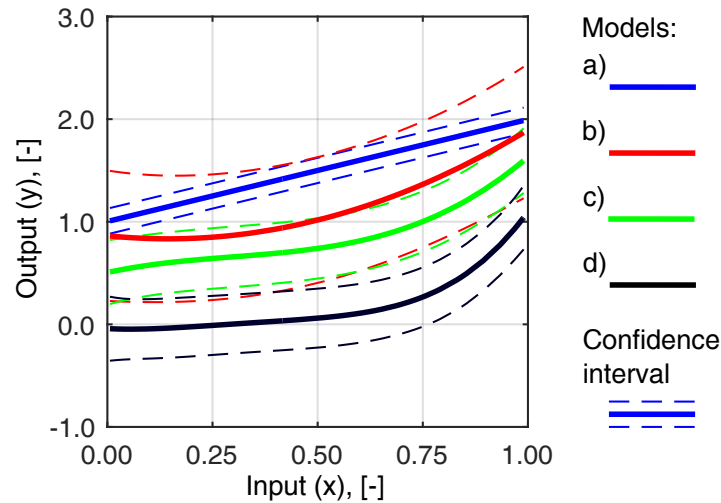


Figure 5.1. Hypothetical set of plausible models in the design space.

that our current knowledge is limited to what we know of  $y$  through the models at hand. This translates into the fact that if the majority of the models are wrong it is expectable that our collective understanding of  $y$  is wrong. In the latter case, it is no surprise that out of a group of wrong models a wrong model (maybe not the worst, anyhow) is selected as the best. There is, obviously, low chance of fishing the appropriate model out of a pool of models in which the plausible ones are in minority.

In the example shown in Figure 5.1, the design space is limited to the outputs from models (a) to (d) regardless of their experimental or numerical nature and their complexity. As long as there is no access to any specific information concerning the performance of the models, they could be assumed to be part of the space and of the same level of importance. In other words, none of them has any advantages whatsoever over the others in representing the reality. In such a case, clearly, the immediate response loses its credit. Take for example the following scenarios. Scenario 1: the outlier model (d) could as well be the closest to the reality which implies mostly wrong models have been collected. Scenario 2: in spite of being an outlier, model (d) represents the experimental data or the most complex model i.e. the considered benchmark has been misleading. Scenario 3: the choice of model (a) or (c) for the best model fails to cover the design space meaning there is a high probability that the output  $y$  takes values out of the prediction bounds of the selected model. Certainly, there can be lots of other scenarios depending on the number of models building up the design space and the prior knowledge about their performance. At this point, it is well understood that not only the choice of the benchmark models but also the uncertainty properties of the models to be validated affect the model selection process and consequently the design space. In the present thesis, I propose an assessment technique which attempts to evaluate the models in the design space based on a systematic comparison considering their uncertainty and sensitivity properties.

## 5.1. Assessment Methodology

To begin with, it is necessary to restate that every model is by definition an abstraction of the reality and hence is treated accordingly unless specific information regarding the performance of the models is available. This is the fundamental idea behind the proposed model selection technique. It is based on the assumption that every single competing model has the probability to be the *best* representation of the reality and therefore a benchmark.

Assume models  $\mathcal{M}_1, \dots, \mathcal{M}_M$  are the  $M$  models in the design space describing  $Y$  in terms of  $K$  parameters  $X_1, \dots, X_K$ . The benchmark model, conventionally being either the experimental model or the most complex one, is denoted as  $\mathcal{M}_{bmk}$  and is a member of the aforementioned  $M$  models. Following the traditional model validation techniques, we have checked the results of models  $\mathcal{M}_i$  where  $i = 1, \dots, M$  and  $i \neq bmk$  against the results from  $\mathcal{M}_{bmk}$  in a one-by-one comparison. Obviously, better agreement with the benchmark model improves the rank of a model in the group. The highest ranked model, consequently, shall be selected as the *best* among all the models and used for further studies. This approach could be too risky since it purely relies on the only choice of the benchmark. Not to forget that it is founded on the precarious assumption that the experimental or the most complex models are definitely the *best* benchmarks. At this point the proposed model selection technique deviates from the traditional validation. As mentioned in the chapter's opening, I assume any plausible model could play the role of the benchmark as long as all the models in the design space are treated equally. The proposed method is not based only on one benchmark but as many as the competing models and does not prejudice the models based on their nature or complexity.

Basically, we are interested to assess our pool of models on the account that any given model from the pool is the *best* model. In the first step,  $\mathcal{M}_j$  where  $j$  can be any value from 1 to  $M$ , is picked as the benchmark. At this stage, models have no advantage over each other particularly stemming from their experimental or numerical nature or complexity level. So, the choice of  $\mathcal{M}_j$  is completely arbitrary. In order to assess the pool of models, there is a need to specify a quantitative measure of how every model  $i$  in the pool, where  $i$  can be any value between 1 and  $M$  except for the predefined  $j$ , compares with respect to the selected benchmark. This measure could be used as a criterion to rank the models based on their performance in predicting results close enough to the benchmark results. In this thesis, I propose the probability of failure in prediction as such a measure.  $P_{ij}$  is defined as the probability that  $\mathcal{M}_i$  fails in producing results in the vicinity of  $\mathcal{M}_j$ . The acceptable lower and upper bounds are assumed to be a standard deviation away from the mean value the  $\mathcal{M}_j$  results. The probability-based comparison of the performance of the models in predicting  $\mathcal{M}_j$  is founded on a straightforward concept and therefore is easy to

comprehend and apply. Moreover, probabilities are always values in the  $[0, 1]$  range and consequently very convenient to work further on.

The probability of failure in prediction can be calculated for any two models, one of which is the benchmark. Computation of the  $P_{ij}$ s for the entire pool of models, i.e.  $M - 1$  pairs of  $\mathcal{M}_i$  (where  $i = 1, \dots, M$  and  $i \neq j$ ) and  $\mathcal{M}_j$ , reveals how the models perform in case  $\mathcal{M}_j$  is the *best* model or the benchmark. Referring back to basic assumption that every plausible model has the potential to play as the benchmark, what is done so far is only one scenario out of  $M$  possible scenarios for the benchmark model. To consider the potential for the other models in the pool, the process described above should be repeated for every single member of as the benchmark. At the end of the iterations, we should end up with  $M \times M$  matrix of  $P_{ij}$ s in which element  $ij$  denotes the probability that model  $i$  fails in predicting model  $j$ . Consequently, we may assume the model with the least probabilities of failure in predicting and being predicted is a reasonable representative of the group of models. But before rushing into the final conclusion, some improvements are made to increase the reliability of the procedure as outlined so far.

In order to calculate the  $P_{ij}$ , the outputs from models  $i$  and  $j$  must be compared along their entire parameter space considering their uncertainty properties, namely,  $\mu$  and  $\sigma$ . Two issues can be recognized here. First, if the models are highly nonlinear, the mean and the standard deviation over the entire parameter space do not appropriately represent the behavior of the models. Second, in the course of relating the models over their parameter space, comparison is unnecessarily done over dimensions corresponding to insignificant parameters. To avoid the aforementioned issues, the recommended implementation for the sensitivity analysis in the previous chapter was used to propose an enhanced model selection technique. In particular, the subdividing approach along each parameter range was employed not only to compare the models along one dimension in the parameter space at a time but also to localize the comparison in smaller subdivisions of each parameter range.

As before, let us assume a design space of  $\mathcal{M}_1, \dots, \mathcal{M}_M$  in which each member model has  $K$  parameters. So, all the models tend to produce the output  $Y$  from the set of inputs  $X_1, \dots, X_K$ . It can, certainly, be expected that not all the models in the design space have exactly the same parameters in terms of definition and number. In this case, decision on the  $K$  parameters to be included in the model selection procedure is based on their relevance to the output. Take, for instance, the four models in Figure 5.2 as the models defining the design space. Altogether, the models have 21 parameters out of which 5 are shared among the models and consequently 14 are unique. Now, every data sample can be defined by the information coming from these 14 parameters regardless of their role in a specific model. In fact, every model is fed with this information and merely takes advantage of the part that is applicable to its function. Obviously, the unused part of the

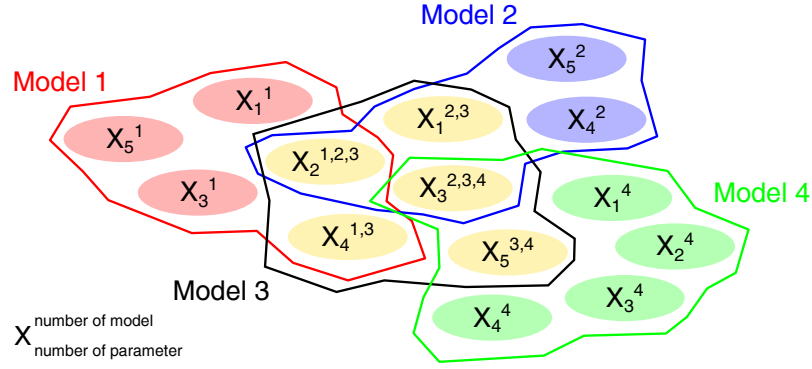


Figure 5.2. Example parameter space for four hypothetical models.

information has no effect on the model response. Accordingly, the collection of parameters to be selected as the parameter space for all the models should at least cover all the corresponding functional needs. In the example mentioned above, the collective parameter space would contain 14 parameters over which all the models could operate regularly. It should be noted that an extensive scatter in the core input parameters of various models describing the same phenomenon suggest that there is a significant uncertainty regarding the influential parameters. Nevertheless, the aforementioned approach to form the parameter space has the advantage that all the potentially influential parameters can be included and model outputs with slightly different parameter spaces can be compared.

To begin with the model selection process,  $\mathcal{M}_j$  and  $\mathcal{M}_i$  (where  $i$  and  $j$  take values between 1 and  $M$  and  $i \neq j$ ) are arbitrarily selected from the pool of models as the benchmark and the model to be checked against it, respectively. Following the same procedure as for the sensitivity analysis, parameter  $k$  (takes any value from 1 to  $K$ ) is picked and the outputs from  $\mathcal{M}_i$  and  $\mathcal{M}_j$  are momentarily studied in the two-dimensional  $Y-X_k$  space. This space is divided into  $S$  subdivisions of equal probability along the  $X_k$ . In each subdivision  $s$  the mean and the standard deviation of the benchmark response are calculated and denoted, in the same order, as  $\mu_j^{sk}$  and  $\sigma_j^{sk}$ . The acceptable bounds for the models to be checked against the benchmark is, therefore, within  $\pm\sigma_j^{sk}$  of the  $\mu_j^{sk}$ . Now, the probability  $P_{ij}^{sk}$  that  $\mathcal{M}_i$  fails in predicting  $\mathcal{M}_j$  in subdivision  $s$  along the range of the parameter  $X_k$  can be calculated following the Equation 5.1.

$$P_{ij}^{sk} = P(\mathcal{M}_i^{sk} \notin [\mathcal{M}_j^{sk} - \sigma_j^{sk}, \mathcal{M}_j^{sk} + \sigma_j^{sk}]) \quad (5.1)$$

The  $P_{ij}^{sk}$  can be calculated for all the  $S$  subdivisions along the parameter range. The average value of the computed  $P_{ij}^{sk}$ s, as given in Equation 5.2, is assumed to be the probability of failure in prediction in the space of the  $k$ th parameter.

$$P_{ij}^k = E_s(P_{ij}^{sk}) \quad (5.2)$$

The above procedure should be repeated in all the  $K$  dimensions of the parameter space resulting in a total number of  $K$  probabilities of failure in prediction for this pair of  $\mathcal{M}_i$  and  $\mathcal{M}_j$ . At this point, the aforementioned  $K$  probabilities could be summed up to form a unique final grade for the performance of model  $i$  in predicting the benchmark  $j$ . The immediate consequence of the summation is that all the parameters have been treated equally in terms of their effect on the benchmark output. Although, sensitivity analysis might prove otherwise, i.e. different input parameters influence the output in different levels from negligible to considerable. The current assessment technique, therefore, should be able to scale the  $P_{ij}^k$ s with respect to the importance of  $X_K$  for  $\mathcal{M}_j$ . The intention is to weigh down the  $P_{ij}^k$ s corresponding to the insignificant parameters while on the contrary the  $P_{ij}^k$ s for the influential parameters are weighed up. This is best done using the first order sensitivity indices by SOBOL (1993) using the conceptual implementation as discussed in the previous chapter and repeated in Equation 5.3 for convenience.

$$S_k = \frac{V_s(E_{X_k}(Y|X_k^s))}{V(Y)} \quad \text{where: } k = 1, \dots, K \quad \text{and} \quad s = 1, \dots, S \quad (5.3)$$

Eventually, the performance of  $\mathcal{M}_i$  in predicting  $\mathcal{M}_j$  can be evaluated according to Equation 5.4 where  $(P_{fp})_{ij}$  is the final probability that  $\mathcal{M}_i$  fails in prediction of  $\mathcal{M}_j$  and  $S_k^j$  is the sensitivity of the output of the benchmark  $j$  to the parameter  $k$ .

$$(P_{fp})_{ij} = \sum_{k=1}^K P_{ij}^k S_k^j \quad (5.4)$$

$(P_{fp})_{ij}$  is always in the  $[0, 1]$  interval which is a very convenient property. Since the choices of  $i$  and  $j$  have  $M$  possibilities each, the final product of the assessment technique so far is a  $M \times M$  matrix of  $(P_{fp})_{ij}$ s. It is worth to mention that the final matrix is not necessarily symmetric, since it brings the sensitivity indices of each individual benchmark into the computations. Element  $ij$  in this matrix is the final probability that  $\mathcal{M}_i$  fails in predicting  $\mathcal{M}_j$ . In other words, each column  $j$  stands for the performance of all models in predicting model  $j$  as the benchmark whereas each row  $j$  shows how model  $j$  has performed in predicting all the other models. If the *best* representative model is assumed to be the best in predicting and being predicted by other models, then it should be the one with the lowest sum of the corresponding row and column, i.e. the lowest grade  $G$  as given in Equation 5.5.

$$G_j = \sum_{i=1}^M (P_{fp})_{ij} + \sum_{i=1}^M (P_{fp})_{ji} \quad (5.5)$$

The lowest (best) graded model shall be announced as the highest-ranked in the studied group of models. As the maximum value of  $(P_{fp})_{ij}$  equals to one, the maximum value of  $G_j$  is simply  $2 \times (M - 1)$ . This maximum can be used to further normalize the grades so that they fit in the  $[0, 1]$  interval, too. We should have in mind that the proposed method does not seek the *best* model. But rather, it searches for the model which is most likely the *best* representative of the design space. In fact, it reduces the risk of choosing an outlier by sticking to a trade-off solution. In order to confirm such statements, the method was applied to a series of mathematical and engineering models of numerical and experimental natures from the previously introduced database. In what follows, the selected problems and the resulting accomplishments of the proposed model selection technique are presented and discussed.

## 5.2. Benchmark Problem

It was mentioned in Section 5.1 that in this study models were not prejudged specifically due to their experimental or complex nature. As a result, in a group of plausible models the quality assessment process involves numerous scenarios depending on the arrangement of the models in the output-input space. One arrangement of interest for instance was shown in Figure 5.1 for a group of five models with an outlier. There can, clearly, be an infinite number of such arrangements depending on the number and behavior of the models as well as the context in which they are applied. The proposed model selection technique was expected to come up with reasonable rankings of the models regardless of their specific arrangement. In order to check if this expectation could be fulfilled simple mathematical functions were selected for a benchmark study. The intention was to create all the possible arrangements of the models with a few parameters controlling their distance and scatter and capture the performance of the proposed method. Some particular arrangements such as the one presented in Figure 5.1 could also be individually presented for additional discussions.

### 5.2.1. General Conditions

The selected functions, designated by  $\mathcal{M}$  as shown in Figure 5.3, included  $\mathcal{M}_m : y = x^m$  in the  $[0, 1]$  interval where  $m = 1, \dots, M$  and  $M$  is the total number of models. They produce quite close results in the mentioned range and therefore are acceptable as com-

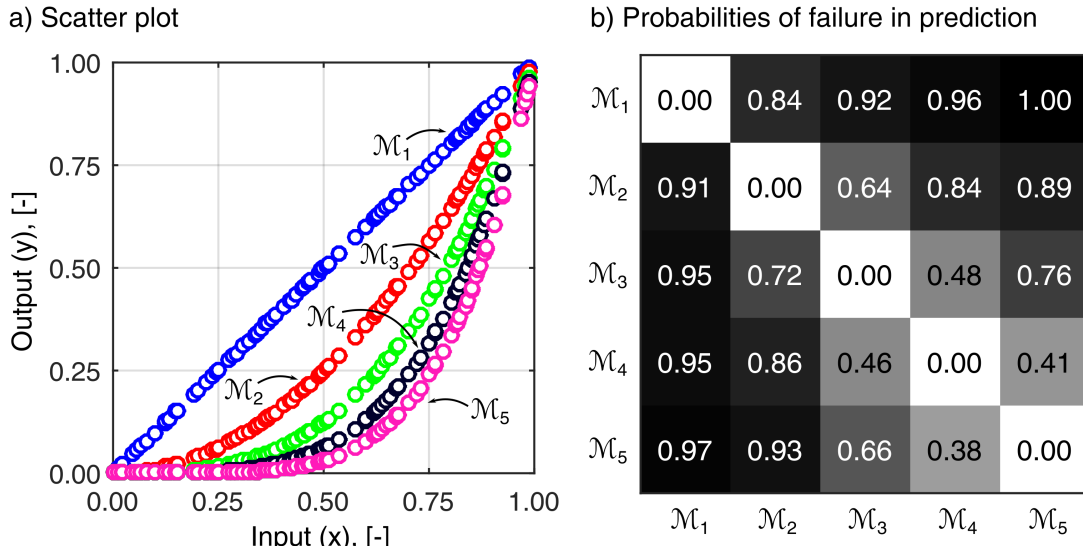


Figure 5.3. Selected benchmark functions: a) scatter plot b) probabilities of failure in prediction.

peting models defining a hypothetical phenomenon. Figure 5.3 additionally includes the probabilities of failure in prediction resulted from the application of the model selection technique (calculated using Equation 5.4). In the original state, accordingly,  $\mathcal{M}_4$  appears to be the best representative of the five models.

Note that the selected models are functions of a single parameter which is rarely the case in practical problems. Yet, they could be appropriate choices to demonstrate the performance of the proposed method in a single dimension since the multidimensional parameter spaces are, in fact, treated individually in each dimension following the same straightforward procedure.

The primary arrangement of the selected models could not be a representative of the practical problems in its original form. The models were, therefore, disturbed using random error terms to create more realistic engineering arrangements. The error term,  $\epsilon$ , as seen in Equation 5.6 was set to be a function of  $\alpha$  controlling the scatter and  $\beta$  regulating the shift from the original state for each model.

$$y^* = y + \epsilon \quad \text{where} \quad \epsilon = \alpha\varepsilon + \beta \quad (5.6)$$

$\varepsilon$  is a vector of the same size as  $y$  containing random values from a uniform distribution in the  $[-1, 1]$  interval. The physical interpretation of these parameters are shown in Figure 5.4 for  $y = x$  considering all the combinations of  $\alpha$  and  $\beta$  given that they only take the values of 0 and 1. It is clear that large values of  $\alpha$  and  $\beta$  lead to large errors through shifting and dispersing the data from its original state.



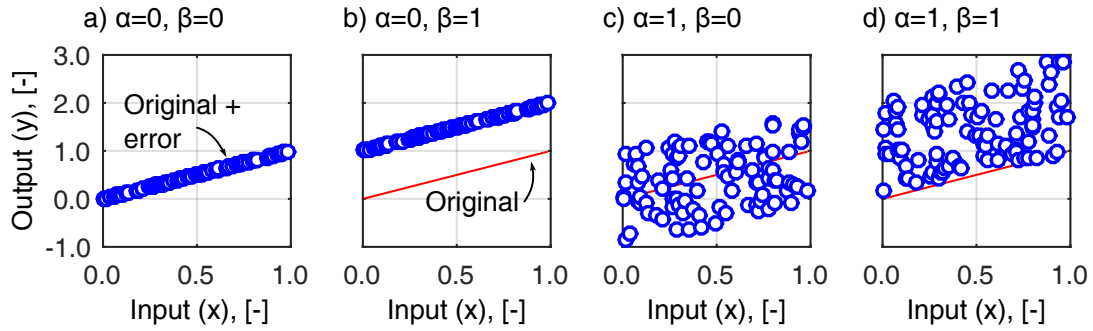


Figure 5.4. Influence of the error parameters  $\alpha$  and  $\beta$  on  $y^*$  when  $y = x$ .

The disturbed functions were, accordingly, calculated by adding the error term to the original functions. In order to clarify the procedure, here the arrangement of the models shown in Figure 5.1 was recreated using the basic functions and error terms presented in Table 5.1. Figure 5.5 illustrates the resulting recreation which in connection to Table 5.1 makes it well clear how the  $\alpha$  and  $\beta$  control the arrangement of the models. Application of the proposed model selection technique on this particular group of models is also shown in Figure 5.5 in the form of the matrix of the probabilities of failure in prediction. It is not surprising that the outlier model (i.e.  $\mathcal{M}_4$ ) has ended up with the largest values, implying that it cannot represent the group of models. In contrast,  $\mathcal{M}_2$  seems to be the best representative following the circumstances. Such an arrangement, in fact, exemplifies the yield displacement estimation results using different methods which are discussed in Section 5.3.

### 5.2.2. Parametric Study

The proposed model selection technique was challenged through a parametric study. All the possible arrangements of four models were created using a full grid of  $\alpha$  and  $\beta$  combinations. The selected four models included  $\mathcal{M}_1 : y_1 = x + \epsilon_1$ ,  $\mathcal{M}_2 : y_2 = x + \epsilon_2$ ,  $\mathcal{M}_3 : y_3 = x + \epsilon_3$  and  $\mathcal{M}_4 : y_4 = x + \epsilon_4$  in each of which the error term was calculated based on Equation 5.6. In order to build all the possible arrangements of the models, the error terms were varied by setting  $\alpha$  and  $\beta$  to 0, 0.5 and 1 standing for small, medium and large values, respectively. It is readily understood that nine different error terms could

Table 5.1. Error parameters used for the recreation of Figure 5.1.

	$\mathcal{M}_1$	$\mathcal{M}_2$	$\mathcal{M}_3$	$\mathcal{M}_4$
Functions	$x + \epsilon_1$	$x^2 + \epsilon_2$	$x^3 + \epsilon_3$	$x^4 + \epsilon_4$
$\alpha$	0.10	0.50	0.25	0.25
$\beta$	1.00	0.80	0.60	0.00

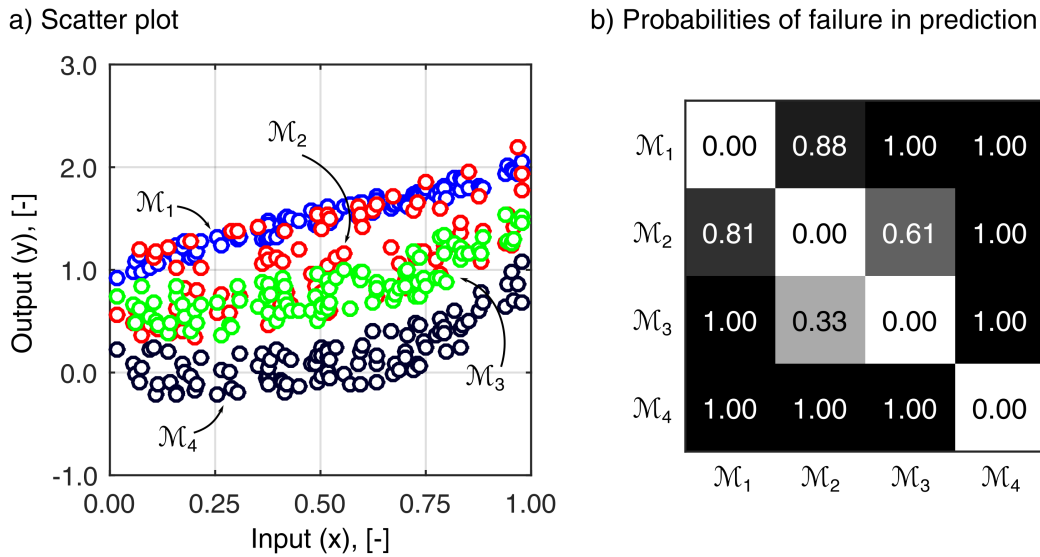


Figure 5.5. Recreation of the models presented in Figure 5.1: a) scatter plot b) probabilities of failure in prediction.

be computed using the full grid combinations of  $\alpha$  and  $\beta$ . The resulting states of the disturbed models can be imagined if we refer to Figure 5.4 which contained the full grid combinations of  $\alpha$  and  $\beta$  in case they took only the values of 0 and 1.

The four assumed models could be disturbed to nine distinct states using the aforementioned error terms. The disturbed models could then be arranged in  $9^4 = 6561$  different arrangements which provided an appropriate benchmark to apply the proposed model selection technique. Therefore, the method was used in each of the 6561 arrangements to rank the models involved. In the primary step, the best (lowest) grades were categorized based on the  $\alpha$  and  $\beta$  combination of the corresponding highest-ranked models. A statistical study on the resulting data, as shown in Figure 5.6 revealed that  $\alpha$  significantly influences the best grade.  $\beta$ , in contrast, seems to be of negligible importance to the best grade.

Obviously, as seen in Figure 5.6, the models with larger  $\alpha$  (i.e. scatter) have gained lower grades in general. It is clear that the proposed model selection technique has a tendency to assign the highest ranks to the more scattered models. This is a direct consequence of the fact that the scattered models have higher chances of covering and accordingly representing the design space. Although, the perpetual choice of the largest scatter as the representative model is not a good strategy and should be avoided. Consequently, the study was further extended to find out if the proposed method always picked the largest scattered model as the highest-ranked regardless of the arrangement of the models. Table 5.2 contains the number of cases out of 6561 total arrangements where the highest-ranked model particularly had the smallest or largest scatter ( $\alpha$ ) or shift ( $\beta$ ) in the corresponding group of models. In some cases all the models had the same values for  $\alpha$  or  $\beta$ . Such cases are

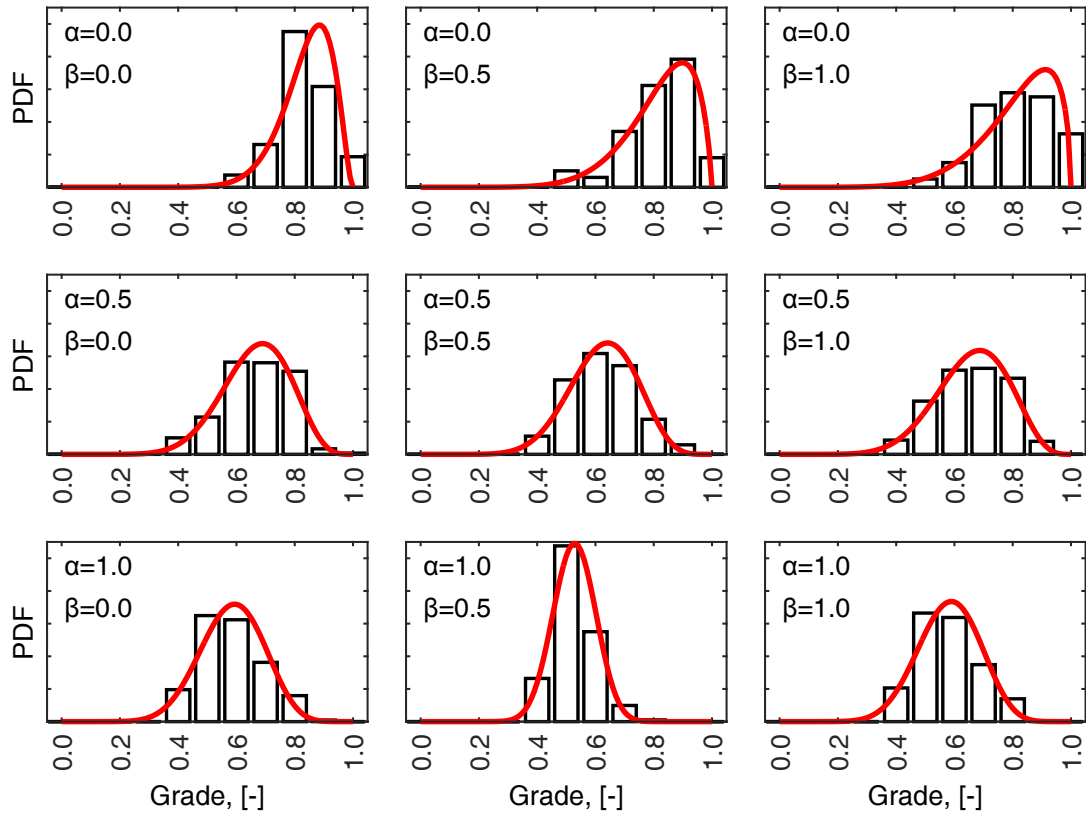


Figure 5.6. Probability distribution of the grades scored by the highest-ranked (lowest graded) models categorized according to the  $\alpha$  and  $\beta$  combinations.

designated as *equal* in Table 5.2. In addition, the same statistical information is provided for the lowest-ranked (worst-graded) models.

It is not surprising that in 54% of the 6561 cases the highest-ranked model had the largest  $\alpha$ . It is, however, interesting that in 3% of the cases the smallest-scattered model was selected as the representative of the group of models. Moreover, in 11% of the cases the largest-scattered model was even ranked as the worst model. The two aforementioned properties prove that the proposed model selection technique does not automatically rank the most scattered model as the best. It, rather, systematically compares the models and

Table 5.2. Status of the parameters  $\alpha$  and  $\beta$  for the highest and lowest-ranked models (values are presented as the percentage of the occurrences out of the total 6561 studied cases).

	Cases where the model had the:					
	smallest		largest		equal	
	$\alpha$	$\beta$	$\alpha$	$\beta$	$\alpha$	$\beta$
Best (lowest) grade	3	22	54	10	4	4
Worst (highest) grade	43	34	11	44	4	4

offers a ranking based on their capability to represent each other. It is also noteworthy that in 44% of the cases the worst model had the largest shift implying that the model was potentially an outlier. Evidently, the proposed method is also able to detect the general trend by disregarding the outliers. In sum, the promising results from the benchmark study qualified the proposed model selection study for further application to real engineering problems.

### 5.3. Engineering Problems

A real example of what was presented in Figure 5.1 can be observed during the yield displacement estimation for RC walls. As mentioned in Section 2.3, the response parameter of interest was chosen to be the yield displacement since it is a characteristic point in the wall behavior. The availability of various approaches and the variability of the resulting approximations of the yield displacement made the choice of a universal approach complicated. In fact, as in the case of Figure 5.1, numerous scenarios regarding the validity of the competing approaches can be considered. Therefore, the problem is an appropriate choice to check the performance of the proposed model selection technique.

The method was applied to the data stored in the database of RC walls (both experimental and numerical parts). Accordingly, two different case studies were performed. The following section is dedicated to more details regarding the studied yield displacement estimation methods. Within the model selection process, the five selected methods were designated with  $m_1, \dots, m_5$ . Experimental, MVLEM and FSIDB models were distinguished by being labeled as  $\mathcal{M}_1, \dots, \mathcal{M}_3$ , respectively.

#### 5.3.1. Studied Yield Displacement Estimation Methods

Among the several available methods to estimate the yield displacement which were discussed previously in Section 2.3, a considerable number (used normally in practical design) rely on the bilinearization techniques. Such methods tend to idealize the non-linear force-deformation relationship and return rough estimates of the yield displacement. Since methods of this kind are quite popular, specifically in design codes, we chose three of them to perform an assessment study. The methods, as shown in Figure 5.7, included the proposal from PAULAY AND PRIESTLEY (1992) and the recommendations by ATC40 (1996) and FEMA273 (1997). In this Figure,  $V$  and  $\Delta$  stand for the base shear and the top displacement, respectively. Along with the aforementioned methods, two empirical relationships introduced by PRIESTLEY ET AL. (2007) and KAZAZ ET AL. (2012) were used to compute the yield displacement.

## 5.3.1.1. PAULAY AND PRIESTLEY (1992)

PAULAY AND PRIESTLEY (1992) suggested the effective secant stiffness to 75% of the ideal yield strength for the elastic branch of the idealized force-deformation curve. Their model assumed a zero post-yield stiffness (see Figure 5.7a).

## 5.3.1.2. ATC40 (1996)

Later, ATC40 (1996) recommended to idealize the capacity curve by a bilinear curve. The code advised to use the initial stiffness of the force-deformation relationship as the elastic stiffness to the yield point for the idealized curve (see Figure 5.7b). The post-yield stiffness had to be found based on the equal energy absorption criterion. This concept dictates that the energy absorbed by the real and idealized systems should be identical, i.e. the area under the real and the idealized curves should be equal.

## 5.3.1.3. FEMA273 (1997)

FEMA273 (1997) introduced a bilinearization technique mainly to determine the structural period. The stiffness of the elastic branch was found such that the idealized curve intersects with the real curve at 60% of the yield strength (see Figure 5.7c). The stiffness of the plastic branch was specified by minimizing the difference between the areas under the curves.

## 5.3.1.4. PRIESTLEY ET AL. (2007)

PRIESTLEY ET AL. (2007) developed simplified relationships as approximations of the yield displacement for the sake of displacement-based design. The relationships addressed several structural types including RC walls. Equation (5.7) conditions the yield curvature of the wall on its length ( $L_w$ ) and the yield strain of the flexural reinforcement ( $\epsilon_y$ ).

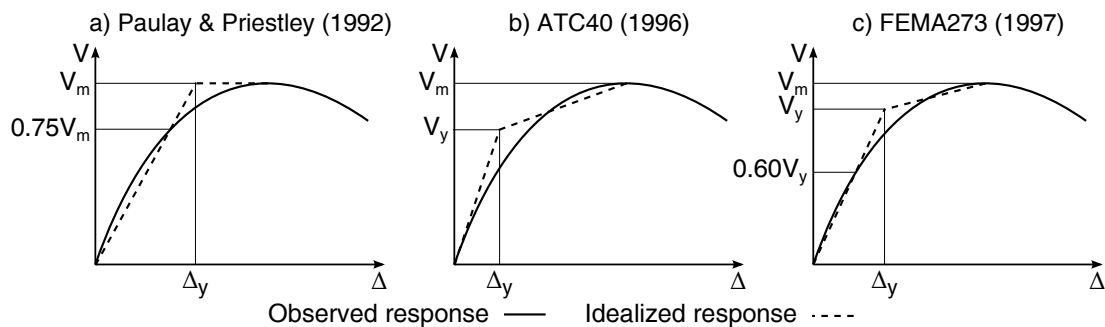


Figure 5.7. Studied bilinearization methods for yield displacement estimation.

$$\phi_y = 2.0(\epsilon_y/L_w) \quad (5.7)$$

It should be noted that in the present study the yield displacement estimation techniques were investigated. Therefore, the yield curvature was converted to the yield displacement by assuming a uniform distribution of the curvature over  $0.5L_w$  along the height of the wall.

#### 5.3.1.5. KAZAZ ET AL. (2012)

In a recent study, KAZAZ ET AL. (2012) proposed empirical relationships for deformation limits of RC walls based on parametric numerical analysis. The parameters included the shear-span-to-wall-length ratio, wall length, axial load ratio, normalized shear stress, the amount of horizontal web reinforcement, and the amount of longitudinal reinforcement at the confined boundary of the wall. Equation (5.8) expresses the yield drift ratio in terms of the wall length ( $L_w$ ) and the longitudinal boundary reinforcement ratio ( $\rho_b$ ).

$$\Delta_y = 0.125(e^{-0.116L_w})(\rho_b^{0.225}) \quad (5.8)$$

#### 5.3.2. Database: Numerical Part

Further investigation on the performance of the proposed model selection technique was primarily limited to the wall samples generated randomly using the MVLEM in the numerical part of the database. Obviously, this provided the possibility to perform relatively large number of analysis on a random basis. Therefore, the results could be statistically more reliable. As mentioned in Section 3.2, the required variable and constant parameters for the numerical simulations were regulated according to those of the experimental counterpart. The parameters defined in Table 3.1 were set to vary in the ranges from Table 3.2. The constant parameters were selected based on the average values of the corresponding parameters in the experimental part of the database as shown in Figure 5.8. The selected values are presented in Table 5.3.

1000 samples were generated using the Latin hypercube sampling (MCKAY ET AL. (1979)) considering uniform distributions along the given ranges of the parameters. MVLEM of each sample was built in OpenSees and nonlinear static analysis was performed (refer to Section 3.2.1 for more information). The yield displacements were, then, calculated following the five approaches described in Section 5.3.1 (i.e.  $m_1$ : PAULAY AND PRIESTLEY (1992),  $m_2$ : FEMA273 (1997),  $m_3$ : ATC40 (1996),  $m_4$ : PRIESTLEY ET AL. (2007) and  $m_5$ : KAZAZ ET AL. (2012)). The results are located on the corresponding force-deformation



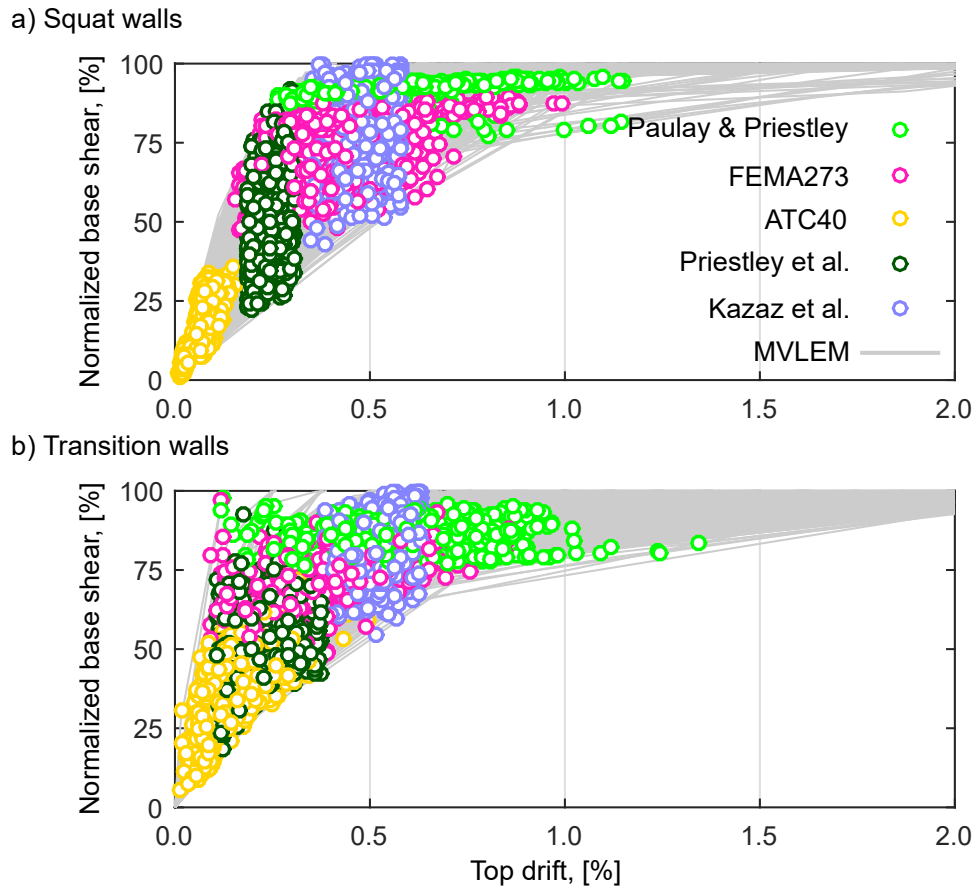


Figure 5.9. Estimated yield drifts for the MVLEM-generated specimens in the numerical part of the database (base shear is normalized to its maximum value for each wall).

of the parameter space. Though, the knowledge is purely qualitative and more importantly subjective. The quantitative measurement of the influence that each parameter imposes on the estimated yield displacement was done using the sensitivity analysis implementation from Chapter 4. The resulting first order sensitivity indices are shown in Figure 5.11. Now, the methods appear to agree on the first order effects for the most part. It is of particular interest that the reinforcement properties are identically recognized as the dominant parameters for all the studied methods since they govern the yielding process.

The question yet to be answered was whether the methods could be evaluated quantitatively. The ultimate goal here was to find the most representative method through which the design space was reasonably covered. To achieve this goal, a systematic comparison of the methods was crucial. The proposed model selection technique was, therefore, applied to the data. Figure 5.12 shows the final matrix of the probabilities of failure in prediction calculated using Equation 5.4. The corresponding grades are presented in Table 5.4. The grades were normalized to their corresponding maximum value as discussed in Section 5.1.



Y, [%]: Estimated yield drift for generated transition walls using:

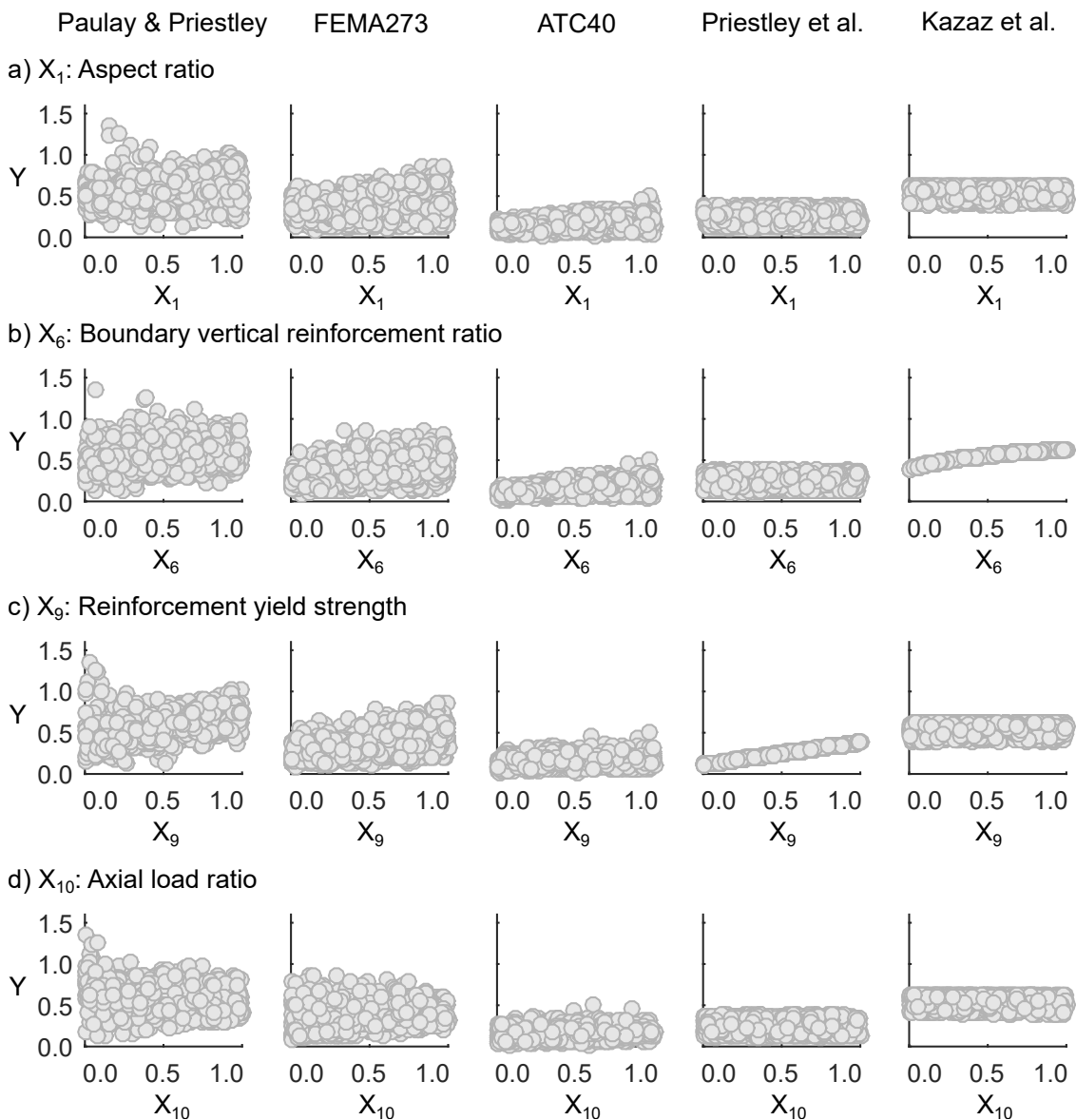


Figure 5.10. Scatter plots of the estimated yield drifts against: a) aspect ratio, b) boundary vertical reinforcement ratio, c) reinforcement yield strength and d) axial load ratio for the MVLEM-generated specimens in the numerical part of the database.

Based on Figure 5.12 and Table 5.4, FEMA273 could be announced as the best representative among all the methods thanks to its lowest probabilities of failure in prediction. ATC40, in contrast, is caught as an outlier and therefore, has shown the worst performance.

The proposed model selection technique presented promising results on the generated simulations. It should be noted, however, that in many practical cases the available data can be orders of magnitude less than what was worked on here. A very good example

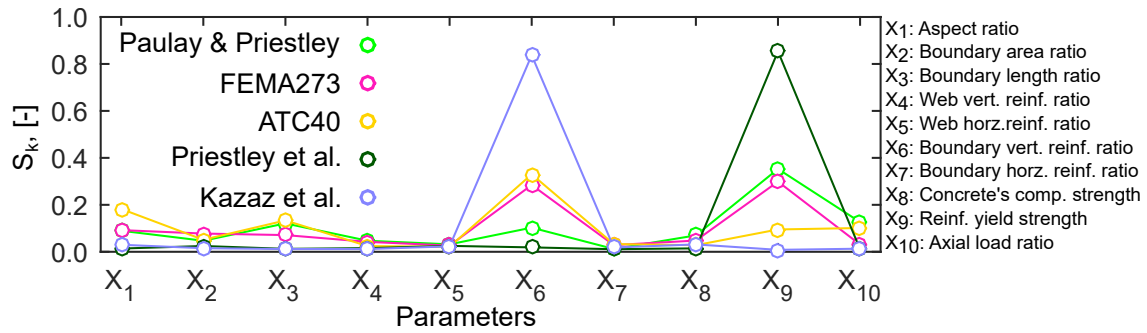
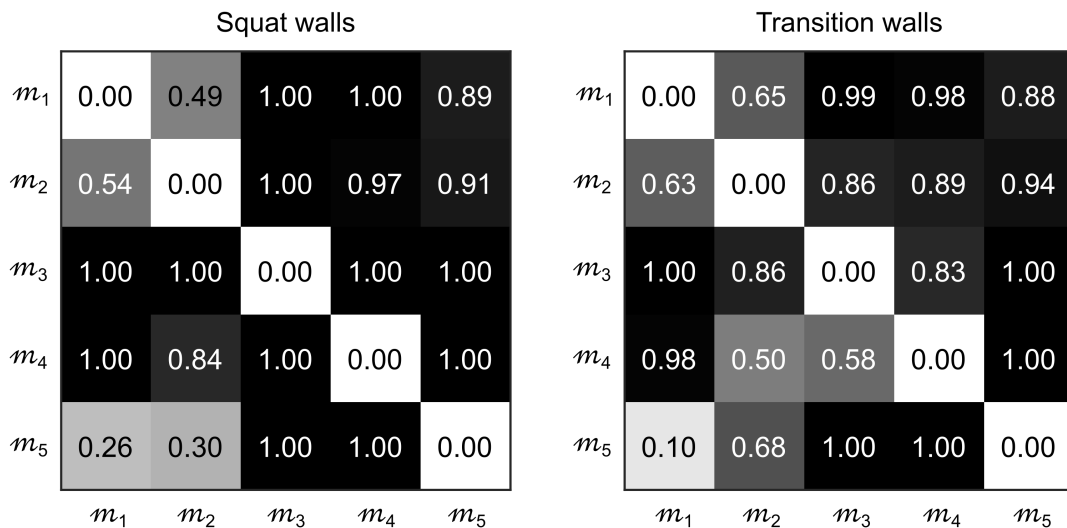


Figure 5.11. First order effects of the input parameters on the estimated yield drifts for the MVLEM-generated specimens in the numerical part of the database.

is the data collected on the yield displacement of RC walls in the experimental part of the database (see Section 3.1). In the final step, the proposed method was applied to the aforementioned set of specimens to challenge its capability of dealing with limited data.



$m_1$ : Paulay & Priestley,  $m_2$ : FEMA273,  $m_3$ : ATC40,  $m_4$ : Priestley et al. and  $m_5$ : Kazaz et al.

Figure 5.12. Estimated probabilities of failure in prediction for the studied methods based on the data from the MVLEM-generated specimens in the numerical part of the database (colors represent the corresponding values with white for 0.00 and black for 1.00).

Table 5.4. Normalized final grades for the studied methods based on the data from the MVLEM-generated specimens in the numerical part of the database.

	Paulay & Priestley	FEMA273	ATC40	Priestley et al.	Kazaz et al.
Squat	0.77	0.76	1.00	0.98	0.79
Transition	0.78	0.75	0.89	0.84	0.83

### 5.3.3. Database: Experimental and Numerical Parts

In the final attempt to check the performance of the proposed model selection technique, the core data included the response parameter of interest from all the specimens recorded in the experimental part of the database. As mentioned earlier in Section 3.1, the specimens were divided into two categories of squat and transition walls with 51 and 55 walls in each category, respectively. The numerical part of the database was additionally involved by recreating each specimen using the MVLEM and the FSIDB. Each specimen was modeled and analyzed by means of the variable and constant parameters identical to the counterpart parameters of the specific specimen. As a result, for every specimen in the experimental part of the database three force-deformation curves coming from experiment, MVLEM and FSIDB were available as shown in Figures A.1 and A.2 for the squat and transition walls, respectively.

The methods described in Section 5.3.1 were used to estimate the yield displacement for the collected specimens. Figures A.1 and A.2, in the same order, depict the results for the individual squat and transition specimens. The collective results are shown in Figures 5.13 and 5.14 for the squat and transition walls, respectively. The immediate reflection is that the figures look quite similar to the Figure 5.9 from the previous section. In the same manner as before, the major observations include the underestimation of the yield displacement by ATC40, quite independent approximations from PRIESTLEY ET AL. (2007) and KAZAZ ET AL. (2012) and finally physically meaningful estimations by PAULAY AND PRIESTLEY (1992) and FEMA273. Again, this is a qualitative assessment which can go even a further step forward by bringing in the observed yield displacement as employed in Section 4.3.3 and shown in Figure 4.21. The estimated yield displacements are compared to the observed counterparts in Figure 5.15 for the transition walls. The figure practically confirms the preliminary qualitative assessment as the PAULAY AND PRIESTLEY (1992) and FEMA273 tend to scatter around the diagonal of the plots. In contrast, the results from PRIESTLEY ET AL. (2007), KAZAZ ET AL. (2012) and ATC40 diverge from the observation which was also anticipated according to the basic evaluation.

Following the preliminary evaluation of the methods, the quantitative assessment was performed using the proposed model selection technique. The assessment was conditioned based on two individual inquiries. The first inquiry concerned the evaluation of  $m_1, \dots, m_5$  given the data resulting from  $\mathcal{M}_1, \dots, \mathcal{M}_3$ . The second inquiry, in contrast, cared for the assessment of  $\mathcal{M}_1, \dots, \mathcal{M}_3$  given the data estimated by  $m_1, \dots, m_5$ . In order to clarify the conditioning, note that the data used in the assessment process was, in fact, a product from a combination of  $\mathcal{M}_i$  ( $i = 1, \dots, 3$ ) and  $m_j$  ( $j = 1, \dots, 5$ ). Take for instance, the force-deformation curve computed through a pushover analysis on MVLEM and the yield displacement approximated using the ATC40 bilinearization on that curve. The final

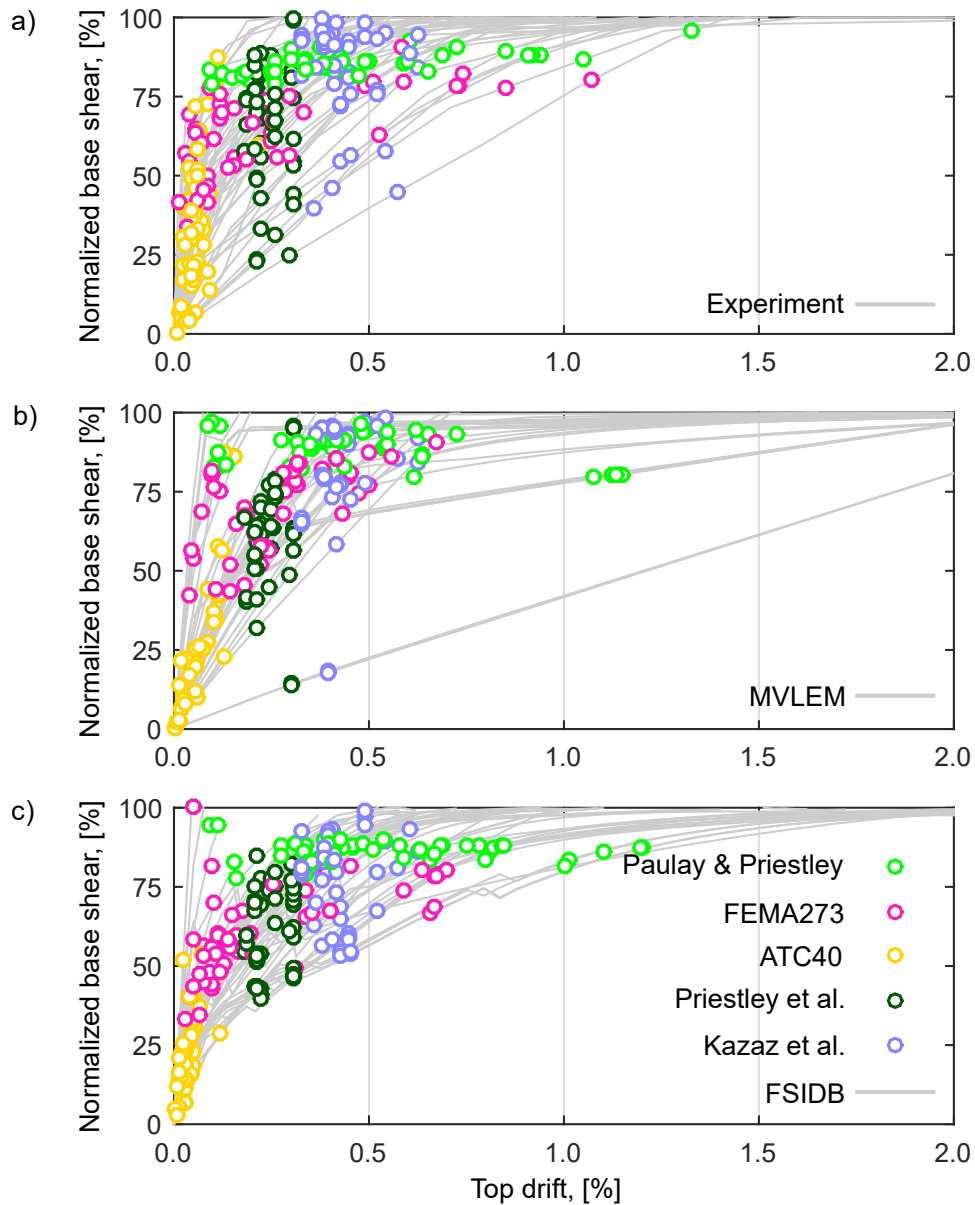


Figure 5.13. Estimated yield drifts for the squat specimens in the experimental part of the database: a) experiment b) MVLEM recreation c) FSIDB recreation (base shear is normalized to its maximum value for each wall).

output product could be easily dependent on the combination of the employed models. Therefore, the two inquiries were considered to capture any potential in this regard. Figure 5.16 presents the probabilities of failure in prediction computed following the first inquiry. Table 5.5 contains the corresponding grades. Generally, the results support the qualitative assessment performed earlier in this section. FEMA273 appears to be the best representative in all cases with PRIESTLEY ET AL. (2007) being the runner-up. On the contrary, ATC40 has ended up with the largest grades confirming its position as the least representative.

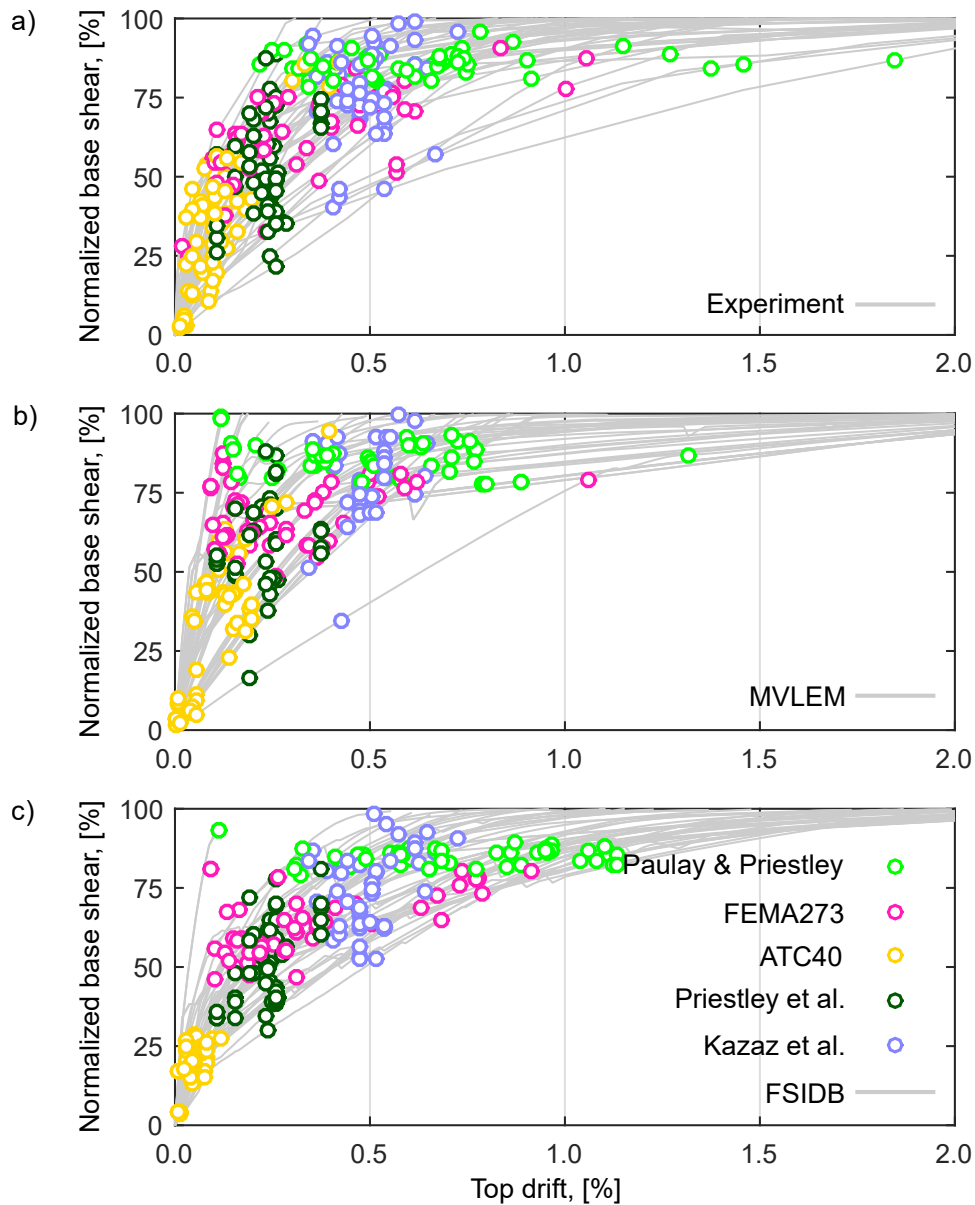


Figure 5.14. Estimated yield drifts for the transition specimens in the experimental part of the database: a) experiment b) MVLEM recreation c) FSIDB recreation (base shear is normalized to its maximum value for each wall).

The information gained from Figure 5.16 and Table 5.5 is not limited to the above-mentioned observations. A comparison between the results for the squat and transition walls, for instance, reveals that grades earned in the latter category are on average larger. The same observation applies to the grades from the FSIDB which are noticeably larger than those from the experiment and MVLEM. Such larger average grades for the models in a group imply that they have less in common. It can be concluded, for example, that FSIDB brings more uncertainty to the yield displacement estimation using the studied methods. This can be clearly seen in Figure 5.17 and Table 5.6 which were produced following

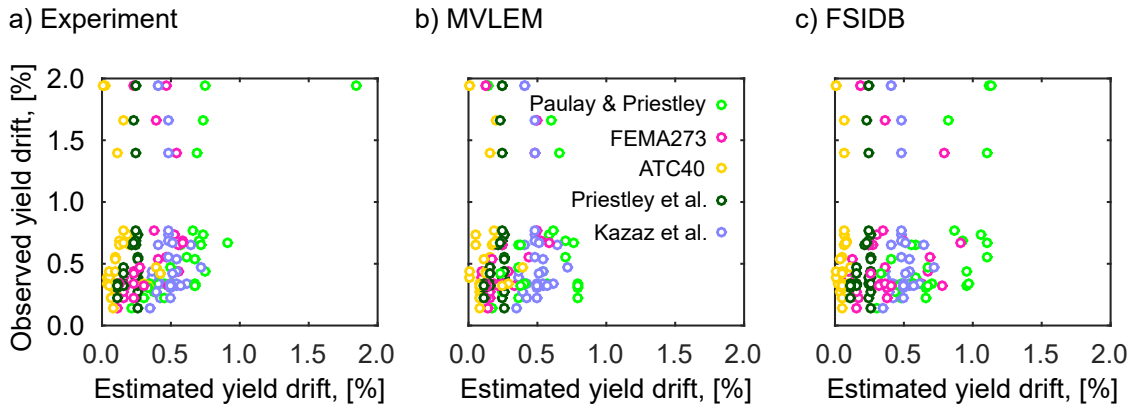


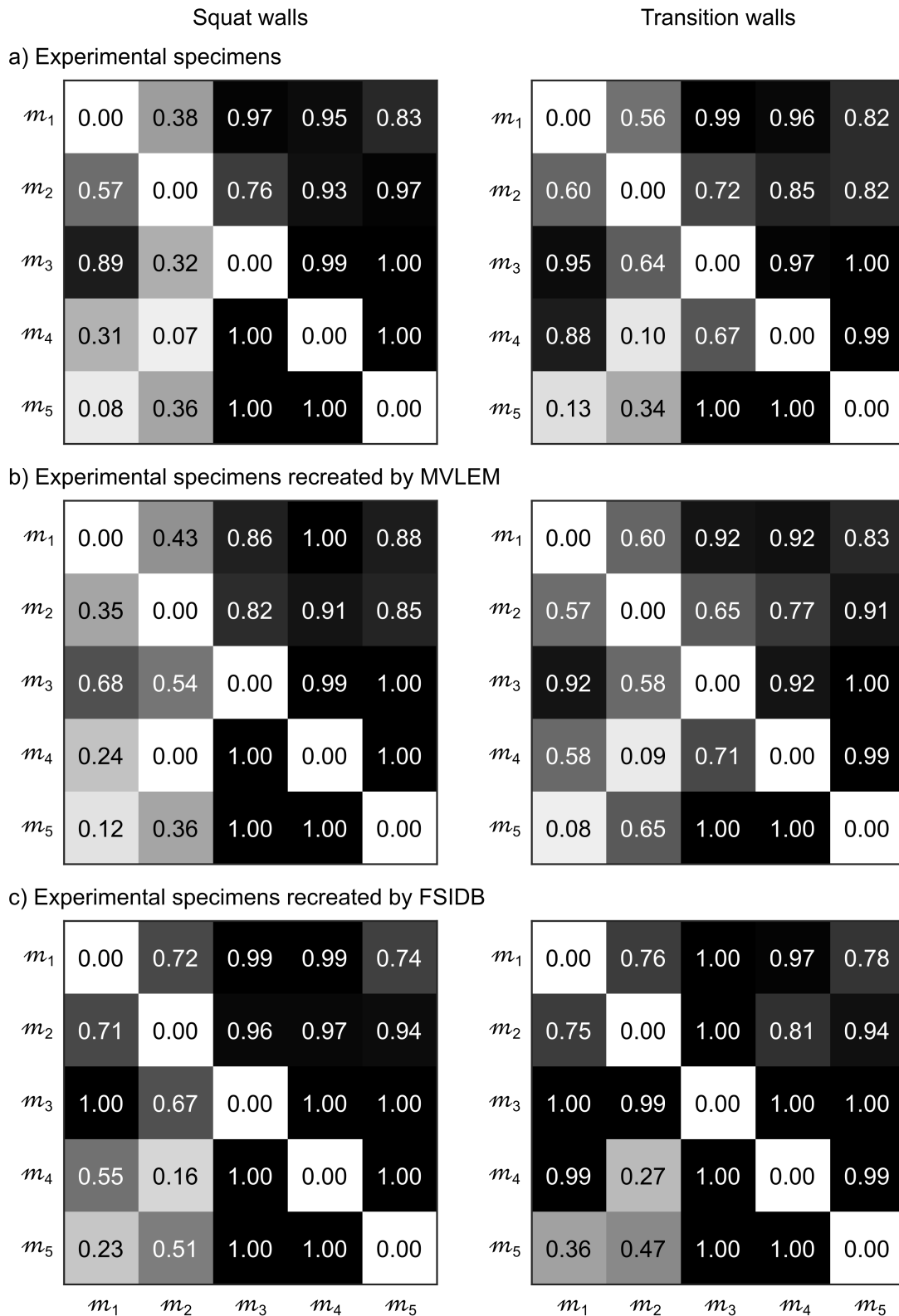
Figure 5.15. Estimated vs observed yield drifts for the transition specimens in the experimental part of the database: a) experiment b) MVLEM recreation c) FSIDB recreation.

the second considered inquiry. Note that, here,  $\mathcal{M}_1, \dots, \mathcal{M}_3$  were assessed given the data estimated using  $m_1, \dots, m_5$ . As expected from the first inquiry assessment, FSIDB has ended up with the largest grades. The experimental model, in contrast, has earned the lowest grades and therefore the highest ranks. Note that no prejudgment was made on the accuracy of the experiments to achieve the latter conclusion. It is interesting, in fact, that the experimental data has appeared to be covering the design space and consequently won the highest rank in the assessment process. The covering characteristic is a result of the uncertainty in the experimental data in the reasonable range of the other models in the design space. This uncertainty is normally ignored in classical one-on-one model validation against experiment.

A second look at Figure 5.17 and Table 5.6 reveals that the grades calculated using the data from PRIESTLEY ET AL. (2007) and KAZAZ ET AL. (2012) are equal for all the involved models. This is due to the fact that PRIESTLEY ET AL. (2007) and KAZAZ ET AL. (2012) are formula-based and compute the yield displacement purely on the account of the wall properties and therefore regardless of its experimental or numerical behavior.

Table 5.5. Normalized final grades for  $m_1, \dots, m_5$  given the data from  $\mathcal{M}_1, \dots, \mathcal{M}_3$ .

	Paulay & Priestley	FEMA273	ATC40	Priestley et al.	Kazaz et al.
Squat walls					
Experiment	0.62	0.54	0.87	0.78	0.78
MVLEM	0.57	0.53	0.86	0.77	0.78
FSIDB	0.74	0.70	0.95	0.83	0.80
Transition walls					
Experiment	0.74	0.58	0.87	0.80	0.76
MVLEM	0.68	0.60	0.84	0.75	0.81
FSIDB	0.83	0.75	1.00	0.88	0.82



$m_1$ : Paulay & Priestley,  $m_2$ : FEMA273,  $m_3$ : ATC40,  $m_4$ : Priestley et al. and  $m_5$ : Kazaz et al.

Figure 5.16. Estimated probabilities of failure in prediction for  $m_1, \dots, m_5$  given the data from a) specimens in the experimental part of the database and their recreation with b) MVLEM and c) FSIDB (colors represent the corresponding values with white for 0.00 and black for 1.00).

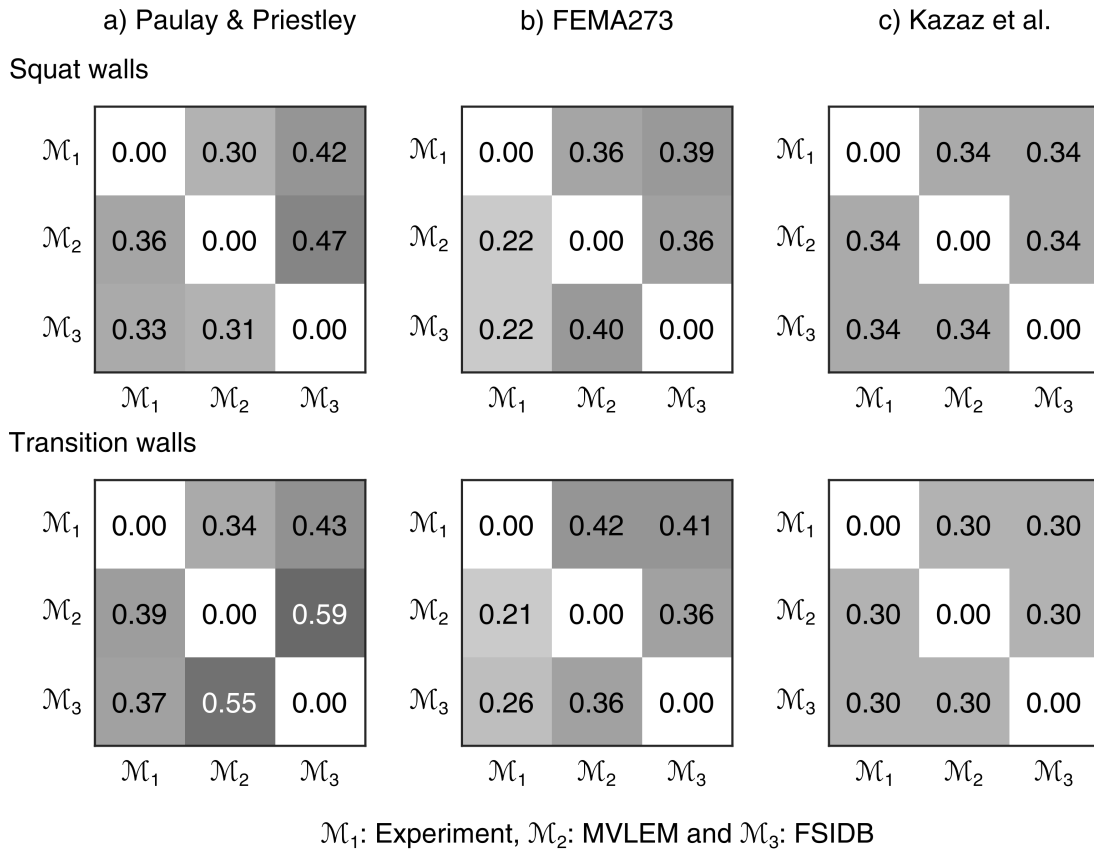


Figure 5.17. Estimated probabilities of failure in prediction for  $\mathcal{M}_1, \dots, \mathcal{M}_3$  given the data from a) Paulay & Priestley, b) FEMA273 and c) Kazaz et al. (colors represent the corresponding values with white for 0.00 and black for 1.00).

Table 5.6. Normalized final grades for  $\mathcal{M}_1, \dots, \mathcal{M}_3$  given the data from  $m_1, \dots, m_5$ .

	Paulay & Priestley	FEMA273	ATC40	Priestley et al.	Kazaz et al.
Squat walls					
Experiment	0.35	0.30	0.47	0.34	0.29
MVLEM	0.36	0.33	0.51	0.34	0.29
FSIDB	0.38	0.34	0.52	0.34	0.29
Transition walls					
Experiment	0.38	0.32	0.46	0.30	0.40
MVLEM	0.48	0.34	0.45	0.30	0.40
FSIDB	0.49	0.35	0.53	0.30	0.40

## 5.4. Discussion of the Results

The previous sections were dedicated to the introduction and justification of the proposed model selection technique. The methodology was comprehensively described and applied to a series of selected problems with an exclusive concentration on the data stored in the database as defined in Chapter 3. A benchmark study was performed using straightfor-



ward mathematical functions in order to learn more about the strengths and weaknesses of the proposed method. The major concern was to assure that the model selection technique did not constantly rank the most scattered models as the best representative models. This was checked through a study on the all possible arrangements of four simple mathematical models with different scatter and distance properties. The results showed that although the method tends to prefer the scattered models it does not automatically select them as the best representatives. In fact, cases were found in which the most scattered models were ranked as the worst models. In addition, the study revealed that the method is able to recognize the outliers. The promising results from the benchmark study justified the further application of the method to the engineering problems.

As mentioned above, the method was further challenged by application to the data coming from the database. The investigation was divided into two individual parts, one involving only the numerical part of the database with generated simulations and the other dealing mainly with the experimental part of the database and its numerical recreation. In the first study, the data to work on random walls were generated by means of the MVLEM and their corresponding yield displacements were computed using five different methods. The advantage of using generated simulations was the statistical reliability offered on the account of having practically unlimited number of samples. the proposed model selection technique was applied to the yield displacement approximations resulted from the selected methods. The ranking agreed well with the qualitative assessment of the models. The outlier model was detected and the models producing more or less constant results for distinct walls were ranked at lower positions.

As the first attempt with the method on engineering problems was successful, the application was further extended to the experimental part of the database. This time the data was significantly less compared to the generated simulations. The sample walls, here, included the experimental specimens and their recreations using the MVLEM and the FSIDB. As the previous problem, the five selected methods were used on the samples to calculate the yield displacement. The final data provided the ground to apply the proposed model selection technique. Again, the resulting assessment matched the qualitative evaluation. The trade-off model was ranked the highest which agreed well with the recorded observed yield displacements. Other interesting outcomes of the latter study included the highest rank of the experiment among the studied models and the additional uncertainty introduced by FSIDB to the yield displacement estimation problem. To sum, the proposed method generally performed well and provided valuable information about the studied group of models.



## 6. Conclusions

The final chapter of the thesis is dedicated to the summary of the study's achievements. Additionally, a quick review of the tackled problems is provided for the sake of convenience. The core challenge of the presented study, as indicated in Section 1.2, was to assess models without necessarily relying on predefined benchmarks as the majority of the existing assessment techniques commonly do. This required that no prejudgments were made on the performance of the models to be assessed, particularly for the experimental data and/or the most complex model out of the group of models to be evaluated. As a result, I proposed a model selection technique which ranks the models based on their ability to represent the studied group of models. The assessment was performed through a systematic comparison of the models considering their uncertainty and sensitivity properties. For the specific purpose of the study, this was mainly done by means of the conceptual implementation of the variance-based sensitivity analysis. The conceptual implementation was separately investigated since it formed the ground for the proposed model selection technique. Here, the major accomplishments and conclusions of the corresponding studies are underlined.

The fundamental investigation targeted the variance-based sensitivity analysis. The proposed conceptual implementation was compared to Saltelli's implementation and EFAST in a variety of analytical and numerical problems with the intention to check its accuracy and efficiency. The results can be summarized as follows:

- The major success was gained in problems with large multidimensional parameter spaces where the other two implementations failed practically.
- The efficiency was established on the basis of the low number of samples required to come to reasonable results.
- The accuracy appeared to be a side effect of the reliable estimation of the mean value as opposed to the tricky approximation of the variance in the other two implementations.

To sum, the applied conceptual implementation is proved to be an efficient as well as accurate tool to ease the calculation of the first order sensitivity measures. Reasonably accurate results can be achieved by performing significantly less number of simulations i.e. making less function calls as addressed in the literature. The aforementioned features

make the implementation an attractive solution to problems dealing with the sensitivity analysis of complex models in which the demanded computational effort is a major concern. Not to mention that in contrast to Saltelli's implementation and EFAST, the conceptual implementation is applicable to the cases where on-demand evaluations of the models are not possible as in the case of experimental data. Cheap and straightforward sensitivity analysis in terms of the computational effort allows for further prioritization and reduction of uncertainties by design of experiment and model updating and selection. Possible modifications to adapt the implementation to the calculation of the total order effects could be the subject of future studies.

Next, the proposed model selection technique was founded on the basis of the successfully examined conceptual implementation. The methodology used in the variance-based sensitivity analysis was employed to involve the uncertainty and sensitivity properties of the models in the comparison and the assessment process. The proposed model selection technique was principally meant to handle the experimental and numerical data collected in the experience-based database on RC structural walls. The organized data in the database provided a firm ground for statistical studies specially on the experimental records. Moreover, the various approaches available for the estimation of the yield displacement for RC walls could very well justify the need for a quantitative evaluation.

In addition to the engineering problems mentioned above, a collection of mathematical problems were used to challenge the method in different conditions in terms of the properties and the arrangement of the models to be evaluated. The achievements can be summarized as follows:

- Although the method favored the more scattered models, it did not constantly rank the most scattered one the highest according to the mathematical benchmark study.
- The method detected the outliers which did not follow the general trend in the group of models.
- Its application to real engineering data of numerical and experimental natures led to quantitative assessment that matched very well with the qualitative evaluation.

A primary advantage of the proposed model selection technique is that it provides information on how any pair of two models in the group of models to be studied compare. This implies that regardless of the ranking that follows the matrix of the probabilities of failure in prediction, the information can be used to learn about the model in the context of the group of models. Take for instance, the case in which we have made the common assumption that the experimental data is the benchmark for validation. In such a case, application of the proposed model selection technique to the group of models including the experiment covers the validation process by default. Here, we are obviously more interested to see how the models have performed in predicting the experimental model.

---

In other words, only the column of the matrix of the probabilities of failure in prediction corresponding to the experiment is of importance to us. It is well clear that although pre-judgments do not affect the results of the proposed model selection technique they can indeed influence the way the results are interpreted.

The major drawback of the technique as mentioned above might be its tendency towards the more scattered models in the design space. Such models are particularly disappointing when it comes to predicting the response of the desired phenomenon out of the boundaries of the available knowledge (e.g. in new ranges of the input parameters). In contrast to the less uncertain models, more scattered models fail at predicting precise outputs for such unknown situations. Yet, it cannot be claimed that the less uncertain models necessarily predict the *best* results. On the contrary, in a group of several very different but certain models defining a phenomenon, the choice of any model as the *best* model results in unreliable predictions of the phenomenon unless the chosen model represents the average of the group. The wrong choice of the *best* model in such cases can be very nonconservative. To tackle this issue, the proposed model selection technique attempts to find a representative model depending on the arrangement of the models in the design space and their uncertainty and sensitivity properties. Accordingly, the choice of the wrong model as the *best* model would not affect the predictions dramatically since the selected model could best predict and be predicted by all the other models in the design space.

Finally, it is worth to mention again that the proposed model selection technique does not (and is not able to) seek the *best* abstraction of a real phenomenon but rather the *best representative* of a group of models. The choice strongly depends on the uncertainty properties and arrangement of the models. The method systematically compares every pair of two models in the group and offers a trade-off through which the design space is reasonably covered. The resulting matrix of probabilities of failure in prediction is a unique collection of quantitative information on how each model compares to the other members of the studied group of models. Moreover, the proposed method does not rely on any specific choice of benchmark data. Therefore, its application is not limited to the problems where experimental data is particularly available.



# A. Database: Experimental Part

Table A.1 provides information regarding the type, sectional geometry, loading condition and failure mode of the 162 specimens before filtration of the database. The studied specimens in the final filtered database are marked. Details regarding the input parameters and the output parameter of interest for the studied specimens are presented in Sections A.1 and A.2 for squat and transition walls, respectively.

Table A.1. Database sources and specimens.

Source	Specimen	Type	Section	Loading	Failure	Quality	Studied
DAZIO ET AL. (2009)	WSH1	2	B	C	N/I	5	×
	WSH2	2	B	C	N/I		✓
	WSH3	2	B	C	N/I		✓
	WSH4	2	B	C	N/I		✓
	WSH5	2	B	C	N/I		✓
	WSH6	2	B	C	N/I		✓
THOMSEN AND WALLACE (1995)	RW1	2	B	C	S/F	5	✓
	RW2	2	B	C	S/F		✓
OESTERLE ET AL. (1976)	R1	2	R	C	S	3	×
	R2	2	R	C	S		×
	B1	2	B	C	S		✓
	B2	2	B	C	S		✓
	B3	2	B	C	S		✓
	B4	2	B	M	S		✓
	B5	2	B	C	F		✓
	B6	2	B	C	S		✓
B7	2	B	C	F		✓	

Wall type: 1 = Squat, 2 = Transition and 3 = Slender.

Section: R = Rectangular and B = Barbell.

Loading: M = Monotonic, C = Cyclic and D = Dynamic.

Failure: S = Shear, F = Flexure, S/F = Shear/Flexure and N/I = No information.

Quality: 1 = Lowest quality to 5 = Highest quality.

Table A.1. Database sources and specimens (continued).

Source	Specimen	Type	Section	Loading	Failure	Quality	Studied
	B8	2	B	C	F		✓
	B9	2	B	C	F		✓
	B10	2	B	C	F		✓
ESCOLANO-MARGARIT ET AL. (2012)	W-MC-C	2	B	C	N/I	5	✓
	W-MC-N	2	R	C	N/I		×
TRAN AND WALLACE (2012A)	RW-A20-P10-S38	2	B	C	N/I	5	✓
	RW-A20-P10-S63	2	B	C	N/I		✓
	RW-A15-P10-S51	1	B	C	N/I		✓
	RW-A15-P10-S78	1	B	C	N/I		✓
	RW-A15-P2.5-S64	1	B	C	N/I		✓
SITTIPUNT AND WOOD (2000)	W1	1	B	C	S	5	✓
	W2	1	B	C	S		✓
	W3	1	B	C	S		✓
	W4	1	B	C	S		✓
LESTUZZI AND BACHMANN (2007)	WDH1-SOFT	2	R	D	N/I	4	×
	WDH2-SOFT	2	R	D	N/I		×
	WDH3-SOFT	2	R	D	N/I		✓
	WDH4-SOFT	2	R	D	N/I		✓
	WDH5-SOFT	2	R	D	N/I		✓
	WDH6-SOFT	2	R	D	N/I		✓
SALONIKIOS ET AL. (1999)	MSW1	1	R	C	S/F	5	✓
	MSW2	1	R	C	S/F		✓
	MSW3	1	R	C	S/F		✓
	MSW4	1	R	C	S/F		✓
	MSW5	1	R	C	S/F		✓
	MSW6	1	R	C	S/F		✓
	LSW1	1	R	C	S/F		✓
	LSW2	1	R	C	S/F		✓
LSW3	1	R	C	S/F		✓	

Wall type: 1 = Squat, 2 = Transition and 3 = Slender.

Section: R = Rectangular and B = Barbell.

Loading: M = Monotonic, C = Cyclic and D = Dynamic.

Failure: S = Shear, F = Flexure, S/F = Shear/Flexure and N/I = No information.

Quality: 1 = Lowest quality to 5 = Highest quality.



Table A.1. Database sources and specimens (continued).

Source	Specimen	Type	Section	Loading	Failure	Quality	Studied
	LSW4	1	R	C	S/F		✓
	LSW5	1	R	C	S/F		✓
MASSONE ET AL. (2009)	WS-T1-S1	1	R	C	S	3	×
	WP-T5-N10-S2	1	R	C	S		✓
CARDENAS ET AL. (1980)	SW-7	1	R	M	F	5	✓
	SW-8	1	R	M	F		×
	SW-9	1	R	M	F		×
	SW-10	1	R	M	N/I		×
	SW-11	1	R	M	N/I		×
	SW-12	1	R	M	N/I		×
BARDA ET AL. (1977)	B1-1	1	B	M	S	5	✓
	B2-1	1	B	M	S		✓
	B3-2	1	B	C	S		✓
	B4-3	1	B	C	S		×
	B5-4	1	B	C	S		×
	B6-4	1	B	C	S		✓
	B7-5	1	B	C	S		✓
	B8-5	1	B	C	S		✓
HIDALGO ET AL. (2002)	1	2	R	C	S	4	×
	2	2	R	C	S		×
	4	2	R	C	S		×
	6	1	R	C	S		×
	7	1	R	C	S		×
	8	1	R	C	S		×
	9	1	R	C	S		×
	10	1	R	C	S		×
	11	1	R	C	S		×
	12	1	R	C	S		×
	13	1	R	C	S		×

Wall type: 1 = Squat, 2 = Transition and 3 = Slender.

Section: R = Rectangular and B = Barbell.

Loading: M = Monotonic, C = Cyclic and D = Dynamic.

Failure: S = Shear, F = Flexure, S/F = Shear/Flexure and N/I = No information.

Quality: 1 = Lowest quality to 5 = Highest quality.

Table A.1. Database sources and specimens (continued).

Source	Specimen	Type	Section	Loading	Failure	Quality	Studied
	14	1	R	C	S		×
	15	1	R	C	S		×
	16	1	R	C	S		×
LEFAS ET AL. (1990)	SW30	2	R	M	F	5	✓
	SW31	2	R	C	F		✓
	SW31R	2	R	C	F		✓
	SW32	2	R	C	F		✓
	SW32R	2	R	C	F		✓
	SW33	2	R	C	F		✓
	SW33R	2	R	C	F		✓
ZHANG AND WANG (2000)	SW7	2	R	C	F	5	✓
	SW8	2	R	C	F		✓
	SW9	2	R	C	F		✓
	SRCW12	2	R	C	F		✓
MANSUR ET AL. (1991)	W2	1	B	C	S	5	✓
	W3	1	B	C	S		✓
	W4	1	B	C	S		✓
GHOUBANI-RENANI ET AL. (2009)	A1M(prototype)	2	R	M	F	5	✓
	A2C(prototype)	2	R	C	S/F		✓
	B1M(model)	2	R	M	F		✓
	B2C(model)	2	R	C	S/F		✓
LOPES (2001)	SW13	1	R	C	F	4	✓
	SW16	1	R	C	S		×
	SW17	1	R	C	S		×
MICKLEBOROUGH ET AL. (1999)	SH-L	2	R	M	S/F	5	×
	SH-H	2	R	M	S/F		×
	SM-L	1	R	M	S/F		×
	SM-H	1	R	M	S/F		×
	SL-L	1	R	M	S/F		×

Wall type: 1 = Squat, 2 = Transition and 3 = Slender.

Section: R = Rectangular and B = Barbell.

Loading: M = Monotonic, C = Cyclic and D = Dynamic.

Failure: S = Shear, F = Flexure, S/F = Shear/Flexure and N/I = No information.

Quality: 1 = Lowest quality to 5 = Highest quality.

Table A.1. Database sources and specimens (continued).

Source	Specimen	Type	Section	Loading	Failure	Quality	Studied
	SL-H	1	R	M	S/F		×
LAYSSI AND MITCHELL (2012)	W1	2	R	C	S	4	✓
	W2	2	R	C	S		✓
TASNIMI (2000)	SHW1	2	R	C	F	5	✓
	SHW2	2	R	C	F		✓
	SHW3	2	R	C	F		✓
	SHW4	2	R	C	F		✓
PALERMO (2002)	DP1	1	B	C	S/F	5	✓
	DP2	1	B	C	S/F		✓
WIRADINATA (1985)	Wall1	1	R	C	S	5	✓
	Wall2	1	R	C	S		✓
TUPPER (1999)	W3	3	B	C	F	5	×
ROTHE AND KNIG (1988)	T01	1	B	D	F	2.5	✓
	T06	1	B	C	F		✓
	T07	1	B	C	F		✓
SHIGA ET AL. (1973)	WB-1	1	B	C	S	3	×
	WB-2	1	B	C	S		×
	WB-3	1	B	C	S		×
	WB-4	1	B	M	S		×
	WB-6	1	B	C	S		×
	WB-7	1	B	C	S		×
	WB-8	1	B	C	S		×
YANEZ ET AL. (1991)	S1	1	R	C	F	5	×
KABEYASAWA ET AL. (1983)	NW-1	2	B	C	F	5	✓
	NW-2	2	B	C	S		✓
	NW-3	2	B	C	S		✓
	NW-4	2	B	C	S		✓
	NW-5	2	B	C	S		✓
	NW-6	2	B	C	S		✓

Wall type: 1 = Squat, 2 = Transition and 3 = Slender.

Section: R = Rectangular and B = Barbell.

Loading: M = Monotonic, C = Cyclic and D = Dynamic.

Failure: S = Shear, F = Flexure, S/F = Shear/Flexure and N/I = No information.

Quality: 1 = Lowest quality to 5 = Highest quality.

Table A.1. Database sources and specimens (continued).

Source	Specimen	Type	Section	Loading	Failure	Quality	Studied
ENDO ET AL. (1980)	W7102	1	B	C	S/F	4.5	✓
	W7401	1	B	M	S/F		✓
	W7402	1	B	C	S/F		✓
	W7403	1	B	M	S/F		✓
	W7404	1	B	C	S/F		✓
	W7502	1	B	M	S/F		✓
	W7503	1	B	C	S/F		✓
	W7506	1	B	C	S/F		✓
	W7605	1	B	C	S/F		✓
	W7606	1	B	C	S/F		✓
IBRAHIM (2000)	prototype	3	B	C	S/F	5	×
SHIMAZAKI (2008)	WP1	2	R	C	S	4.5	✓
LOWES ET AL. (2011)	PW1	1	R	C	F	5	✓
	PW2	1	R	C	F		✓
	PW3	1	R	C	F		✓
	PW4	1	R	C	F		✓
HIRAISHI ET AL. (1983)	W1	2	B	C	S	4	✓
	W2	2	B	C	S		✓
LOMBARD (1999)	1	1	R	C	F	5	×
SHIU ET AL. (1981)	CI-1	2	R	C	S	5	✓
ATHANASOPOULOU (2010)	S1	1	R	C	S/F	5	×
	S2	1	R	C	S/F		×
	S4	1	R	C	S/F		×
	S5	1	R	C	S/F		×
	S6	1	R	C	S/F		×
	S7	1	R	C	S/F		×
	S8	1	R	C	S/F		×
	S9	1	R	C	S/F		×
	S10	1	R	C	S/F		×

Wall type: 1 = Squat, 2 = Transition and 3 = Slender.

Section: R = Rectangular and B = Barbell.

Loading: M = Monotonic, C = Cyclic and D = Dynamic.

Failure: S = Shear, F = Flexure, S/F = Shear/Flexure and N/I = No information.

Quality: 1 = Lowest quality to 5 = Highest quality.

## A.1. Squat Walls

Table A.2. Database parameters for squat walls: geometry and material.

Source	Specimen	$\frac{H}{L}$	$\frac{A_b}{A}$	$\frac{L_b}{L}$	$f'_c$	$f_y$
TRAN AND WALLACE (2012A)	RW-A15-P10-S51	1.50	0.15	0.25	48.0	515.0
	RW-A15-P10-S78	1.50	0.15	0.25	56.0	440.0
	RW-A15-P2.5-S64	1.50	0.15	0.25	56.0	440.0
SITTIPUNT AND WOOD (2000)	W1	1.43	0.55	0.33	36.6	450.0
	W2	1.43	0.55	0.33	35.8	450.0
	W3	1.43	0.55	0.33	37.8	450.0
	W4	1.43	0.55	0.33	36.3	450.0
SALONIKIOS ET AL. (1999)	MSW1	1.50	0.40	0.40	26.1	610.0
	MSW2	1.50	0.40	0.40	26.2	610.0
	MSW3	1.50	0.40	0.40	24.1	610.0
	MSW4	1.50	0.40	0.40	24.6	610.0
	MSW5	1.50	0.40	0.40	22.0	610.0
	MSW6	1.50	0.40	0.40	27.5	610.0
	LSW1	1.00	0.40	0.40	22.2	610.0
	LSW2	1.00	0.40	0.40	21.6	610.0
	LSW3	1.00	0.40	0.40	23.9	610.0
	LSW4	1.00	0.40	0.40	23.2	610.0
LSW5	1.00	0.40	0.40	24.9	610.0	
MASSONE ET AL. (2009)	WP-T5-N10-S2	0.89	0.09	0.09	31.4	424.0
CARDENAS ET AL. (1980)	SW-7	1.00	0.20	0.20	43.0	593.7
BARDA ET AL. (1977)	B1-1	0.50	0.41	0.11	29.0	489.5
	B2-1	0.50	0.41	0.11	16.3	496.4
	B3-2	0.50	0.41	0.11	27.0	510.2
	B6-4	0.50	0.41	0.11	21.2	496.4
	B7-5	0.25	0.41	0.11	25.7	496.4
	B8-5	1.00	0.41	0.11	23.4	489.5
MANSUR ET AL. (1991)	W2	0.67	0.45	0.10	31.4	429.0
	W3	0.67	0.45	0.10	31.3	429.0
	W4	0.67	0.45	0.10	37.4	359.0
LOPES (2001)	SW13	1.10	0.35	0.35	44.0	414.0
PALERMO (2002)	DP1	0.70	0.73	0.06	21.7	605.0
	DP2	0.70	0.73	0.07	18.8	605.0
WIRADINATA (1985)	Wall1	0.50	0.29	0.29	25.0	425.0

Table A.2. Database parameters for squat walls: geometry and material (continued).

Source	Specimen	$\frac{H}{L}$	$\frac{A_b}{A}$	$\frac{L_b}{L}$	$f'_c$	$f_y$
	Wall2	0.25	0.29	0.29	22.0	425.0
ROTHE AND KNIG (1988)	T01	1.50	0.38	0.40	24.3	419.6
	T06	1.50	0.55	0.40	33.7	419.6
	T07	1.50	0.55	0.40	30.9	419.6
ENDO ET AL. (1980)	W7102	0.88	0.47	0.22	24.6	447.3
	W7401	0.88	0.47	0.22	20.2	414.0
	W7402	0.88	0.47	0.22	22.9	414.0
	W7403	0.88	0.47	0.22	28.4	414.0
	W7404	0.88	0.47	0.22	23.9	414.0
	W7502	0.88	0.47	0.22	22.9	366.9
	W7503	0.88	0.47	0.22	21.8	366.9
	W7506	0.88	0.47	0.22	27.7	366.9
	W7605	1.30	0.47	0.22	27.1	422.8
	W7606	0.88	0.47	0.22	26.1	422.8
LOWES ET AL. (2011)	PW1	1.20	0.34	0.34	36.1	517.1
	PW2	1.20	0.34	0.34	40.3	517.1
	PW3	1.20	0.39	0.39	34.3	517.1
	PW4	1.20	0.34	0.34	29.5	517.1

Table A.3. Database parameters for squat walls: reinforcement and loading.

Source	Specimen	$\rho_{vw}$	$\rho_{hw}$	$\rho_{vb}$	$\rho_{hb}$	$\frac{P}{f_c A}$
TRAN AND WALLACE (2012A)	RW-A15-P10-S51	0.0029	0.0033	0.0459	0.0086	0.10
	RW-A15-P10-S78	0.0062	0.0075	0.0860	0.0086	0.10
	RW-A15-P2.5-S64	0.0051	0.0062	0.0860	0.0086	0.03
SITTIPUNT AND WOOD (2000)	W1	0.0039	0.0052	0.0229	0.0044	0.00
	W2	0.0052	0.0079	0.0229	0.0054	0.00
	W3	0.0105	0.0052	0.0229	0.0044	0.00
	W4	0.0157	0.0079	0.0229	0.0054	0.00
SALONIKIOS ET AL. (1999)	MSW1	0.0057	0.0057	0.0170	0.0110	0.07
	MSW2	0.0028	0.0028	0.0130	0.0110	0.07
	MSW3	0.0028	0.0028	0.0130	0.0110	0.07
	MSW4	0.0028	0.0069	0.0130	0.0170	0.07
	MSW5	0.0028	0.0069	0.0130	0.0170	0.07
	MSW6	0.0057	0.0057	0.0170	0.0170	0.07
	LSW1	0.0057	0.0057	0.0170	0.0170	0.07
	LSW2	0.0028	0.0028	0.0130	0.0170	0.07
	LSW3	0.0028	0.0028	0.0130	0.0170	0.07
	LSW4	0.0028	0.0069	0.0130	0.0170	0.07
LSW5	0.0028	0.0069	0.0130	0.0170	0.07	
MASSONE ET AL. (2009)	WP-T5-N10-S2	0.0028	0.0023	0.0133	0.0023	0.10
CARDENAS ET AL. (1980)	SW-7	0.0085	0.0027	0.0830	0.0027	0.08
BARDA ET AL. (1977)	B1-1	0.0050	0.0050	0.0180	0.0110	0.25
	B2-1	0.0050	0.0050	0.0640	0.0110	0.45
	B3-2	0.0050	0.0050	0.0410	0.0110	0.27
	B6-4	0.0025	0.0050	0.0410	0.0110	0.34
	B7-5	0.0050	0.0050	0.0410	0.0110	0.28
	B8-5	0.0050	0.0050	0.0410	0.0110	0.31
MANSUR ET AL. (1991)	W2	0.0055	0.0110	0.0330	0.0150	0.00
	W3	0.0055	0.0110	0.0330	0.0150	0.00
	W4	0.0062	0.0248	0.0330	0.0150	0.00

Table A.3. Database parameters for squat walls: reinforcement and loading (continued).

Source	Specimen	$\rho_{vw}$	$\rho_{hw}$	$\rho_{vb}$	$\rho_{hb}$	$\frac{P}{f_c A}$
LOPES (2001)	SW13	0.0039	0.0093	0.0593	0.0279	0.00
PALERMO (2002)	DP1	0.0079	0.0074	0.0270	0.0058	0.07
	DP2	0.0079	0.0074	0.0270	0.0058	0.02
WIRADINATA (1985)	Wall1	0.0018	0.0021	0.0138	0.0100	0.00
	Wall2	0.0018	0.0021	0.0138	0.0100	0.00
ROTHE AND KNIG (1988)	T01	0.0141	0.0047	0.0071	0.0047	0.00
	T06	0.0200	0.0094	0.0100	0.0038	0.00
	T07	0.0113	0.0094	0.0057	0.0038	0.01
ENDO ET AL. (1980)	W7102	0.0024	0.0024	0.0085	0.0031	0.00
	W7401	0.0024	0.0024	0.0085	0.0031	0.00
	W7402	0.0024	0.0024	0.0085	0.0031	0.00
	W7403	0.0024	0.0024	0.0085	0.0031	0.00
	W7404	0.0024	0.0024	0.0085	0.0031	0.00
	W7502	0.0024	0.0024	0.0170	0.0031	0.00
	W7503	0.0024	0.0024	0.0170	0.0031	0.00
	W7506	0.0024	0.0024	0.0170	0.0031	0.00
	W7605	0.0028	0.0028	0.0250	0.0032	0.00
	W7606	0.0028	0.0028	0.0250	0.0032	0.00
LOWES ET AL. (2011)	PW1	0.0030	0.0030	0.0341	0.0111	0.10
	PW2	0.0030	0.0030	0.0341	0.0111	0.13
	PW3	0.0163	0.0030	0.0200	0.0122	0.10
	PW4	0.0030	0.0030	0.0341	0.0111	0.12



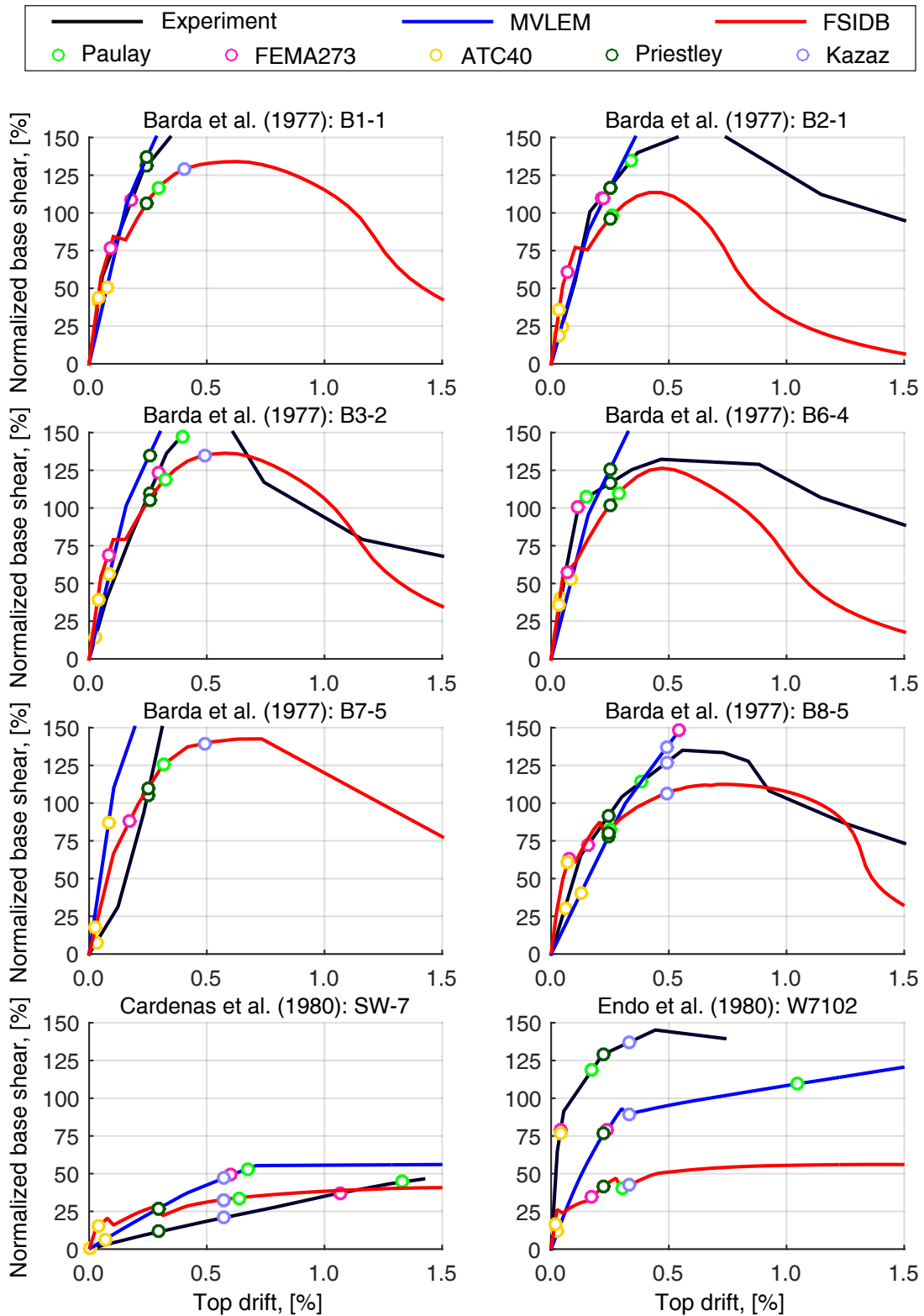


Figure A.1. Database force-deformation plots and the estimated yield drifts for the squat walls.

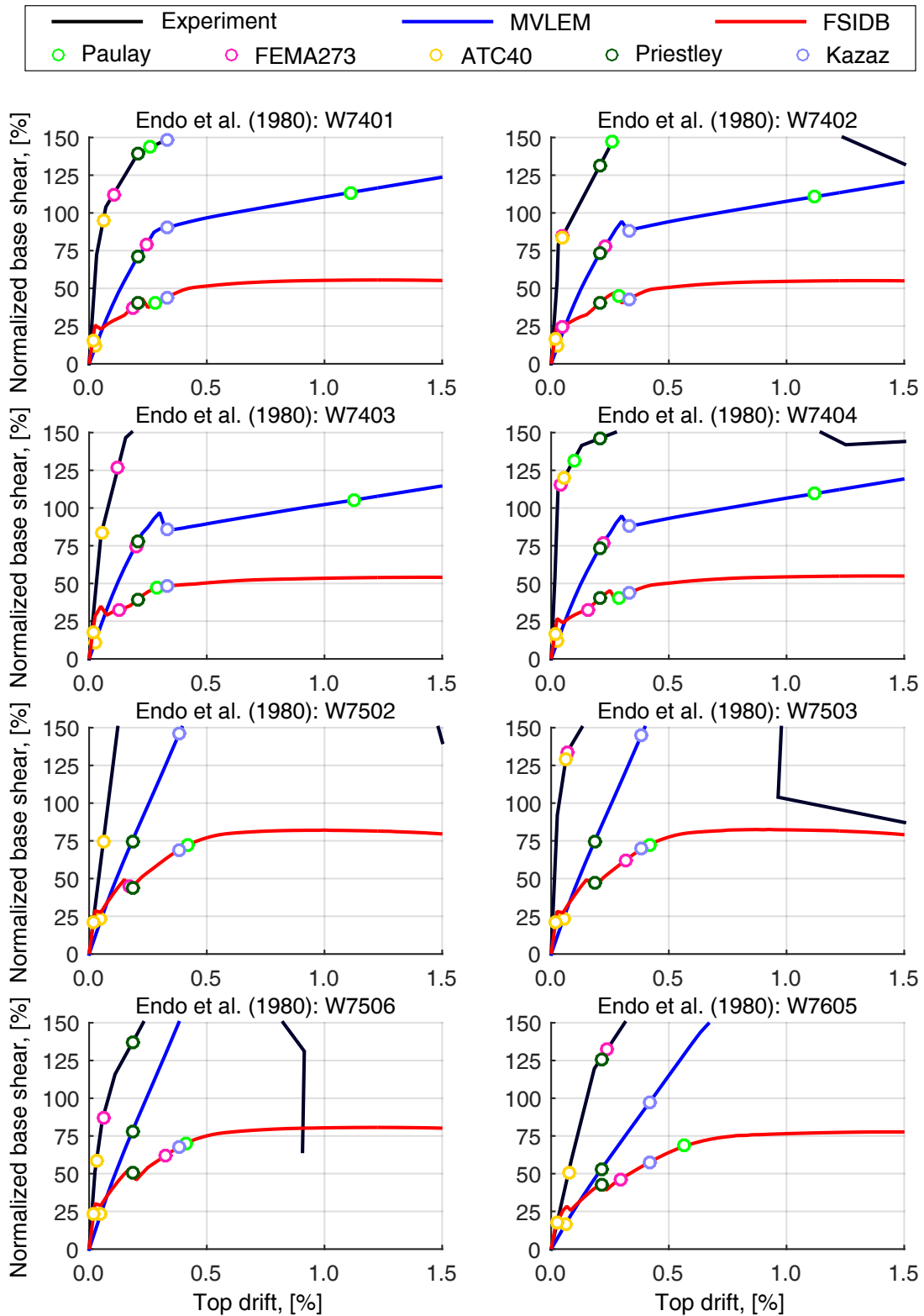


Figure A.1. Database force-deformation plots and the estimated yield drifts for the squat walls (continued).

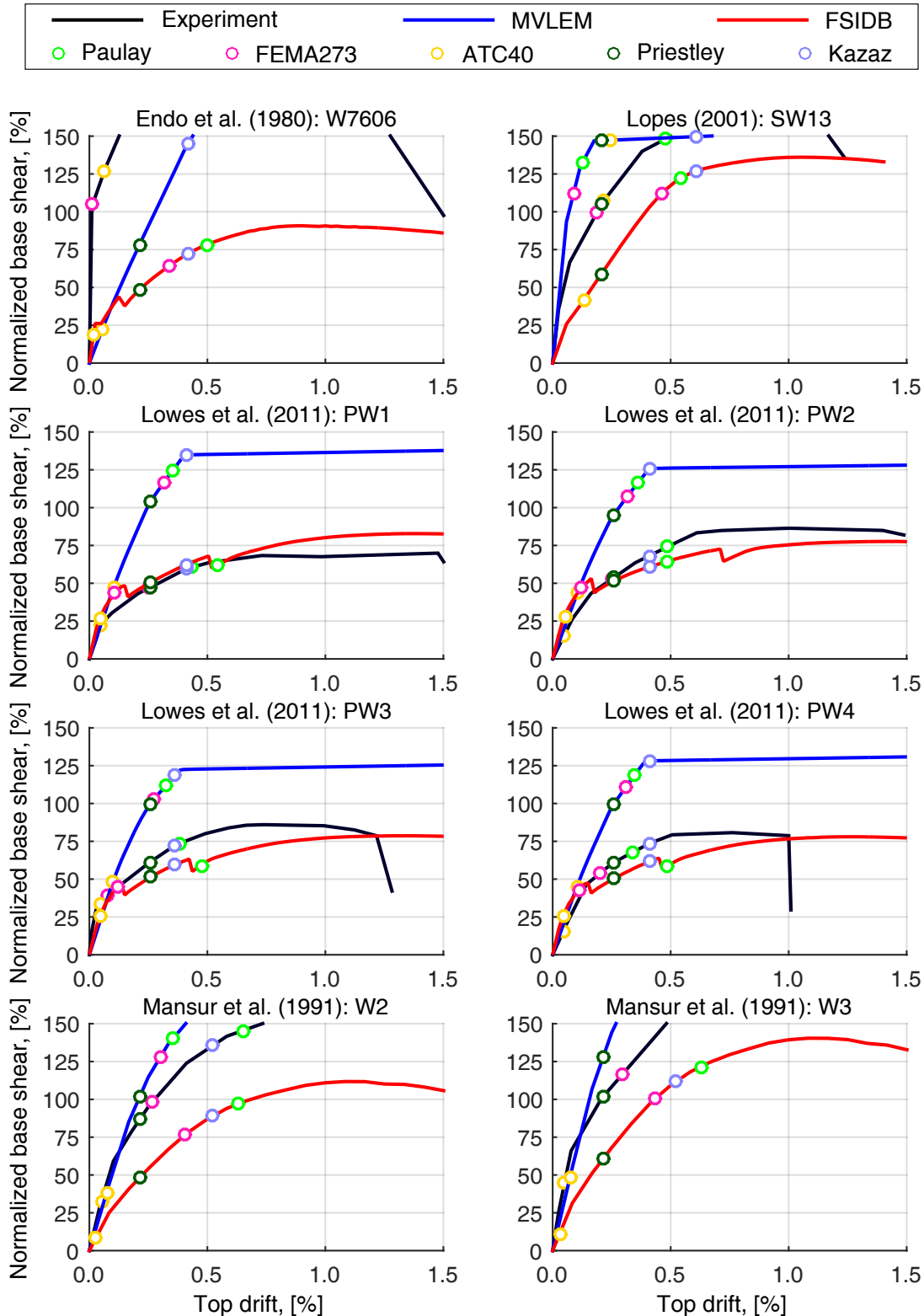


Figure A.1. Database force-deformation plots and the estimated yield drifts for the squat walls (continued).

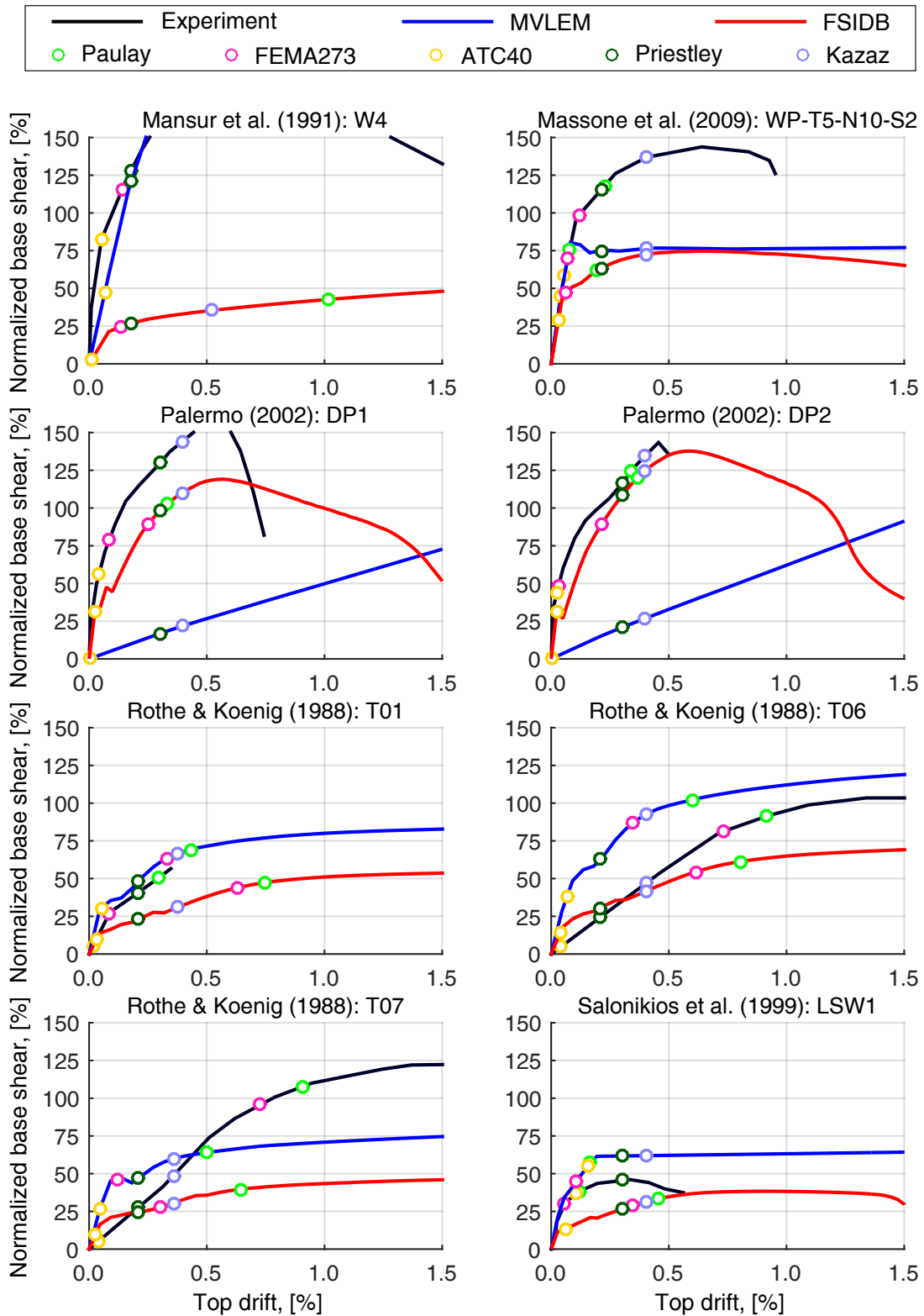


Figure A.1. Database force-deformation plots and the estimated yield drifts for the squat walls (continued).

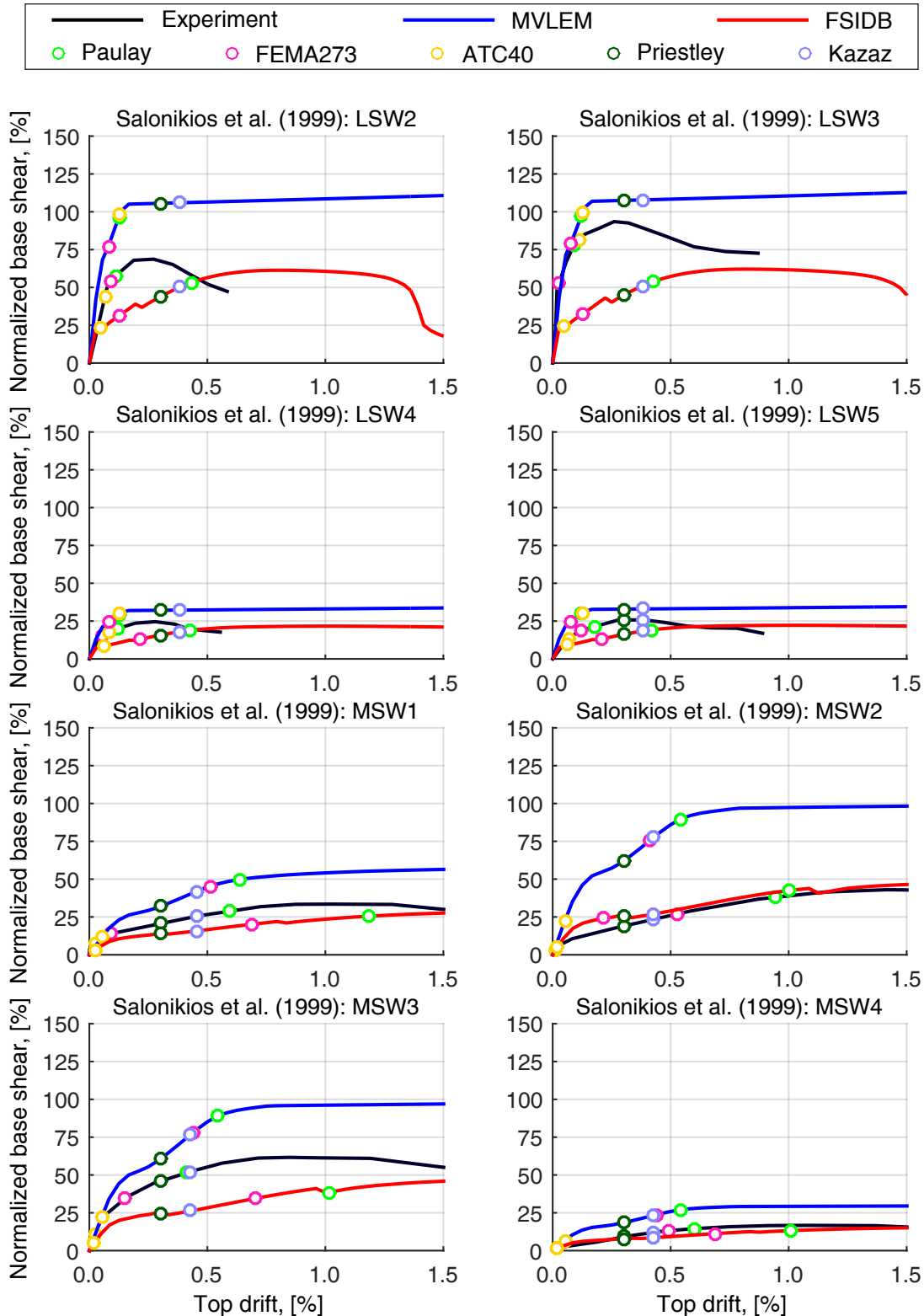


Figure A.1. Database force-deformation plots and the estimated yield drifts for the squat walls (continued).

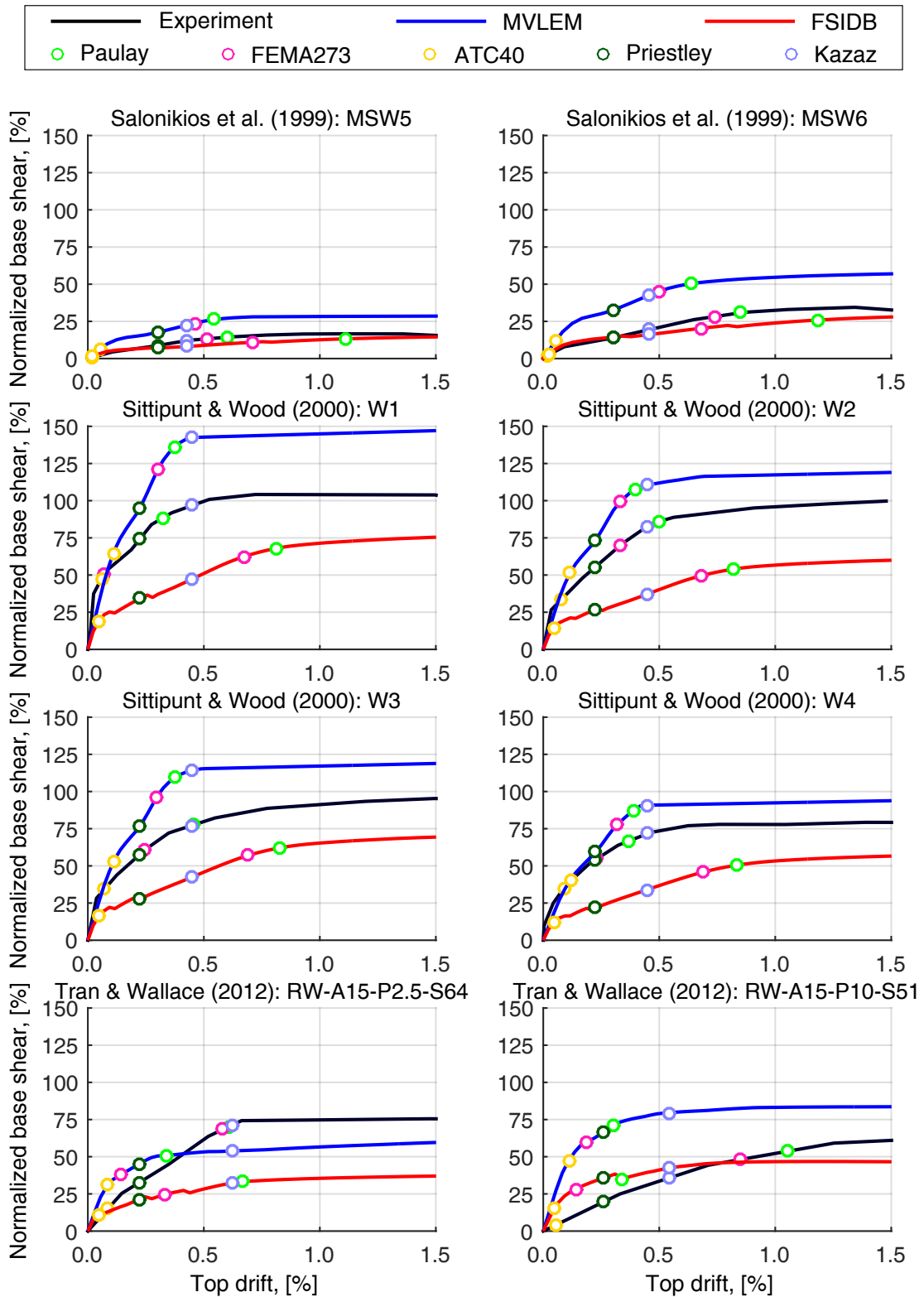


Figure A.1. Database force-deformation plots and the estimated yield drifts for the squat walls (continued).

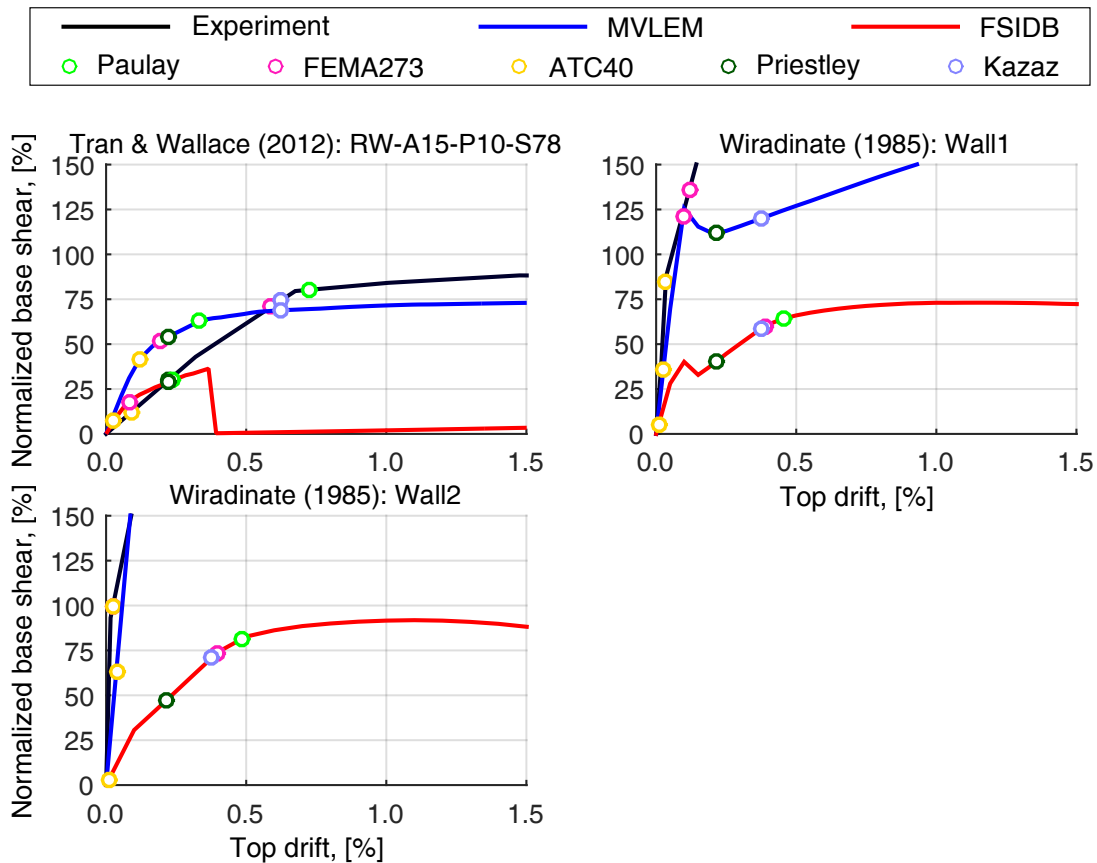


Figure A.1. Database force-deformation plots and the estimated yield drifts for the squat walls (continued).

## A.2. Transition Walls

Table A.4. Database parameters for transition walls: geometry and material.

Source	Specimen	$\frac{H}{L}$	$\frac{A_b}{A}$	$\frac{L_b}{L}$	$f'_c$	$f_y$
DAZIO ET AL. (2009)	WSH2	2.28	0.10	0.15	40.5	484.9
	WSH3	2.28	0.13	0.20	39.2	489.0
	WSH4	2.28	0.23	0.23	40.9	518.9
	WSH5	2.28	0.13	0.20	38.3	518.9
	WSH6	2.26	0.22	0.33	45.6	518.9
THOMSEN AND WALLACE (1995)	RW1	3.00	0.16	0.25	31.6	448.0
	RW2	3.00	0.16	0.25	34.0	448.0
OESTERLE ET AL. (1976)	B1	2.39	0.59	0.32	52.9	520.6
	B2	2.39	0.59	0.32	53.6	532.3
	B3	2.39	0.59	0.32	47.3	478.5
	B4	2.39	0.59	0.32	45.0	504.7
	B5	2.39	0.59	0.32	45.3	502.0
	B6	2.39	0.59	0.32	21.8	511.6
	B7	2.39	0.59	0.32	49.3	489.5
	B8	2.39	0.59	0.32	41.9	482.0
	B9	2.39	0.59	0.32	44.1	461.3
	B10	2.39	0.59	0.32	45.6	475.1
ESCOLANO-MARGARIT ET AL. (2012)	W-MC-C	2.40	0.08	0.15	30.7	482.7
TRAN AND WALLACE (2012A)	RW-A20-P10-S38	2.00	0.15	0.25	48.0	515.0
	RW-A20-P10-S63	2.00	0.15	0.25	48.0	440.0
LESTUZZI AND BACHMANN (2007)	WDH3-SOFT	2.83	0.22	0.22	36.5	474.2
	WDH4-SOFT	2.83	0.22	0.22	36.3	481.4
	WDH5-SOFT	2.83	0.22	0.22	36.5	553.9
	WDH6-SOFT	2.83	0.22	0.22	42.6	567.5
LEFAS ET AL. (1990)	SW30	2.00	0.43	0.43	30.1	520.0
	SW31	2.00	0.43	0.43	35.2	520.0
	SW31R	2.00	0.43	0.43	34.9	520.0
	SW32	2.00	0.43	0.43	53.6	520.0
	SW32R	2.00	0.43	0.43	38.2	520.0
	SW33	2.00	0.43	0.43	49.2	520.0
	SW33R	2.00	0.43	0.43	38.1	520.0
ZHANG AND WANG (2000)	SW7	2.50	0.29	0.29	29.7	305.0



Table A.4. Database parameters for transition walls: geometry and material (continued).

Source	Specimen	$\frac{H}{L}$	$\frac{A_b}{A}$	$\frac{L_b}{L}$	$f'_c$	$f_y$
	SW8	2.50	0.29	0.29	32.0	305.0
	SW9	2.50	0.29	0.29	35.4	305.0
	SRCW12	2.50	0.29	0.29	28.1	305.0
GHOORBANI-RENANI ET AL. (2009)	A1M(prototype)	2.07	0.23	0.23	28.3	400.0
	A2C(prototype)	2.07	0.23	0.23	28.3	400.0
	B1M(model)	2.08	0.22	0.22	28.3	400.0
	B2C(model)	2.08	0.22	0.22	28.3	400.0
LAYSSI AND MITCHELL (2012)	W1	2.83	0.08	0.08	31.2	470.0
	W2	2.83	0.14	0.14	30.4	470.0
TASNIMI (2000)	SHW1	3.00	0.40	0.40	21.6	216.0
	SHW2	3.00	0.40	0.40	21.6	216.0
	SHW3	3.00	0.40	0.40	22.5	216.0
	SHW4	3.00	0.40	0.40	23.5	216.0
KABEYASAWA ET AL. (1983)	NW-1	1.80	0.43	0.24	87.6	753.0
	NW-2	1.80	0.43	0.24	93.6	753.0
	NW-3	1.80	0.43	0.24	55.5	753.0
	NW-4	1.80	0.43	0.24	54.6	753.0
	NW-5	1.80	0.43	0.24	60.3	753.0
	NW-6	1.80	0.43	0.24	65.2	753.0
SHIMAZAKI (2008)	WP1	2.00	0.35	0.35	44.0	387.0
HIRAISHI ET AL. (1983)	W1	1.75	0.36	0.18	26.5	377.0
	W2	1.75	0.36	0.18	26.5	377.0
SHIU ET AL. (1981)	CI-1	2.90	0.30	0.30	23.3	472.9

Table A.5. Database parameters for transition walls: reinforcement and loading.

Source	Specimen	$\frac{H}{L}$	$\frac{A_b}{A}$	$\frac{L_b}{L}$	$f'_c$	$f_y$
DAZIO ET AL. (2009)	WSH2	0.0027	0.0025	0.0209	0.0075	0.06
	WSH3	0.0046	0.0025	0.0226	0.0075	0.06
	WSH4	0.0048	0.0025	0.0197	0.0025	0.06
	WSH5	0.0024	0.0025	0.0101	0.0099	0.13
	WSH6	0.0045	0.0025	0.0160	0.0137	0.11
THOMSEN AND WALLACE (1995)	RW1	0.0029	0.0033	0.0365	0.0137	0.10
	RW2	0.0029	0.0033	0.0365	0.0091	0.10
OESTERLE ET AL. (1976)	B1	0.0026	0.0027	0.0111	0.0055	0.00
	B2	0.0026	0.0055	0.0367	0.0111	0.00
	B3	0.0026	0.0027	0.0111	0.0273	0.00
	B4	0.0026	0.0027	0.0111	0.0273	0.00
	B5	0.0026	0.0055	0.0367	0.0382	0.00
	B6	0.0026	0.0055	0.0367	0.0278	0.13
	B7	0.0026	0.0055	0.0367	0.0382	0.08
	B8	0.0026	0.0137	0.0367	0.0464	0.09
	B9	0.0026	0.0055	0.0367	0.0382	0.09
	B10	0.0026	0.0055	0.0197	0.0382	0.08
ESCOLANO-MARGARIT ET AL. (2012)	W-MC-C	0.0029	0.0055	0.0877	0.0098	0.09
TRAN AND WALLACE (2012A)	RW-A20-P10-S38	0.0025	0.0027	0.0459	0.0086	0.10
	RW-A20-P10-S63	0.0051	0.0062	0.1010	0.0086	0.10
LESTUZZI AND BACHMANN (2007)	WDH3-SOFT	0.0036	0.0035	0.0085	0.0069	0.03
	WDH4-SOFT	0.0036	0.0035	0.0085	0.0069	0.03
	WDH5-SOFT	0.0049	0.0028	0.0100	0.0028	0.03
	WDH6-SOFT	0.0049	0.0028	0.0100	0.0028	0.03
LEFAS ET AL. (1990)	SW30	0.0150	0.0035	0.0330	0.0066	0.00
	SW31	0.0150	0.0035	0.0330	0.0066	0.00
	SW31R	0.0150	0.0035	0.0330	0.0066	0.00
	SW32	0.0150	0.0035	0.0330	0.0066	0.00
	SW32R	0.0150	0.0035	0.0330	0.0066	0.00
	SW33	0.0150	0.0035	0.0330	0.0066	0.00

Table A.5. Database parameters for transition walls: reinf. and loading (continued).

Source	Specimen	$\frac{H}{L}$	$\frac{A_b}{A}$	$\frac{L_b}{L}$	$f'_c$	$f_y$
	SW33R	0.0150	0.0035	0.0330	0.0066	0.00
ZHANG AND WANG (2000)	SW7	0.0060	0.0100	0.0615	0.0210	0.24
	SW8	0.0060	0.0100	0.0450	0.0210	0.35
	SW9	0.0060	0.0170	0.1256	0.0250	0.24
	SRCW12	0.0060	0.0170	0.0270	0.0250	0.35
GHOUBANI-RENANI ET AL. (2009)	A1M(prototype)	0.0060	0.0066	0.0265	0.0100	0.00
	A2C(prototype)	0.0060	0.0066	0.0265	0.0100	0.00
	B1M(model)	0.0059	0.0066	0.0570	0.0100	0.00
	B2C(model)	0.0059	0.0066	0.0570	0.0100	0.00
LAYSSI AND MITCHELL (2012)	W1	0.0018	0.0053	0.0870	0.0053	0.00
	W2	0.0019	0.0053	0.0941	0.0053	0.00
TASNIMI (2000)	SHW1	0.0021	0.0028	0.0226	0.0028	0.00
	SHW2	0.0021	0.0028	0.0226	0.0028	0.00
	SHW3	0.0021	0.0028	0.0226	0.0028	0.00
	SHW4	0.0021	0.0028	0.0226	0.0028	0.00
KABEYASAWA ET AL. (1983)	NW-1	0.0047	0.0047	0.0236	0.0283	0.14
	NW-2	0.0047	0.0047	0.0236	0.0283	0.13
	NW-3	0.0024	0.0024	0.0236	0.0196	0.17
	NW-4	0.0024	0.0024	0.0314	0.0196	0.20
	NW-5	0.0047	0.0047	0.0314	0.0196	0.16
	NW-6	0.0047	0.0047	0.0398	0.0196	0.17
SHIMAZAKI (2008)	WP1	0.0266	0.0187	0.0415	0.0254	0.08
HIRAIISHI ET AL. (1983)	W1	0.0031	0.0031	0.0135	0.0038	0.05
	W2	0.0048	0.0047	0.0340	0.0057	0.05
SHIU ET AL. (1981)	CI-1	0.0024	0.0054	0.0520	0.0095	0.00

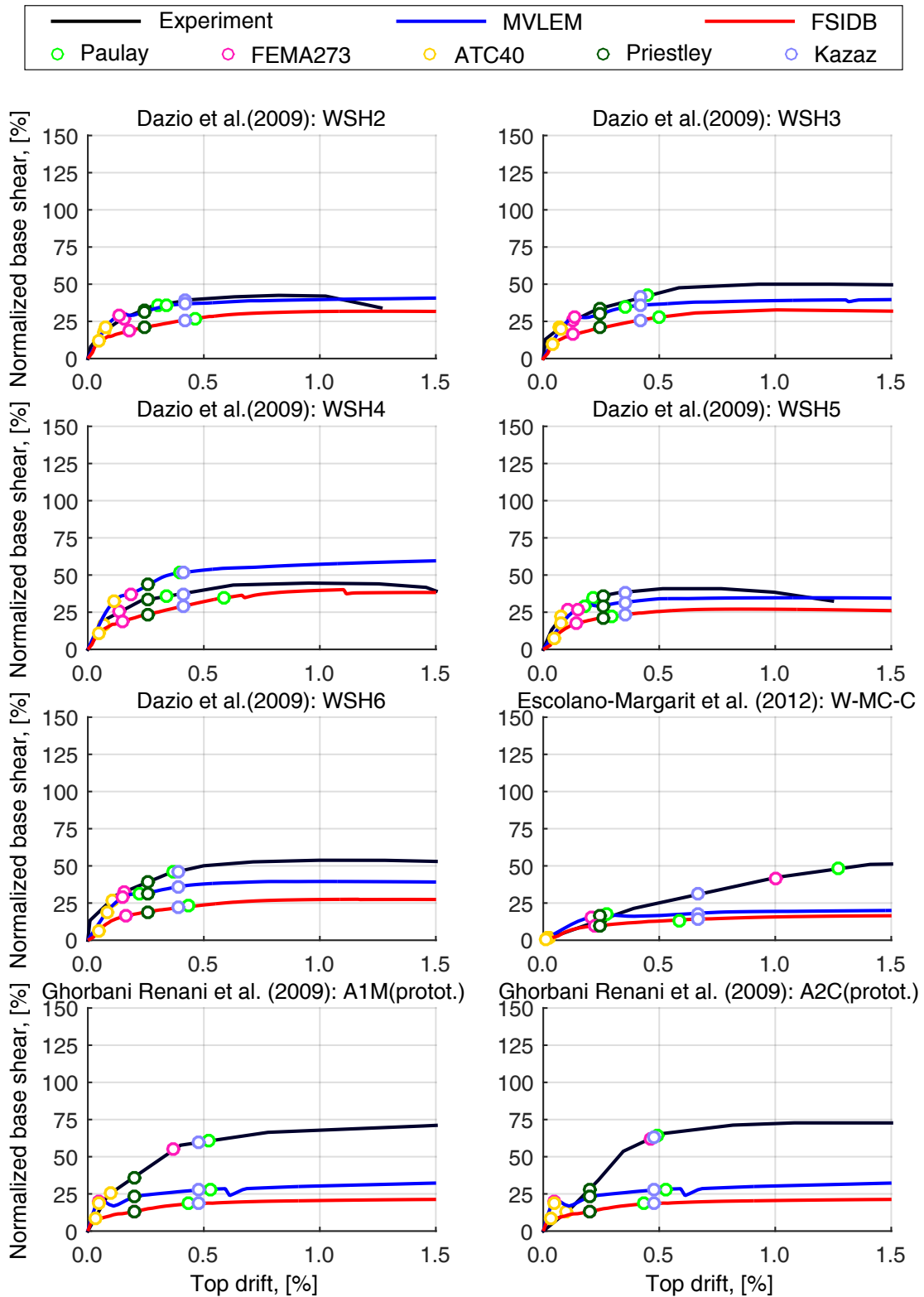


Figure A.2. Database force-deformation plots and the estimated yield drifts for the transition walls.

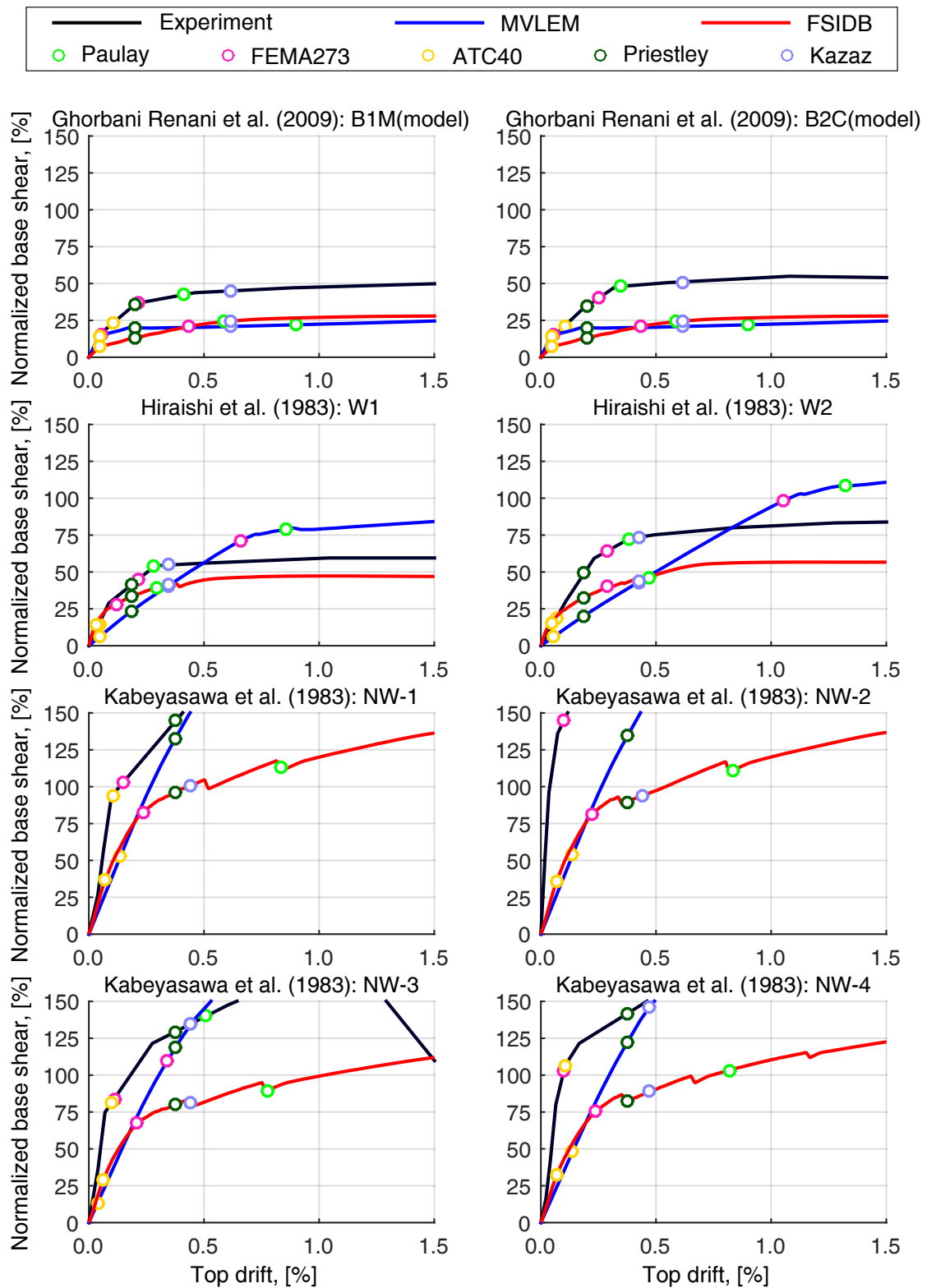


Figure A.2. Database force-deformation plots and the estimated yield drifts for the transition walls (continued).

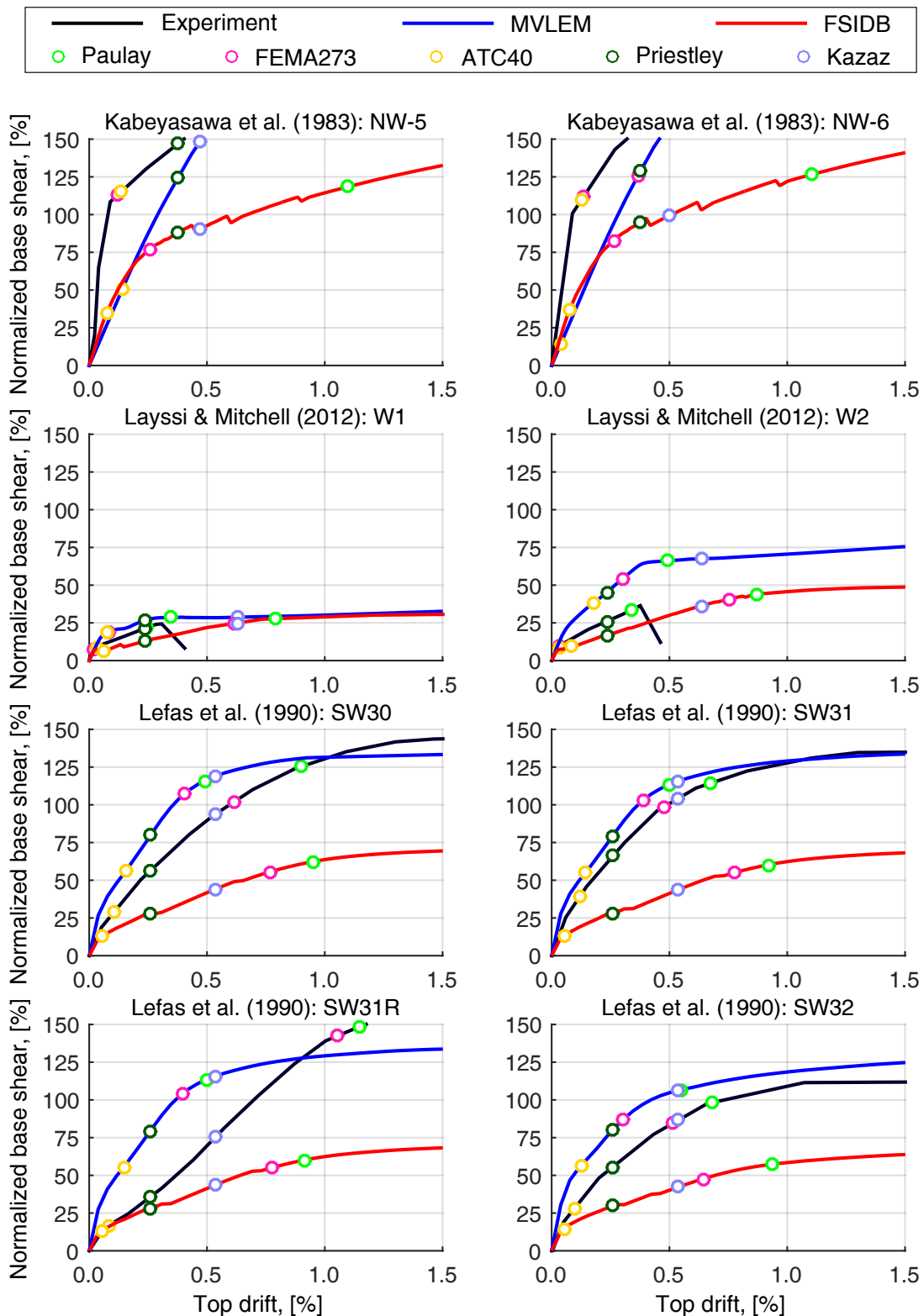


Figure A.2. Database force-deformation plots and the estimated yield drifts for the transition walls (continued).

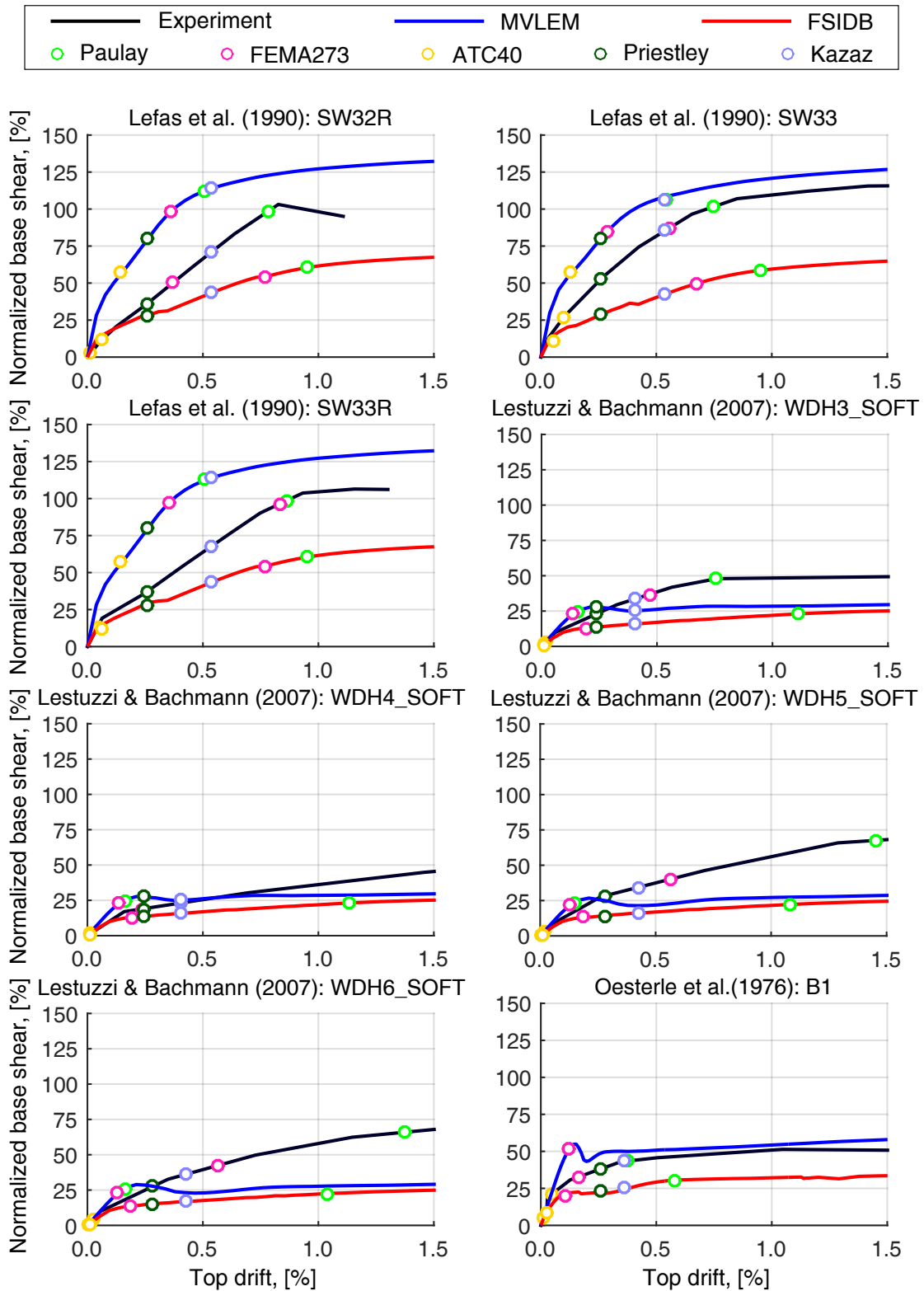


Figure A.2. Database force-deformation plots and the estimated yield drifts for the transition walls (continued).

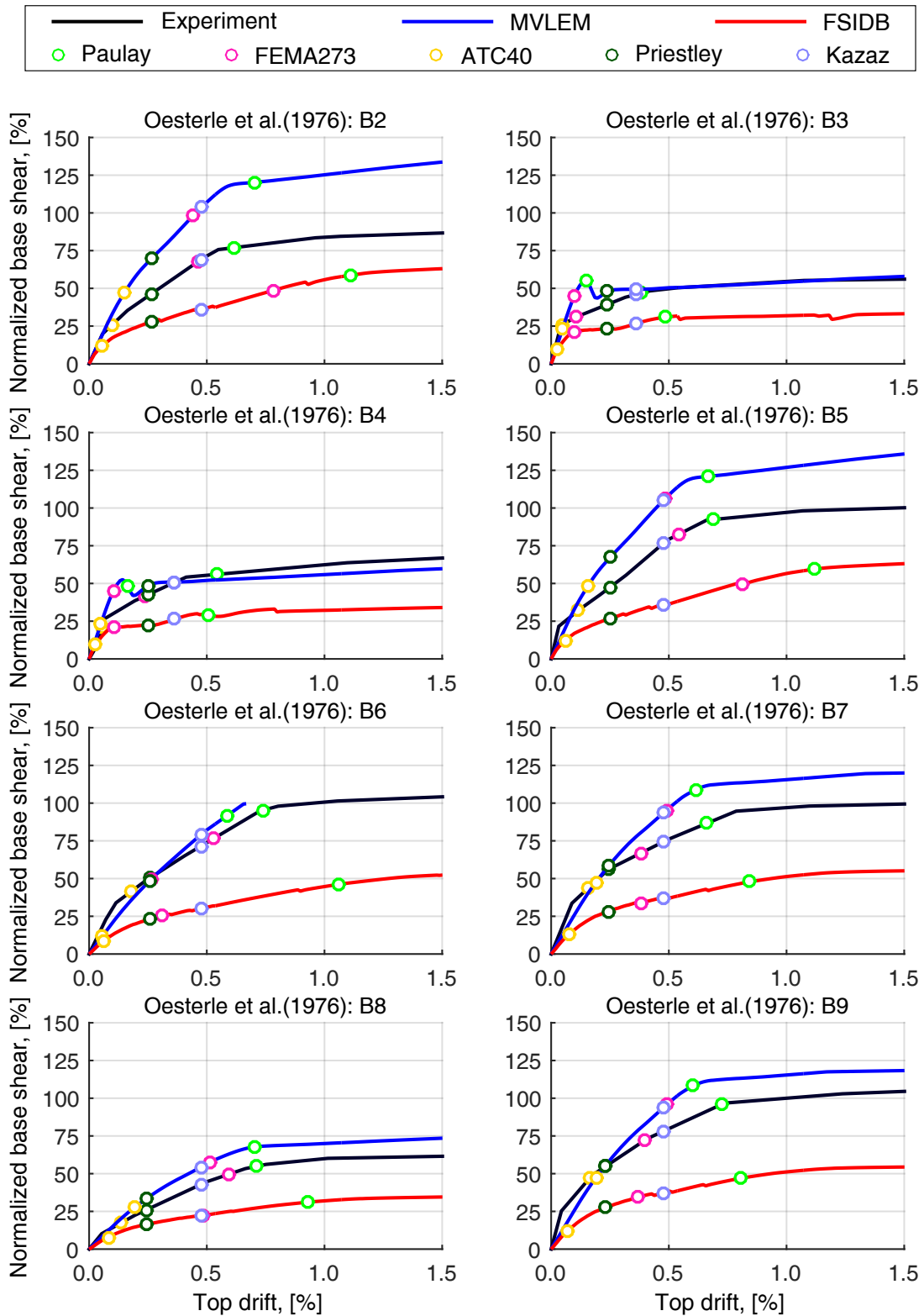


Figure A.2. Database force-deformation plots and the estimated yield drifts for the transition walls (continued).



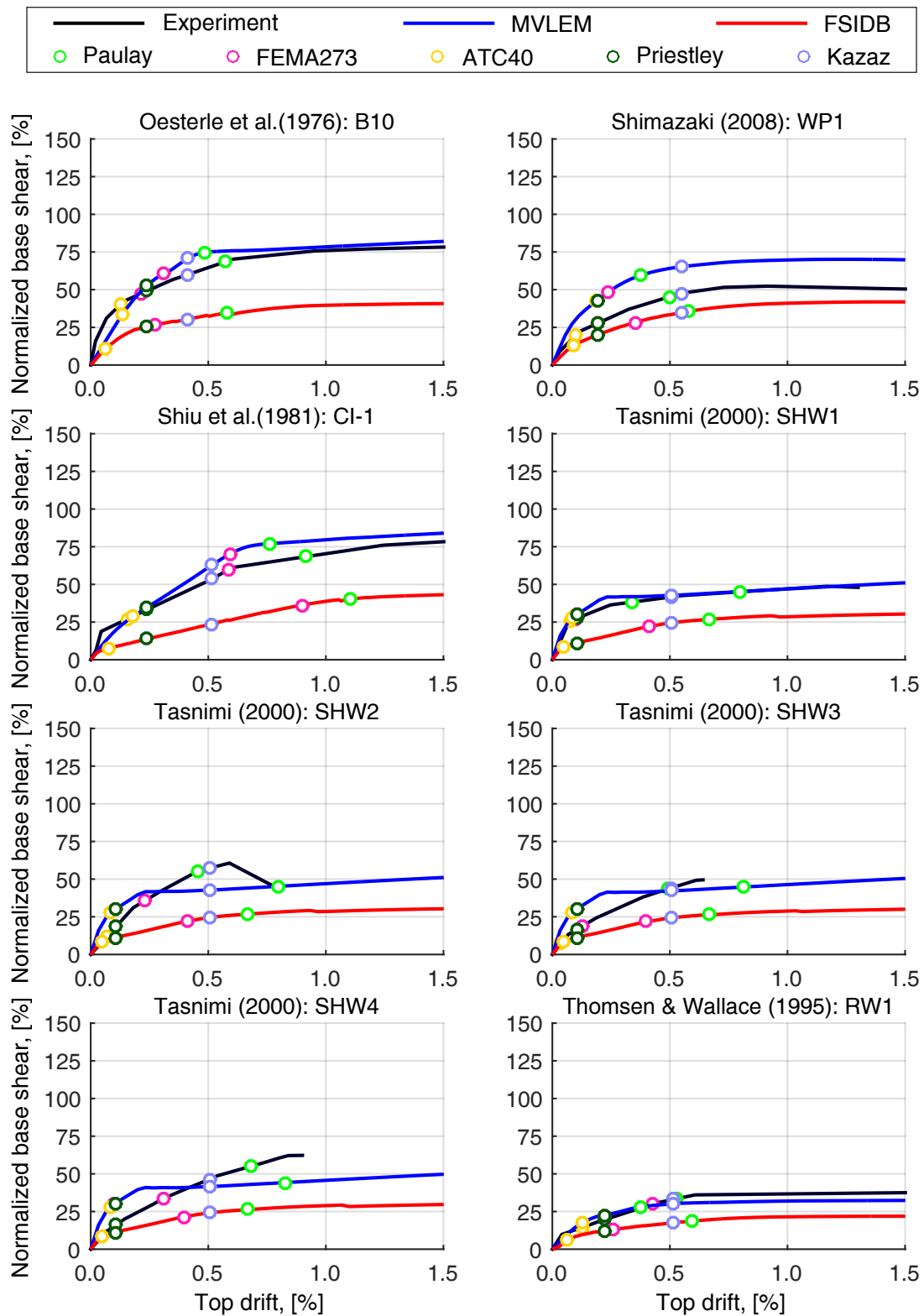


Figure A.2. Database force-deformation plots and the estimated yield drifts for the transition walls (continued).

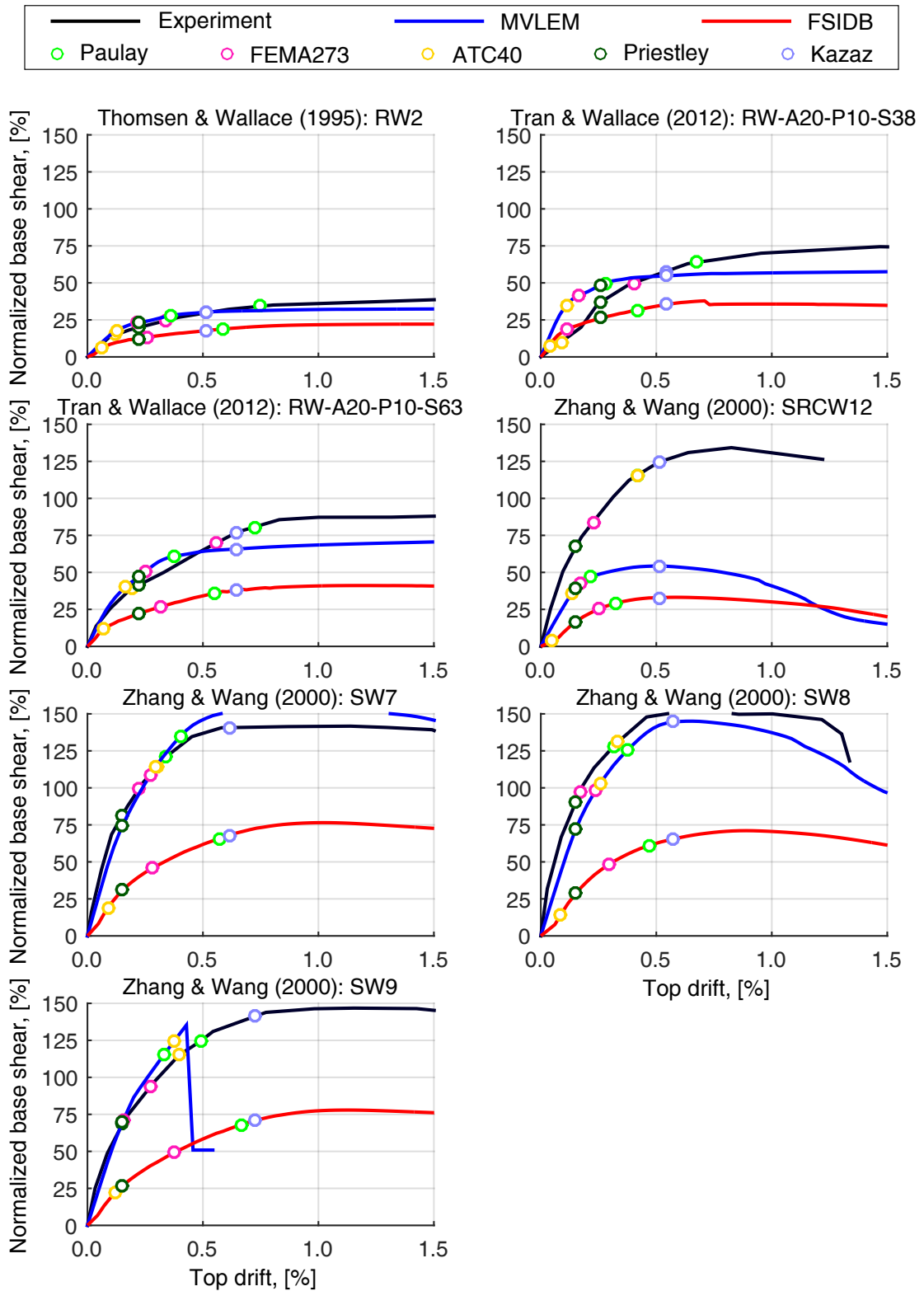


Figure A.2. Database force-deformation plots and the estimated yield drifts for the transition walls (continued).

# Bibliography

- Aaleti, S. R. (2009). *Behavior of Rectangular Concrete Walls Subjected to Simulated Seismic Loading*. Ph. D. thesis, Iowa State University.
- Akaike, H. (1973). Information Theory and an Extension of the Maximum Likelihood Principle. In P. B. N. and F. Csaki (Eds.), *Second International Symposium on Information Theory*, pp. 267–281.
- ATC40 (1996). *Seismic Evaluation and Retrofit of Concrete Buildings.*, Applied Technology Council, Redwood, California, US.
- Athanasopoulou, A. (2010). *Shear Strength and Drift Capacity of Reinforced Concrete and High-performance Fiber Reinforced Concrete Low-rise Walls Subjected to Displacement Reversals*. Ph. D. thesis, University of Michigan.
- Austrell, P. E., O. Dahlblom, J. Lindemann, A. Olsson, K. G. Olsson, K. Persson, H. Petersson, M. Ristinmaa, G. Sandberg, and P. A. Wernberg (2004). *CALFEM, A Finite Element Toolbox, Version 3.4*. Lund, Sweden: Division of Structural Mechanics at Lund University.
- Baker, J. W. and C. A. Cornell (2003). Uncertainty Specification and Propagation for Loss Estimation Using FOSM Methods. Technical report, Department of Civil and Environmental Engineering, Stanford University.
- Bao, Y. and S. K. Kunnath (2010). Simplified Progressive Collapse Simulation of RC Frame-wall Structures. *Engineering Structures* 32, 3153–3162.
- Barbosa, A. R. (2011). *Simplified Vector-Valued Probabilistic Seismic Hazard Analysis and Probabilistic Seismic Demand Analysis: Application to the 13-Story NEHRP Reinforced Concrete Frame-Wall Building Design Example*. Ph. D. thesis, University of California, San Diego.
- Barda, F., J. M. Hanson, and W. Corley (1977). Shear Strength of Low-Rise Walls with Boundary Elements. *ACI Special Publications: Reinforced Concrete in Seismic Zones SP53(8)*, 149–202.
- Belarbi, H. and T. C. C. Hsu (1994). Constitutive Laws of Concrete in Tension and Reinforcing Bars Stiffened by Concrete. *ACI Structural Journal* 91(4), 465–474.
- Beyer, K., A. Dazio, and M. J. N. Priestley (2011, March-April). Shear Deformations of Slender Reinforced Concrete Walls under Seismic Loading. *ACI Structural Journal* 108(2), 167–177.
- Birely, A. C. (2012). *Seismic Performance of Slender Reinforced Concrete Structural*

- Walls. Ph. D. thesis, Department of Civil and Environmental Engineering, University of Washington.
- Bouchon, M., N. Orbovic, and B. Fouré (2004, August 1-6). Tests on Reinforced Concrete Low-Rise Shear Walls Under Static Cyclic Loading. In *13th World Conference on Earthquake Engineering*, Vancouver, B.C., Canada.
- Box, G. E. P. and N. R. Draper (1987). *Empirical Model-Building and Response Surfaces*. Oxford, England: John Wiley & Sons.
- Browne, M. W. (2000). Cross-Validation Methods. *Journal of Mathematical Psychology* 44, 108–132.
- Buckland, S. T., K. P. Burnham, and N. H. Augustin (1997). Model Selection: An Integral Part of Inference. *Biometrics* 53, 603618.
- Burnham, K. P. and D. R. Anderson (2002). *Model Selection and Multimodel Inference: A Practical Information-Theoretic Approach*. Springer.
- Cardenas, A. E., H. G. Russell, and W. G. Corley (1980). Strength of Low-Rise Structural Walls. *ACI Special Publications SP63(10)*, 221–241.
- Cavanaugh, J. E. (1999). A Large-Sample Model Selection Criterion Based on Kullback's Symmetric Divergence. *Statistics & Probability Letters* 42(4), 333–343.
- Chib, S., M. Clyde, G. Woodworth, and A. Zaslavsky (2003). *Subjective and Objective Bayesian Statistics*. New York: John Wiley & Sons.
- Chinneck, J. W. (2006). *Practical Optimization: A Gentle Introduction*. Ottawa, Canada: Systems and Computer Engineering, Carleton University. To be Published.
- Christopher Frey, H. and S. R. Patil (2002). Identification and Review of Sensitivity Analysis Methods. *Risk Analysis* 22(3), 553–578.
- Cukier, R. I., C. M. Fortuin, K. E. Shuler, A. G. Petschek, and J. H. Schaibly (1973). Study of the Sensitivity of Coupled Reaction Systems to Uncertainties in Rate Coefficients. I Theory . *Journal of Chemical Physics* 59(8), 3873–3878.
- Darani, F. M. and A. S. Moghadam (2012). Analytical Study on the Effect of Boundary Element Characteristics on the Behavior of Low-Rise Concrete Shear Walls. In *15th World Conference on Earthquake Engineering*, Lisbon, Portugal.
- Dashti, F., S. Malekpour, and A. Davaran (2012). Local and Global Response Simulation of a Reinforced Concrete Wall Specimen. In *15th World Conference on Earthquake Engineering*, Lisbon, Portugal.
- Dazio, A., K. Beyer, and H. Bachmann (2009). Quasi-Static Cyclic Tests and Plastic Hinge Analysis of RC Structural Walls. *Engineering Structures* 31, 1556–1571.
- Dazio, A., T. Wenk, and H. Bachmann (1999, March). Versuche an Stahlbetontragwänden unter zyklisch-statischer Einwirkung. Technical report, Institut für Baustatik und Konstruktion, Eidgenössische Technische Hochschule Zürich, Zürich.
- De Borst, R., J. J. C. Remmers, A. Needleman, and M.-A. Abellan (2004). Discrete

- vs Smearred Crack Models for Concrete Fracture: Bridging the Gap. *International Journal for Numerical and Analytical Methods in Geomechanics* 28, 583607.
- deLeeuw, J. (1992). Introduction to Akaike (1973) Information Theory and an Extension of the Maximum Likelihood Principle. In S. Kotz and N. Johnson (Eds.), *Breakthroughs in Statistics*, Springer Series in Statistics, pp. 599–609. Springer New York.
- Draper, D. (1995). Assessment and Propagation of Model Uncertainty. *Journal of the Royal Statistical Society B(57)*, 4570.
- Dziak, J. J., D. L. Coffman, L. S. T., and R. Li (2012). Sensitivity and Specificity of Information Criteria. Technical Report 12-119, The Pennsylvania State University.
- EAG (2013). Guidance on Detailed Engineering Evaluation of Earthquake Affected Non-residential buildings - Part 3: Technical Guidance., Engineering Advisory Group (EAG). Section 9: Reinforced Concrete Wall Buildings.
- Endo, T., H. Adachi, and M. Nakanishi (1980, September 8-13). Force-Deformation Hysteresis Curves of Reinforced Concrete Walls. In *7th World Conference on Earthquake Engineering*, Istanbul, Turkey.
- ervenka, V., D. Novk, D. Lehk, and R. Pukl (2005, March 20-25). Identification of Shear Wall Failure Mode. In *11th International Conference on Fracture, ICF11*, Turin, Italy.
- Escolano-Margarit, D., A. Klenke, S. Pujol, and A. Benavent-Climent (2012). Failure Mechanism of Reinforced Concrete Structural Walls with and without Confinement. In *15th World Conference on Earthquake Engineering*, Lisbon, Portugal.
- Fazileh, F. (2011). *Displaccmct-Based Seismic Design of RC Wall-Frame Buildings and Asymmetric Plan Buildings*. Ph. D. thesis, Carleton University.
- FEMA273 (1997). NEHRP Guidelines for the Seismic Rehabilitation of Buildings., Applied Technology Council (ATC-33 Project).
- FEMA356 (2000). Prestandard and Commentary for the Seismic Rehabilitation of Buildings., American Society of Civil Engineers.
- Filippou, F. C., E. P. Popov, and V. V. Bertero (1983). Effects of Bond Deterioration on Hysteretic Behavior of Reinforced Concrete Joints. Technical Report UCB/EERC-83/19, Earthquake Engineering Research Center, University of California, Berkeley.
- Fischinger, M., K. Rejec, and T. Isakovic (2012). Modeling Inelastic Shear Response of RC Walls. In *15th World Conference on Earthquake Engineering*, Lisbon, Portugal.
- Fischinger, M., T. Vidic, and F. P. (1992). *Nonlinear Seismic Analysis and Design of Reinforced Concrete Buildings*, Chapter Nonlinear Seismic Analysis Of Structural Walls Using The Multiple-Vertical-Line-Element Model, pp. 191–202. Elsevier Applied Science.
- Fischinger, M., T. Vidic, J. Selih, P. Fajfar, H. Y. Zhang, and F. Damjanic (1990, 4-6

- April). Validation of a Macroscopic Model for Cyclic Response Prediction of RC Walls. In *2nd International Conference on Computer Aided Analysis and Design of Concrete Structures*, Volume 2, Zell am See, Austria, pp. 1131–1142.
- Gaber, N., G. Foley, P. Pascual, N. Stiber, and E. Sunderland (2009). Guidance on the Development, Evaluation and Application of Environmental Models. EPA/100/K-09/003, Council for Regulatory Environmental Modeling .
- Galal, K. and H. El-Sokkary (2008, October 12-17). Advancement In Modeling of RC Shear Walls. In *14th World Conference on Earthquake Engineering*, Beijing, China.
- Gallitire, E., P. Labbe, N. Ile, J. M. Reynouard, and E. Viallet (2007, August 12-17). Reinforced Concrete Shear Walls Damage Characterisation for Seismic Loads: Crack Width Evaluation and Alternative Methods. In *19th International Conference on Structural Mechanics in Reactor Technology*, Toronto, Canada.
- Geisser, S. (1975). The Predictive Sample Reuse Method with Applications. *Journal of the American Statistical Association* 70(350), 320–328.
- Ghobarah, A. and M. Youssef (1999). Modelling of Reinforced Concrete Structural Walls. *Engineering Structures* 21, 912–923.
- Ghorbani-Renani, I., N. Velev, R. Tremblay, D. Palermo, B. Massicotte, and P. Leger (2009). Modeling and Testing Influence of Scaling Effects on Inelastic Response of Shear Walls. *ACI Structural Journal* 106(3), 358–367.
- Gulec, C. K. and A. S. Whittaker (2009, September 15). Performance-Based Assessment and Design of Squat Reinforced Concrete Shear Walls. Technical Report MCEER-09-0010, MCEER, University at Buffalo, State University of New York.
- Gulec, C. K., A. S. Whittaker, and J. Hooper (2009, August 9-14). Fragility Functions for Seismic Performance Assessment of Safety-Related Reinforced Concrete Nuclear Structures. In *20th International Conference on Structural Mechanics in Reactor Technology (SMiRT 20)*, Espoo, Finland.
- Hagen, G. R. (2012). Performance-Based Analysis of a Reinforced Concrete Shear Wall Building. Master's thesis, California Polytechnic State University.
- Hannewald, P. and K. Beyer (2012). Plastic Hinge Models for the Seismic Assessment of Reinforced Concrete Wall-type Piers with Detailing Deficiencies. In *15th World Conference on Earthquake Engineering*, Lisbon, Portugal.
- Hart, C. R., D. A. Kuchma, L. N. Lowes, D. E. Lehman, K. P. Marley, and A. C. Birely (2008). Test of RC Walls Using Advanced Load-Control and Instrumentation Methods. In *14th World Conference on Earthquake Engineering*.
- Hidalgo, P. A., R. M. Jordan, and M. P. Martinez (2002). An Analytical Model to Predict the Inelastic Seismic Behavior of Shear-Wall, Reinforced Concrete Structures. *Engineering Structures* 24, 85–98.
- Hiraishi, H., M. Yoshimura, H. Isoishi, and S. Nakata (1983). Planar Tests on Rein-

- forced Concrete Shear Wall Assemblies - U.S.-Japan Cooperative Research Program. Technical report, Building Research Institute, Ministry of Construction.
- Hjort, N. L. and G. Claeskens (2003). Frequentist Model Average Estimators. *Journal of the American Statistical Association* 98, 879-899.
- Hoeting, J. A., D. Madigan, A. E. Raftery, and C. T. Volinsky (1999). Bayesian Model Averaging: A Tutorial. *Statistical Science* 14(4), 382-417.
- Hora, S. C. and R. L. Iman (1986). A Comparison of Maximus/Bounding and Bayes/Monte Carlo for Fault Tree Uncertainty Analysis. Technical Report SAND85-2839, Sandia National Laboratories, Albuquerque, New Mexico.
- Ibrahim, M. M. (2000). *Linear and Nonlinear Flexural Stiffness Models for Concrete Walls in High-Rise Buildings*. Ph. D. thesis, University of British Columbia.
- Iman, R. L. and S. C. Hora (1990). A Robust Measure of Uncertainty Importance for Use in Fault Tree System Analysis. *Risk Analysis* 10(3), 401-406.
- Ishigami, T. and T. Homma (1990, 3-5 December). An Importance Quantification Technique in Uncertainty Analysis for Computer Models. In *1st International Symposium on Uncertainty Modeling and Analysis*, Maryland, USA.
- Jalali, A. and F. Dashti (2010). Nonlinear Behavior of Reinforced Concrete Shear Walls Using Macroscopic and Microscopic Models. *Engineering Structures* 32, 2959-2968.
- Judge, G. G. and R. C. Mittelhammer (2007). Estimation and Inference in the Case of Competing Sets of Estimating Equations. *Journal of Econometrics* 138(2), 513 - 531. 'Information and Entropy Econometrics' A Volume in Honor of Arnold Zellner.
- Jünemann, R., J. C. De La Llera, M. A. Hube, L. A. Cifuentes, and E. Kausel (2015). A Statistical Analysis of Reinforced Concrete Wall Buildings Damaged During the 2010, Chile Earthquake. *Engineering Structures* 82, 168-185.
- Jünemann, R., M. Hube, J. C. De La Llera, and E. Kausel (2012). Characteristics of Reinforced Concrete Shear Wall Buildings Damaged During 2010 Chile Earthquake. In *15th World Conference on Earthquake Engineering*, Lisbon, Portugal.
- Kabeyasawa, T. and J. I. Milev (1997, August 17-22). Modeling of Reinforced Concrete Shear Walls under Varying Axial Load. In *14th International Conference on Structural Mechanics*, Lyon, France.
- Kabeyasawa, T., H. Shiohara, S. Otani, and H. Aoyama (1983). Analysis of the Full-Scale Seven-Story Reinforced Concrete Test Structure. *Journal of Faculty of Engineering, University of Tokyo* 37(2), 432-478.
- KADAŞ, K. (2006). Influence of Idealized Pushover Curves on Seismic Response. Master's thesis, Middle East Technical University.
- Kazaz, I., P. Gülkan, and A. Yakut (2012). Deformation Limits for Structural Walls with Confined Boundaries. *Earthquake Spectra* 28(3), 1019-1046.

- Keitel, H. and A. Dimmig-Osburg (2010). Uncertainty and Sensitivity Analysis of Creep Models for Uncorrelated and Correlated Input Parameters. *Engineering Structures* 32, 3758–3767.
- Kent, D. C. and R. Park (1971). Inelastic Behavior of Reinforced Concrete Members with Cyclic Loading. *Bulletin of New Zealand Society for Earthquake Engineering* 4(1), 108–125.
- Kieseppa, I. A. (1997). Akaike Information Criterion, Curve-Fitting and the Philosophical Problem of Simplicity. *British Journal for the Philosophy of Science* 48, 21–48.
- Kolozvari, K., K. Orakcal, and J. W. Wallace (2015). Modeling of Cyclic Shear-Flexure Interaction in Reinforced Concrete Structural Walls. I: Theory. *Journal of Structural Engineering* (141(5)).
- Kolozvari, K., T. Tran, J. W. Wallace, and K. Orakcal (2012). Modeling of Cyclic Shear-Flexure Interaction in Reinforced Concrete Structural Walls. In *15th World Conference on Earthquake Engineering*, Lisbon, Portugal.
- Kono, S., K. Sakamoto, M. Sakashita, T. Mukai, M. Tani, and H. Fukuyama (2012). Effects of Boundary Columns on the Seismic Behavior of Cantilever Structural Walls. In *15th World Conference on Earthquake Engineering*.
- Layssi, H. and D. Mitchell (2012, June 13-15). Experiments on Seismic Retrofit and Repair of Reinforced Concrete Shear Walls. In *6th International Conference on FRP Composites in Civil Engineering (CICE)*, Rome, Italy.
- Lee, T. H. and K. M. Mosalam (2003, July 6-7). Sensitivity of Seismic Demand of a Reinforced Concrete Shear-Wall Building. In *9th International Conference on Application of Statistics and Probability in Civil Engineering (ICASP9)*, San Francisco, California, US.
- Lee, T. H. and K. M. Mosalam (2005). Seismic Demand Sensitivity of Reinforced Concrete Shear-Wall Building Using FOSM Method. *Earthquake Engineering and Structural Dynamics* 34, 1719–1736.
- Lefas, I. D., M. D. Kotsovos, and N. N. Ambraseys (1990). Behavior of Reinforced Concrete Structural Walls: Strength, Deformation Characteristics and Failure Mechanism. *ACI Structural Journal* 87(1), 23–31.
- Lestuzzi, P. and H. Bachmann (2007). Displacement Ductility and Energy Assessment from Shaking Table Tests on RC Structural Walls. *Engineering Structures* 29, 1708–1721.
- Lombard, J. C. (1999). Seismic Strengthening and Repair of Reinforced Concrete Shear Walls Using Externally Bonded Carbon Fibre Tow Sheets. Master's thesis, Department of Civil and Environmental Engineering, Carlton University.
- Lopes, M. S. (2001). Experimental Shear-Dominated Response of RC Walls. Part I: Objectives, Methodology and Results. *Engineering Structures* 23, 229–239.



- Lowes, L. N., D. E. Lehman, A. C. Birely, D. A. Kuchma, C. R. Hart, and K. P. Marley (2011). Behavior, Analysis, and Design of Complex Wall Systems: Planar Wall Test Program Summary Document. Technical report, Network for Earthquake Engineering Simulation.
- Magna, C. E. and S. K. Kunnath (2012). Simulation of Nonlinear Seismic Response of Reinforced Concrete Structural Walls. In *15th World Conference on Earthquake Engineering*, Lisbon, Portugal.
- Mallows, C. L. (1973). Some Comments on  $C_p$ . *Technometrics* 15(4), 661–675.
- Mander, J. B., M. J. N. Priestley, and R. Park (1988). Theoretical Stress-Strain Model for Confined Concrete. *Journal of Structural Engineering* 114(8), 1804–1825.
- Mansur, M. A., T. Balendra, and S. C. H'ng (1991, January 13 -16). Tests on Reinforced Concrete Low-Rise Shear Walls under Cyclic Loading. In *International Workshop on Concrete Shear in Earthquake*, Houston, Texas.
- Marzban, S. (2010, June). Effect of Soil-Foundation-Structure Interaction on the Seismic Performance of Reinforced Concrete Frames. Master's thesis, Amirkabir University of Technology (Tehran Polytechnic), Tehran. in Persian.
- Massone, L. M., K. Orakcal, and J. W. Wallace (2004, August 1-6). Flexural and Shear Responses in Slender RC Shear Walls. In *13th World Conference on Earthquake Engineering*, Vancouver, B.C., Canada.
- Massone, L. M., K. Orakcal, and J. W. Wallace (2009). Modeling of Squat Structural Walls Controlled by Shear. *ACI Structural Journal* 106(5), 646–655.
- Matsuura, T., T. Matsumoto, and K. Shimazaki (2012). Experimental Study on 3-Dimensional Reinforced Concrete Core Wall for Super High Rise Buildings. In *15th World Conference on Earthquake Engineering*, Lisbon, Portugal.
- Mazzoni, S., F. McKenna, M. H. Scott, and G. L. Fenves (2006). *Open System for Earthquake Engineering Simulation User Command-Language Manual*. Pacific Earthquake Engineering Research Center, University of California. Berkeley.
- McKay, M. D., R. J. Beckman, and W. J. Conover (1979). A Comparison of Three Methods for Selecting Values of Input Variables in the Analysis of Output from a Computer Code. *Technometrics* 21(2), 239-245.
- McKenna, F., G. L. Fenves, and M. H. Scott (2000). Open System for Earthquake Engineering Simulation (OpenSees).
- Menegotto, M. and P. Pinto (1973). Method of Analysis for Cyclically Loaded Reinforced Concrete Plane Frames Including Changes in Geometry and Nonelastic Behavior of Elements under Combined Normal Force and Bending. In *IABSE Symposium on Resistance and Ultimate Deformability of Structures Acted on by Well-Defined Repeated Loads*, Lisbon, Portugal.
- Mickleborough, N. C., F. Ning, and C. M. Chan (1999). Prediction of Stiffness of Reinforced Concrete Shearwalls under Service Load. *ACI Structural Journal* 96(6),

- 10181026.
- Mo, Y. L., J. Zhong, and T. T. C. Hsu (2008). Seismic Simulation of RC Wall-Type Structures. *Engineering Structures* 30, 31673175.
- Mokhtari, A. and H. Christopher Frey (2005). Review and Recommendation of Methods for Sensitivity and Uncertainty Analysis for the Stochastic Human Exposure and Dose Simulation (SHEDS) Models - Volume 1: Review of Available Methods for Conducting Sensitivity and Uncertainty Analysis in Probabilistic Models. Technical report, Alion Science and Technology, 1000 Park Forty Plaza, Durham, NC.
- Most, T. (2012, June 13-15). Variance-Based Sensitivity Analysis in the Presence of Correlated Input Variables. In *5th Conference Reliable Engineering Computing (REC)*, Brno, Czech Republic.
- Nagae, T., K. Tahara, K. Fukuyama, T. Matsumori, H. Shiohara, T. Kabeyasawa, S. Kono, M. Nishiyama, J. Moehle, J. W. Wallace, R. Sause, and W. Ghannoum (2012). Test Results of Four-Story Reinforced Concrete and Post-Tensioned Concrete Buildings: The 2010 E-Defense Shaking Table Test. In *15th World Conference on Earthquake Engineering*, Lisbon, Portugal.
- Oesterle, R. G., J. D. Aristizabal-Ochoa, A. E. Fiorato, H. E. Russel, and W. G. Corley (1979). Earthquake Resistant Structural Walls - Tests of Isolated Walls - Phase II. Technical report, National Science Foundation, Construction Technology Laboratories, Portland Cement Association, Skokie, Illinois.
- Oesterle, R. G., A. E. Fiorato, L. S. Johal, J. E. Carpenter, H. E. Russle, and W. G. Corley (1976). Earthquake Resistant Structural Walls - Tests of Isolated Walls. Technical report, National Science Foundation, Construction Technology Laboratories, Portland Cement Association, Skokie, Illinois.
- Orakcal, K., L. M. Massone, and J. W. Wallace (2006). Analytical Modeling of Reinforced Concrete Walls for Predicting Flexural and Coupled-Shear-Flexural Responses. Technical Report PEER 2006/07, Pacific Earthquake Engineering Research Center, October.
- Orakcal, K., J. W. Wallace, and J. P. Conte (2004). Flexural Modeling of Reinforced Concrete Walls-Model Attributes. *ACI Structural Journal* 101(5), 688–398.
- Palermo, D. (2002). *Behaviour and Analysis of Reinforced Concrete Walls Subjected to Reversed Cyclic Loading*. Ph. D. thesis, Department of Civil Engineering, University of Toronto.
- Panagiotou, M. (2008). *Seismic Design, Testing and Analysis of Reinforced Concrete Wall Buildings*. Ph. D. thesis, University of California, San Diego.
- Park, R. (1988, August 2-9). State of the Art Report: Ductility Evaluation from Laboratory and Analytical Testing. In *9th World Conference on Earthquake Engineering*, Tokyo, Japan.

- Park, Y. J. and C. H. Hofmayer (1994, December). Shear Wall Experiments and Design in Japan. In *5th Symposium on Current Issues Related to Nuclear Power Plant Structures, Equipment and Piping*, Lake Buena Vista, Florida, US.
- Paulay, T. and M. J. N. Priestley (1992). *Seismic Design of Reinforced Concrete and Masonry Buildings*. John Wiley & Sons.
- Pearson, K. (1901). LIII. On Lines and Planes of Closest Fit to Systems of Points in Space. *The London, Edinburgh, and Dublin Philosophical Magazine and Journal of Science* 2(11), 559–572.
- Peng, X. N. and Y. L. Wong (2011). Experimental Study on Reinforced Concrete Walls under Combined Flexure, Shear and Torsion. *Magazine of Concrete Research* 63(6), 459–471.
- Popovics, S. (1973). A Numerical Approach to the Complete Stress-Strain Curve of Concrete. *Cement and Concrete Research* 3(5), 583–599.
- Priestley, M. J. N., G. M. Calvi, and M. J. Kowalsky (2007). *Displacement-Based Seismic Design of Structures*. Pavia, Italy: IUSS Press.
- Priestley, M. J. N. and M. J. Kowalsky (1998). Aspects of Drift and Ductility Capacity of Rectangular Cantilever Structural Walls. *Bulletin of the New Zealand National Society for Earthquake Engineering* 31(2), 73–85.
- Priestley, M. J. N. and R. Park (1987). Strength and Ductility of Concrete Bridge Columns under Seismic Loading. *ACI Structural Journal* 84, 61–76.
- Raftery, A. E., D. Madigan, and J. A. Hoeting (1997). Bayesian Model Averaging for Regression Models. *Journal of the American Statistical Association* 92, 179191.
- Raftery, A. E. and Y. Zheng (2003). Long-Run Performance of Bayesian Model Averaging. *Working Paper, University of Washington*.
- Ratto, M. and A. Pagano (2010). Using Recursive Algorithms for the Efficient Identification of Smoothing Spline Anova Models. *Advances in Statistical Analysis* 94, 367–388.
- Ratto, M., A. Pagano, and P. Young (2007). State Dependent Parameter Metamodelling and Sensitivity Analysis. *Computer Physics Communications* 77(11), 863–876.
- Razvi, S. (1995). *Confinement of Normal and High-Strength Concrete Columns*. Ph. D. thesis, Department of Civil Engineering, University of Ottawa.
- Reich, B. J., C. B. Storlie, and H. D. Bondell (2009). Variable Selection in Bayesian Smoothing Spline ANOVA Models: Application to Deterministic Computer Codes. *Technometrics* 51(2), 110–120.
- Rothe, D. and G. Knig (1988, August 2-9). Behavior and Modelling of Reinforced Concrete Structural Wall Elements. In *9th World Conference on Earthquake Engineering*, Tokyo-Kyoto, Japan.
- Salonikios, T. N. (2004, August 1-6). Analytical Approach to the Measured Deformation Characteristics of R/C Shear Walls. In *13th World Conference on Earthquake*

- Engineering*, Vancouver, B. C., Canada.
- Salonikios, T. N., A. J. Kappos, I. A. Tegos, and G. G. Penelis (1999). Cyclic Load Behavior of Low-Slenderness Reinforced Concrete Walls: Design Basis and Test Results. *ACI Structural Journal* 96(4), 649–661.
- Saltelli, A. (2002). Making Best Use of Model Evaluations to Compute Sensitivity Indices. *Computer Physics Communications* 145, 280297.
- Saltelli, A., P. Annoni, I. Azzini, F. Campolongo, M. Ratto, and S. Tarantola (2010). Variance Based Sensitivity Analysis of Model Output. Design and Estimator for the Total Sensitivity Index. *Computer Physics Communications* 181, 259–270.
- Saltelli, A. and R. Bolado (1998). An Alternative Way to Compute Fourier Amplitude Sensitivity Test . *Computational Statistics & Data Analysis* 26, 445–460.
- Saltelli, A., M. Ratto, T. Andres, F. Campolongo, J. Cariboni, D. Gatelli, M. Saisana, and S. Tarantola (2008). *Global Sensitivity Analysis: The Primer*. John Wiley and Sons, Ltd.
- Saltelli, A., S. Tarantola, and K. Chan (1999). A Quantitative Model-Independent Method for Global Sensitivity Analysis of Model Output. *Technometrics* 41(1), 39–56.
- Satterthwaite, F. E. (1959). Random Balance Experimentation. *Technometrics* 1(2), 111–137.
- Schwarz, G. (1978). Estimating the Dimension of a Model. *The Annals of Statistics* 6(2), 461–464.
- Scott, B. D., R. Park, and M. J. N. Priestley (1982). Stress-Strain Behavior of Concrete Confined by Overlapping Hoops at Low and High Strain Rates. *ACI Journal Proceedings* 79(1), 13–27.
- Sewell, M. (2008). Model selection. *Department of Computer Science, University College London*.
- Shibata, R. (1981). An Optimal Selection of Regression Variables. *Biometrika* 68(1), 45–54.
- Shiga, T., A. Shibata, and S. Takahashi (1973, June 25-29). Experimental Study on Dynamic Properties of Reinforced Concrete Shear Walls. In *5th World Conference on Earthquake Engineering*, Rome, Italy.
- Shimazaki, K. (2008, October 12-17). Reinforced Concrete Shear Walls with Debonded Diagonal Reinforcements for the Damage-less Reinforced Concrete Building. In *14th World Conference on Earthquake Engineering*, Beijing, China.
- Shiu, K. N., J. I. Daniel, J. I. Aristizabal-Ochoa, A. E. Fiorato, and W. Corley (1981). Earthquake Resistant Structural Walls - Tests of Walls with and without Openings. Technical report, The National Science Foundation.
- Sittipunt, C. and S. L. Wood (2000, January 30- February 4). Development of Reinforcement Details to Improve the Cyclic Response of Slender Structural Walls. In

- 12th World Conference on Earthquake Engineering*, Auckland, New Zealand.
- Sobol, I. M. (1993). Sensitivity Estimates for Nonlinear Mathematical Models. *Mathematical Modeling and Computational Experiment 1*, 407–414.
- Sobol, I. M. (2003). Theorems and Examples on High Dimensional Model Representation. *Reliability Engineering and System Safety 79*, 187–193.
- Stone, M. (1974). Cross-Validatory Choice and Assessment of Statistical Predictions. *Journal of the Royal Statistical Society Series B (Methodological)*, 36(2), 111–147.
- Storlie, C. B., H. D. Bondell, B. J. Reich, and H. H. Zhang (2011). Surface Estimation, Variable Selection and the Nonparametric Oracle Property. *Statistica Sinica 21*, 679–705.
- Storlie, C. B., L. P. Swiler, J. C. Helton, and C. J. Sallaberry (2009). Implementation and Evaluation of Nonparametric Regression Procedures for Sensitivity Analysis of Computationally Demanding Models. *Reliability Engineering and System Safety 94(11)*, 1735–1763.
- Su, R. K. L. and S. M. Wong (2007). Seismic Behaviour of Slender Reinforced Concrete Shear Walls Under High Axial Load Ratio. *Engineering Structures 29*, 1957–1965.
- Sudret, B. (2008). Global Sensitivity Analysis Using Polynomial Chaos Expansions. *Reliability Engineering and System Safety 93*, 964–979.
- Sullivan, T. J., G. M. Calvi, and M. J. N. Priestley (2004, August 1-6). Initial Stiffness versus Secant Stiffness in Displacement-Based Design. In *13th World Conference on Earthquake Engineering*, Vancouver, B.C., Canada.
- Taleb, R., H. Bechtoula, M. Sakashita, S. Kono, and N. Bourahla (2012). Behaviour of Reinforced Concrete Walls with Different Opening Locations: Experiment and FEM Analysis. In *15th World Conference on Earthquake Engineering*, Lisbon, Portugal.
- Tang, Y. and J. Zhang (2011). Probabilistic Seismic Demand Analysis of a Slender RC Shear Wall Considering SoilStructure Interaction Effects. *Engineering Structures 33*, 218229.
- Tarantola, S., D. Gatelli, and T. A. Mara (2006). Random Balance Designs for the Estimation of First Order Global Sensitivity Indices. *Reliability Engineering and System Safety 91*, 717727.
- Tasnimi, A. A. (2000). Strength and Deformation of Mid-Rise Shear Walls Under Load Reversal. *Engineering Structures 22*, 311–322.
- Thomsen, J. H. and J. W. Wallace (1995, Potsdam, Newyork). Displacement-based Design of Reinforced Concrete Structural Walls: An Experimental Investigation of Walls with Rectangular and T-shaped Cross-Sections. Technical Report CU/CEE-95-06, Department of Civil and Environmental Engineering, Clarkson University.
- Thomson, E. D., M. E. Perdomo, R. Picn, M. E. Marante, and J. Flrez-Lpez (2009).

- Simplified Model for Damage in Squat RC Shear Walls. *Engineering Structures* 31, 2215–2223.
- Tjhin, T. N., A. M. A., and J. W. Wallace (2004, August 1-6). Yield Displacement Estimates for Displacement-based Seismic Design of Ductile Reinforced Concrete Structural Wall Buildings. In *13th World Conference on Earthquake Engineering*, Vancouver, B.C., Canada.
- Tran, T. and J. W. Wallace (2012a). Experimental Study of the Lateral Load Response of Moderate Aspect Ratio Reinforced Concrete Structural Walls. Technical Report 2012/12, Department of Civil and Environmental Engineering, University of California, Los Angeles.
- Tran, T. A. and J. W. Wallace (2012b). Experimental Study of Nonlinear Flexural and Shear Deformations of Reinforced Concrete Structural Walls. In *15th World Conference on Earthquake Engineering*, Lisbon, Portugal.
- Tuna, Z. (2012). *Seismic Performance, Modeling and Failure Assessment of Reinforced Concrete Shear Wall Buildings*. Ph. D. thesis, University of California, Los Angeles.
- Tupper, B. (1999). Seismic Response of Reinforced Concrete Walls with Steel Boundary Elements. Master's thesis, Department of Civil Engineering and Applied Mechanics, McGill University.
- Vu-Bac, N., T. Lahmer, Y. Zhang, X. Zhuang, and T. Rabczuk (2014). Stochastic Predictions of Interfacial Characteristic of Polymeric Nanocomposites (PNCs). *Composites Part B Engineering* 59, 8095.
- Vulcano, A. and V. V. Bertero (1987, November). Analytical Models for Predicting the Lateral Response of RC Shear Wall: Evaluation of Their Reliability. Technical Report UCB/EERC-87/19, Earthquake Engineering Research Center.
- Wei, C. Z. (1992). On Predictive Least Squares Principles. *The Annals of Statistics* 20(1), 1–42.
- Wherry, R. J. (1931). A New Formula for Predicting the Shrinkage of the Coefficient of Multiple Correlations. *The Annals of Mathematical Statistics* 2(4), 440–457.
- Wiradinata, S. (1985). Behaviour of Squat Walls Subjected to Load Reversals. Master's thesis, Department of Civil Engineering, University of Toronto.
- Wood, S. L., J. K. Wight, and J. P. Moehle (1987). The 1985 Chile Earthquake Observations on Earthquake-Resistant Construction in Vina Del Mar. Technical report, University of Illinois at Urbana-Champaign.
- Wyllie, L. A. J. (1989). Lessons from the Armenian Earthquake. *Concrete International* 11(8), 21–26.
- Xiaolei, H., C. Xuwei, J. Cheang, M. Guiniu, and W. Peifeng (2008, 12-17 October). Numerical Analysis of Cyclic Loading Test of Shear Walls based on OpenSees. In *14th World Conference on Earthquake Engineering*, Beijing, China.

- Xu, C. and G. Z. Gertner (2008a). A General First-Order Global Sensitivity Analysis Method. *Reliability Engineering and System Safety* 93, 1060–1071.
- Xu, C. and G. Z. Gertner (2008b). Uncertainty and Sensitivity Analysis for Models with Correlated Parameters. *Reliability Engineering and System Safety* 93, 1563–1573.
- Yanez, F. V., R. Park, and T. Paulay (1991, November 20-23). Seismic Behaviour of Reinforced Concrete Structural Walls with Regular and irregular Openings. In *Pacific Conference on Earthquake Engineering*, New Zealand.
- Yeow, T., G. MacRae, R. Dhakal, and B. Bradley (2012). Seismic Sustainability Assessment of Structural Systems: Frame or Wall Structures? In *15th World Conference on Earthquake Engineering*, Lisbon, Portugal.
- Zhang, Y. and Z. Wang (2000). Seismic Behavior of Reinforced Concrete Shear Walls Subjected to High Axial Loading. *ACI Structural Journal* 97(5), 739–750.